KAERI/TR-2061/2002

MASTER-3.0: Multi-purpose Analyzer for Static and Transient Effects of Reactors (MASTER-3.0 코드 방법론)

Korea Atomic Energy Research Institute

제 출 문

한국원자력연구소장 귀하

본 보고서를 "MASTER-3.0 코드 방법론"에 관한 기술보고서로 제출합니다.

2002 년 3 월

연구기관명 : 한국원자력연구소

참여연구원

주 저 자 : 조 병 오 (일체형원자로노심설계기술개발)

공동저자 : 주 한 규 (일체형원자로노심설계기술개발)

조 진 영 (일체형원자로노심설계기술개발)

송 재 승 (일체형원자로노심설계기술개발)

지 성 균 (일체형원자로노심설계기술개발)

요 약

MASTER-3.0 (Multi-purpose Analyzer for Static and Transient Effects of Reactors) 코드는 정상상태 및 천이상태의 사각형 또는 육각형 핵연료집합체로 구성된 원자로를 3차원으로 모사할 수 있는 노심설계 코드이다. 다군 또는 2군 중성자 확산방정식을 풀기 위해 사각형 핵연료집합체를 사용하는 노심에는 NIM (Nodal Integration Method), NEM (Nodal Expansion Method), AFEN (Analytic Function Expansion Nodal Method)/NEM 혼용 방법, NNEM (Non-linear Nodal Expansion Method), NANM (Non-linear Analytic Nodal Method) 방법들이 사용자의 선택에 따라 이용 가능하며, 육각형 핵연료집합체를 사용하는 노심에는 NTPEN (Non-linear Triangle-based Polynomial Expansion Nodal Method) 방법, AFEN (Analytic Function Expansion Nodal)/NEM 혼용 방법 또는 NLFM (Non-linear Local Fine-Mesh Method) 이 이용되고 있다. 계산의 효율 증대 및 시간 단축을 위하여 coarse-mesh rebalancing, Krylov Subspace 방법, 에너지군 축약/확대 방법, asymptotic extrapolation 방법들이 사용되고 있다. MASTER-3.0 코드는 CASMO-3 또는 HELIOS 로부터 마련된 각 핵종의 미시단면적으로 연소계산을 수행한다. 또한, MSS-IAS (Method of Successive Smoothing with Improved Analytic Solution)를 이용하여 각 핵연료집합체 내의 핵연료봉에 관한 정보를 구할 수 있다. 열수력 계산을 위해서 핵연료 온도표를 이용하는 기능과 COBRA3-C/P 또는 MATRA 코드로 계산하는 기능도 갖추고 있다. MASTER-3.0 코드는 실제 설계에 효율적으로 사용되기 위하여 WH형과 CE형 노심 및 SMART 원자로를 비롯한 일반 가압경수로 노심에서 설계 단계별로 필요로 하는 자료를 출력하는 기능도 갖추고 있다.

Abstract

MASTER-3.0 (Multi-purpose Analyzer for Static and Transient Effects of Reactors) is a nuclear design code based on the multi-group diffusion theory to calculate the steady-state and transient pressurized water reactor core in a 3-dimensional Cartesian or hexagonal geometry. Its neutronics model solves the space-time dependent neutron diffusion equations with NIM (Nodal Integration Method), NEM (Nodal Expansion Method), AFEN (Analytic Function Expansion Nodal Method)/NEM Hybrid Method, NNEM (Non-linear Nodal Expansion Method) or NANM (Non-linear Analytic Nodal Method) for a Cartesian geometry and with NTPEN (Non-linear Triangle-based Polynomial Expansion Nodal Method), AFEN (Analytic Function Expansion Nodal)/NEM Hybrid Method or NLFM (Non-linear Local Fine-Mesh Method) for a hexagonal one. Coarse mesh rebalancing, Krylov Subspace method, energy group restriction/prolongation method and asymptotic extrapolation method are implemented to accelerate the convergence of iteration process. MASTER-3.0 performs microscopic depletion calculations using microscopic cross sections provided by CASMO-3 or HELIOS and also has the reconstruction capability of pin information by use of MSS-IAS (Method of Successive Smoothing with Improved Analytic Solution). For the thermal-hydraulic calculation, fuel temperature table or COBRA3-C/P or MATRA model can be used selectively. In addition, MASTER-3.0 is designed to cover various PWRs including SMART as well as WH- and CE-type reactors, providing all data required in their design procedures.

Table of Contents

List of Tables

List of Figures

1. Introduction

Korea Atomic Energy Research Institute (KAERI) has recently developed the nuclear design code MASTER-3.0 (Multi-purpose Analyzer for Static and Transient Effects of Reactor) for the core design of pressurized water reactors (PWRs) based on the reactor physics technologies accumulated through joint R&D programs with leading vendors and more than ten years of experiences in nuclear design activities regarding WH, CE and FRAMATOME reactors.

Since most core analysis codes are designed for specific reactor types, they have some restrictions or inconvenience in applying them to reactors built by other vendors. Considering these aspects the MASTER-3.0 code is designed to be applicable for various types of reactors using advanced reactor physics methodologies, numerical analysis methods and modern programming techniques. It is also implemented with the standard FORTRAN-77 language on the UNIX operating system and Windows system.

MASTER-3.0 is designed to analyze the steady-state and transient core behaviors in a three-dimensional Cartesian or Hexagonal geometry based on the multi-group diffusion theory. The major calculation modules for the design application consist of depletion, steady-state flux, transient flux, pin power, pin burnup, xenon dynamics, adjoint flux, thermal hydraulics (T/H) and design specific activities including fuel management. These modules are integrated to constitute the MASTER-3.0 code package so that no extra efforts may be required for interfacing or transferring data between different calculation modules unlike other code systems.

MASTER-3.0 has several options for neutronics solution methods: the nodal expansion method (NEM), the nodal integration method (NIM), the analytic function expansion nodal method (AFEN), the non-linear nodal expansion method (NNEM) and the non-linear analytic nodal method (NANM) for Cartesian Geometry, and non-linear triangle-based polynomial expansion method (NTPEN), analytic function expansion nodal method (AFEN) and the non-linear local fine-mesh method (NLFM)

for hexagonal geometry. It performs fuel depletion using microscopic cross sections produced by CASMO-3 or HELIOS. In order to preserve quantities of heterogeneous solution within an assembly it employs the equivalence theory with the assembly discontinuity factor (ADF) as well as the simplified equivalence theory (SET) introducing the heterogeneity factor. All constants required to deplete nuclides are optionally fetched from CASMO-3 or HELIOS to keep consistency between cell and dimensional codes. Exceptionally, however, the delta macroscopic cross section concept is used for control rods and the equivalent macroscopic cross section based on SET is provided for radial reflectors. The equivalent reflector cross sections in the rectangular geometry are provided beforehand through one-dimensional modeling so that they can preserve all quantities of the response matrix elements in the heterogeneous geometry of the core-reflector interface region. This concept is extended to the L-shape reflectors by an approximation of scattering cross sections. While in the hexagonal geometry, the equivalent reflector cross sections are determined from the 2-dimensional HELIOS calculation with the actual heterogeneous core-reflector node representation.

The solution methods for the transient flux calculation module in MASTER-3.0 are identical to those of steady-state flux calculation module except for the additional solution methods regarding time-discretization. For this purpose the implicit first order Euler method combined with frequency transformation is used. The transient flux calculation module predicts the core average power, T/H related quantities and detailed fuel pin powers at rapid changes of reactor conditions such as control rod position, boron concentration, inlet mass flow, inlet temperature and pressure. Any transient calculation can be started with an arbitrary convergent steady-state reactor core solution. At each time step, the sequence of neutronics calculation followed by T/H with updating processes is gone through once, then the transient time is advanced. The time step width is automatically determined after checking the behavior of relative changes of the neutronic and T/H solutions during the time step.

MASTER-3.0 has the microscopic depletion module consistent to the spectral codes: CASMO-3 and HELIOS. It contains depletion modules for fuel, burnable poison and fission product. MASTER-3.0 uses the fully or semi weighted predictor-corrector method to minimize the errors coming from a relatively large time step. Those

methods were turned out to be very accurate for both normal and burnable poisoned fuel assemblies even with a large time step. Meanwhile, since the nodewise cross sections are generated through the flux and volume weighting with the reflective boundary condition, neglecting the large intranodal cross section gradients induced by depletion and thermal feedback leads to a deterioration of accuracy of the modern advanced nodal methods. Thus, the burnup correction model is included to take into account the spatial dependence of cross sections in solving the equivalent one-dimensional diffusion equation for the transverse integrated flux.

In MASTER-3.0 two different core T/H calculation modules are optionally available depending upon the nature of problems to solve: One is to use the fuel temperature versus linear power density table for simple T/H calculations and the other is to apply the detailed T/H codes, COBRA3-C/P and MATRA, for steady-state and transient thermal analysis of rod bundle nuclear fuel elements which is intrinsically integrated in the code. Even though the simple table might be accurate enough to estimate T/H conditions for the normal steady-state operation, COBRA3-C/P or MATRA can be used to simulate more sophisticated transient reactor conditions in view of T/H.

MASTER-3.0 calculates the local heterogeneous fuel pin power distributions in each axial segment within fuel assembly by modulation of the local homogeneous distributions based on the Method of the Successive Smoothing with Improved Analytic Solution (MSS-IAS) and heterogeneous power formfunctions. These pin power distributions are served to yield the axially integrated pin powers.

The detailed fuel pin burnup is accumulated using the pin powers in a similar fashion to the node burnup. During depletion calculation, the pin power from the previous case is weighted with that from the present one to yield the average pin power for this depletion step. Since the burnup is proportional to the power integration over time, the increase of pin burnup is directly calculated by multiplying the node average burnup increase by the pin-to-node power ratio. This change is then added to the existing pin burnup.

During reactor operation the reactor core can be placed in a slow transient state induced by load follow operations. Using the xenon dynamics module in MASTER-3.0 such a behavior can be traced by solving iteratively the time-dependent iodine/xenon and promethium/samarium differential equations with the steady-state flux solution process. The iteration process is performed until the flux shapes and their concentrations are converged.

In addition to the steady-state solution an adjoint module has been included in MASTER-3.0. This module calculates the adjoint flux with the forward steady-state solution and the kinetic parameters such as effective delayed neutron fractions, delayed neutron precursor decay constants and prompt neutron life time.

The control rod model has been implemented in MASTER-3.0 considering the heterogeneous effects of partially inserted rod. This uses the flux volume weighted cross sections to minimize cusping effects in the axial direction.

The iterative process to obtain the solution is accelerated either by the well-known Coarse-mesh rebalancing (CMR) procedure with the vectorized Gauss-Seidel method or by the Krylov Subspace method or by energy group restriction/prolongation method depending on the neutronics solution methods. As an additional acceleration procedure the asymptotic extrapolation is employed for the acceleration of the neutronics solutions for partial currents, transverse leakages and neutron fluxes.

A backward nodal method which determines absorption cross sections in order to obtain the given fluxes and eigenvalue is also implemented in MASTER-3.0. It is of use for various design and analysis applications such as axial power shape matching.

MASTER-3.0 is designed to provide the required information for SMART as well as WH- and CE-type reactors which have different design procedures and requirements each other. For example, it can produce all data required in WH-type design procedure, whereas it is able to describe a 12-finger type of control rods, depletion of Rh-detector and power-to-reaction rate coefficients w′ of detector position which are needed for the CE-type reactor design.

The goal of this report is to describe in detail the methodologies employed in each module of MASTER-3.0. The following sections start with derivation of the neutronics solution, the primary part of this code, and in turn include assembly homogenization, reflector modeling, reconstruction, depletion, burnup correction, T/H feedback, iteration strategy, kinetic parameters, modeling of control rod and detector and xenon dynamics.

2. Steady-State Neutronics Methodology

2.1 Cartesian Geometry

2.1.1 Nodal Expansion Method

The nodal expansion method (NEM) [1,2,3] starts with the multigroup neutron diffusion equation in P_1-form.

$$\nabla \cdot J_g(r) + [\Sigma_{ag}(r) + \sum_{g'>g} \Sigma_{gg'}(r)]\varphi_g(r) = \sum_{g'<g} \Sigma_{g'g}(r)\varphi_{g'}(r) + \frac{1}{k}\sum_{g'} \sum_{j} \chi^j_{pg} \nu\Sigma^j_{fg'}(r)\varphi_{g'}(r) + \chi_{ex} S^{ext}_g(r) \quad (2.1\text{-}1a)$$

$$J_g(r) + D_g(r)\nabla\varphi_g(r) = 0 \quad (2.1\text{-}1b)$$

where φ_g = neutron flux in group g,

J_g = neutron current in group g,

Σ_{ag} = absorption cross section in group g,

$\Sigma_{g'g}$ = scattering cross section from g' to g,

$\nu\Sigma^j_{fg}$ = ν-fission cross section of fissionable isotope j in group g,

k = eigenvalue,

χ^j_{pg} = prompt fission spectrum of fissionable isotope j in group g,

χ_{ex} = external source spectrum in group g,

S^{ext}_g = external source in group g.

Integrating Eq. (2.1-1) over a node volume leads to the exact nodal balance equation as follows:

$$\sum_{u=x,y,z} \frac{1}{a_u^m}\left[\left(j_{gul}^{-m} + j_{gur}^{+m}\right) - \left(j_{gul}^{+m} + j_{gur}^{-m}\right)\right] + \left(\Sigma_{ag}^m + \sum_{g'>g} \Sigma_{gg'}^m\right)\phi_g^m$$
$$= \sum_{g'<g} \Sigma_{g'g}^m \phi_{g'}^m + \frac{1}{k} \sum_{g'} \sum_{j} \chi_{pg}^j \nu\Sigma_{fg'}^{jm} \phi_{g'}^m \qquad (2.1\text{-}2a)$$

$$j_{gus}^{+m} - j_{gus}^{-m} = -D_g^m \left.\frac{\partial \psi_{gu}^m}{\partial u}\right|_S \qquad (2.1\text{-}2b)$$

where a_u^m = mesh size in the direction u (=x,y,z) of node m,

$j_{gus}^{\pm m}$ = incoming and outgoing currents in group g at the surfaces s (=l,r) of node m.

The notations are clarified in Fig. 2-1. The surface average fluxes are defined by

$$\psi_{gus}^m = \frac{1}{A_u^m} \int_0^{a_v^m} \int_0^{a_w^m} \varphi_g(r)\,dv\,dw \qquad (2.1\text{-}3)$$

where A_u^m = transverse area to u-direction.

The surface average fluxes can be expanded into a quartic polynomial

$$\psi_g^m(u) = \sum_{i=0}^{4} a_{igu} \xi_i(u) \qquad (2.1\text{-}4)$$

where $\xi_0(u) = 1$,

$\xi_1(u) = 2u - 1$,

$\xi_2(u) = 6u(1-u) - 1$,

$\xi_3(u) = 6u(1-u)(2u-1)$,

$\xi_4(u) = 6u(1-u)(5u^2 - 5u + 1)$.

The first three coefficients of the right hand side of Eq. (2.1-4) can be expressed by nodal balance equations and continuity conditions, and the third and fourth order coefficients a_{3gu} and a_{4gu} can be determined by solving the 1-dimensional equivalent diffusion equations:

$$-\frac{\partial}{\partial u}D_g^m\frac{\partial}{\partial u}\psi_{gu}^m+(\Sigma_{agu}^m+\sum_{g'>g}\Sigma_{gg'u}^m)\psi_{gu}^m$$
$$=\sum_{g'<g}\Sigma_{g'gu}^m\psi_{g'u}^m+\frac{1}{k}\sum_{g'}\sum_{j}\chi_{pg}^j\nu\Sigma_{fg'}^{jm}\psi_{g'u}^m-D_g^mL_{gu}^m \qquad (2.1\text{-}5)$$

where $L_{gu}^m=-\frac{1}{A_u^m}\int_0^{a_v^m}\int_0^{a_w^m}(\frac{d^2}{dv^2}+\frac{d^2}{dw^2})\varphi_g(r)dvdw$

To find a_{0gu} one can integrate the transverse integrated flux over the u-direction and to obtain a_{1gu} and a_{2gu} one can evaluate the transverse integrated flux at the surfaces of the node in the u-direction. The complete polynomial form of Eq. (2.1-4) can be then written as follows:

$$\psi_{gu}(u)=\phi_g\xi_0(u)+\frac{\psi_{gur}-\psi_{gul}}{2}\xi_1(u)+(\phi_g-\frac{\psi_{gur}+\psi_{gul}}{2})\xi_2(u)$$
$$+a_{3gu}\xi_3(u)+a_{4gu}\xi_4(u) \qquad (2.1\text{-}6)$$

Using the diffusion theory expression $\psi_{gus}^m=2(j_{gus}^{+m}+j_{gus}^{-m})$ and inserting Eq. (2.1-6) into Eq. (2.1-2b), the equations for the outgoing currents on the left and right surfaces are given as functions of the incoming currents and the nodal flux.

$$j_{gul}^{-m}=c_{1gu}^m(\phi_g^m+a_{4gu})+c_{2gu}^mj_{gul}^{+m}+c_{3gu}^mj_{gur}^{-m}-c_{4gu}^ma_{3gu}$$
$$j_{gur}^{+m}=c_{1gu}^m(\phi_g^m+a_{4gu})+c_{3gu}^mj_{gul}^{+m}+c_{2gu}^mj_{gur}^{-m}+c_{4gu}^ma_{3gu} \qquad (2.1\text{-}7)$$

The coefficients of the outgoing currents equations are rational functions of $D_{gu}=D_g^m/a_u$,

where D_g^m is the diffusion constant of energy group g.

$$c_{1gu} = \frac{D_{gu}}{1/6 + 2D_{gu}}, \qquad c_{2gu} = 1 - 4c_{1gu} - c_{3gu}, \tag{2.1-8}$$

$$c_{3gu} = \frac{-c_{1gu}}{3/4 + 3D_{gu}}, \qquad c_{4gu} = c_{1gu} - 6D_{gu}c_{3gu}.$$

The final form of the nodal balance equations Eq. (2.1-2a) becomes

$$\begin{aligned}
&(t_{ag}^m + \sum_{g'>g} \Sigma_{gg'}^m + \sum_{u=x,y,z} \frac{2c_{1gu}^m}{a_u^m})\phi_g^m \\
&\quad = \sum_{g'<g} \Sigma_{g'g}\phi_{g'}^m + \frac{1}{k}\sum_{g'}\sum_{j} \chi_{pg}^j \nu\Sigma_{fg'}^{jm}\phi_{g'}^m \\
&\quad + \sum_{u=x,y,z} \frac{1}{a_u^m}\left[(1 - c_{2gu}^m - c_{3gu}^m)(j_{gul}^{+m} + j_{gur}^{-m}) - 2c_{1gu}^m a_{4gu}^m\right]
\end{aligned} \tag{2.1-9}$$

and this can be solved iteratively.

According to the weighted residual method, integrating Eq. (2.1-5) with the weighting function ξ_1 or ξ_2 presented in Eq. (2.1-4) results in the following form:

$$\begin{aligned}
(60\frac{D_{gu}}{a_u} + \Sigma_g)a_{3gu} &= -\frac{5}{3}\Sigma_g a_{1gu} \\
&+ \sum_{g'<g} \Sigma_{g'g}(\frac{5}{3}a_{1g'u} + a_{3g'u}) \\
&+ \sum_{g'} (\frac{5}{3}a_{1g'u} + a_{3g'u})\frac{1}{k}\sum_{j} \chi_{pg}^j \nu\Sigma_{fg'}^j \\
&- \frac{5}{3}D_g b_{1gu}
\end{aligned} \tag{2.1-10a}$$

$$
\begin{aligned}
(140\frac{D_{gu}}{a_u}+\Sigma_g)a_{4gu} &= \frac{7}{3}\Sigma_g a_{2gu} \\
&+\sum_{g'<g}\Sigma_{g'g}(-\frac{7}{3}a_{2g'u}+a_{4g'u}) \\
&+\sum_{g'}(-\frac{7}{3}a_{2g'u}+a_{4g'u})\frac{1}{k}\sum_{j}\chi_{pg}^{j}\nu\Sigma_{fg'}^{j} \\
&+\frac{7}{3}D_g b_{2gu}
\end{aligned}
\qquad \text{(2.1-10b)}
$$

where $\Sigma_g = \Sigma_{ag} + \sum_{g'>g}\Sigma_{gg'}$,

b_{1gu} , b_{2gu} = coefficients of the transverse leakage expansion function (see Eq.(5-1)).

One can obtain the coefficients a_{3gu} and a_{4gu} with Eqs. (2.1-10a) and (2.1-10b). For the acceleration of an iterative solution, a vectorized red-black Gauss-Seidel method, a multi-level coarse-mesh rebalancing and an asymptotic extrapolation are used. These will be discussed for details later in this manual.

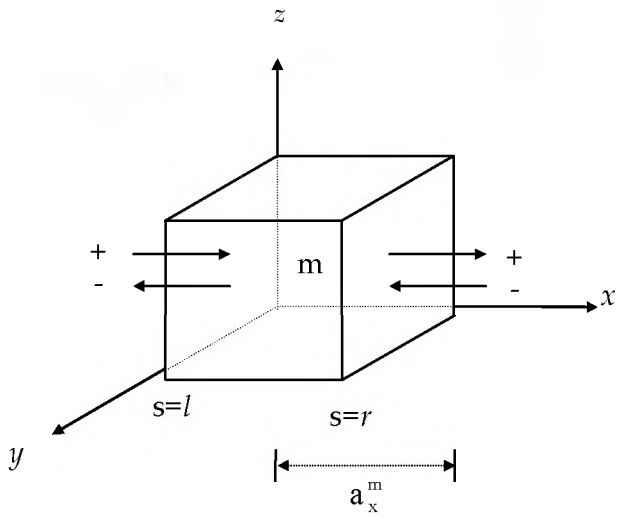

Figure 2-1 Illustration of Mesh Geometry

2.1.2 Nodal Integration Method

The Nodal Integration Method (NIM) [4] is shortly characterized by exact integration of resulting 1-dimensional equation with the transverse leakage shape approximated by a parabola. The starting point for the derivation of NIM is a set of equivalent 1-D diffusion equations.

$$\begin{aligned} D_1 \frac{d^2\psi_{1u}}{du^2} - \Sigma_{r1}\psi_{1u} + \frac{\nu\Sigma_{f2}}{k}\psi_{2u} &= D_1 L_{1u} \\ D_2 \frac{d^2\psi_{2u}}{du^2} - \Sigma_{a2}\psi_{2u} + \Sigma_{12}\psi_{1u} &= D_2 L_{2u} \end{aligned} \qquad (2.1\text{-}11)$$

where D_g = diffusion coefficient of group g,

L_{gu} = transverse leakage of group g in u-direction,

$$\Sigma_{r1} = \Sigma_{a1} + \Sigma_{12} - \frac{\nu\Sigma_{f1}}{k}.$$

The transverse leakage L_{gu} is orthogonal to the spatial direction u. The equations above can be rewritten as

$$\begin{aligned} \frac{d^2\psi_{1u}}{du^2} - c_1\psi_{1u} + c_2\psi_{2u} &= L_{1u} \\ \frac{d^2\psi_{2u}}{du^2} - c_3\psi_{2u} + c_4\psi_{1u} &= L_{2u} \quad (u = x, y, z) \end{aligned} \qquad (2.1\text{-}12)$$

where $c_1 = \frac{\Sigma_{r1}}{D_1}, c_2 = \frac{\nu\Sigma_{f2}}{D_1 k}, c_3 = \frac{\Sigma_{a2}}{D_2}, c_4 = \frac{\Sigma_{12}}{D_2}$.

This is a coupled system of ordinary, linear, inhomogeneous differential equations of second order with constant coefficients. The equations above can be solved analytically with a quadratic approximation of the one-dimensional transverse leakages

$$L_{gu} = \sum_{v=0}^{2} b_{gv}\xi_v(u) \tag{2.1-13}$$

where $\xi_0(u) = 1$,

$\xi_1(u) = 2u - 1$,

$\xi_2(u) = 6u(1-u) - 1$.

The solution can be expressed as

$$\psi_{1u} = k_1\cosh\kappa_1 u + k_2\sinh\kappa_1 u + \alpha(k_3\cos\kappa_2 u + k_4\sin\kappa_2 u) + \sum_{v=0}^{2} f_{1v}\xi_v(u) \tag{2.1-14}$$

$$\psi_{2u} = \beta(k_1\cosh\kappa_1 u + k_2\sinh\kappa_1 u) + k_3\cos\kappa_2 u + k_4\sin\kappa_2 u + \sum_{v=0}^{2} f_{2v}\xi_v(u)$$

The eigenvalues are derived from

$$\kappa_{1,2}^2 = \frac{c_1 + c_3}{2} \pm \sqrt{\left(\frac{c_1 - c_3}{2}\right)^2 + c_2 c_4} \tag{2.1-15}$$

The coupling parameters are

$$\alpha = \frac{c_2}{c_1 - \kappa_2^2}, \beta = \frac{c_4}{c_3 - \kappa_1^2}. \tag{2.1-16}$$

The solution is simplified in reflector nodes since α vanishes. The eigenvalues are as follows:

$$\kappa_1^2 = c_1, \kappa_2^2 = c_3, c_1 \neq c_3.$$

The flux continuity condition is used to determine the coefficients f_{gv} of the inhomogeneous part of the solution. The node average flux ϕ_g results from the integration of the 1-D flux solution over the total node length in u-direction.

$$\phi_g = \frac{1}{a}\int_0^a \psi_{gu}\,du \tag{2.1-17}$$

where a = node width.

The integration of Eq. (2.1-17) leads to the following matrix:

$$\begin{pmatrix} f_{10} \\ f_{20} \end{pmatrix} = \begin{pmatrix} \phi_1 \\ \phi_2 \end{pmatrix} - \begin{bmatrix} \frac{\sinh\kappa_1 a}{\kappa_1 a} & \frac{\cosh\kappa_1 a - 1}{\kappa_1 a} & \alpha\frac{\sin\kappa_2 a}{\kappa_2 a} & \alpha\frac{1-\cos\kappa_2 a}{\kappa_2 a} \\ \beta\frac{\sinh\kappa_1 a}{\kappa_1 a} & \beta\frac{\cosh\kappa_1 a - 1}{\kappa_1 a} & \frac{\sin\kappa_2 a}{\kappa_2 a} & \frac{1-\cos\kappa_2 a}{\kappa_2 a} \end{bmatrix} \begin{pmatrix} k_1 \\ k_2 \\ k_3 \\ k_4 \end{pmatrix} \tag{2.1-18}$$

The coefficients f_{g1} and f_{g2} are obtained by inserting Eq. (2.1-14) into Eq. (2.1-12) and by comparing the coefficients of the linearly independent expansion functions ξ_1 and ξ_2, respectively.

$$\begin{pmatrix} f_{1i} \\ f_{2i} \end{pmatrix} = \frac{1}{c_2 c_4 - c_1 c_3} \begin{bmatrix} c_3 & c_2 \\ c_4 & c_1 \end{bmatrix} \begin{pmatrix} b_{1i} \\ b_{2i} \end{pmatrix}, \quad (i = 1, 2). \tag{2.1-19}$$

The node boundary conditions are used to determine the integration constants k_i (i=1,..,4) and written as

$$\begin{aligned} 4j^{+}_{gul} &= \psi_g(0) - 2D_g \left.\frac{d\psi_{gu}}{du}\right|_{u=0} \\ 4j^{-}_{gur} &= \psi_g(a) + 2D_g \left.\frac{d\psi_{gu}}{du}\right|_{u=a} \end{aligned} \tag{2.1-20}$$

where j^{+}_{gul} = incoming current on the left boundary of a node,

j^{-}_{gur} = incoming current on the right boundary of a node.

The incoming currents of the node concerned are obtained using the continuity conditions. To simplify notation the incoming current vector $\mathbf{J}^{in}_{u}$ is written as

$$\mathbf{J}^{in}_{u} = \left[j^{+}_{1ul}, j^{+}_{2ul}, j^{-}_{1ur}, j^{-}_{2ur} \right]^{T} \tag{2.1-21}$$

where the superscript T denotes transposition.

In the same manner the following vectors are introduced.

$$\mathbf{\Phi} = \left[\phi_1, \phi_2, \phi_1, \phi_2 \right]^{T} \tag{2.1-22}$$

$$\mathbf{V} = 4 \left(\frac{D_1}{a}(f_{11} + 3f_{12}), -\frac{D_2}{a}(f_{21} + 3f_{22}), \frac{D_1}{a}(f_{11} - 3f_{12}), \frac{D_2}{a}(f_{21} - 3f_{22}) \right)^{T}$$

$$\mathbf{W} = \left[-f_{11} - f_{12}, -f_{21} - f_{22}, f_{11} - f_{12}, f_{21} - f_{22} \right]^{T}$$

The evaluation of the node boundary conditions then results in

$$4\mathbf{J}^{in}_{u} = \mathbf{Q}\left[k_1, k_2, k_3, k_4 \right]^{T} + \mathbf{V} + \mathbf{W} + \mathbf{\Phi} \tag{2.1-23}$$

where $\mathbf{Q}$ is a 4x4 matrix. The constants k_i are formally determined by the incoming currents, the node average fluxes and the transverse leakages. For the construction of an efficient iteration algorithm the diffusion boundary condition

$$\psi_u = 2(\mathbf{J}^{in}_{u} + \mathbf{J}^{out}_{u}) \tag{2.1-24}$$

yields

$$\mathbf{J}_u^{out} = \frac{1}{2}\mathbf{P}\left[k_1, k_2, k_3, k_4\right]^T + \frac{1}{2}(\mathbf{W} + \mathbf{\Phi} - \mathbf{J}_u^{in} \tag{2.1-25}$$

where $\mathbf{P}$ is a 4x4 matrix. By eliminating the integration constants the outgoing currents in direction u can be obtained. Denoting the fourth order unity matrix as $\mathbf{I}_4$ leads to the resulting outgoing current equation

$$\mathbf{J}_u^{out} = \frac{1}{2}(\mathbf{P}_u\mathbf{Q}_u^{-1} - \mathbf{I}_4)(4\mathbf{J}_u^{in} - \mathbf{V}_u - \mathbf{W}_u - \mathbf{\Phi} + \mathbf{J}_u^{in} - \frac{1}{2}\mathbf{V}_u . \tag{2.1-26}$$

The multiplication of matrices $\mathbf{PQ}^{-1}$ can favorably be partitioned into 2x2 submatrices $\mathbf{E}$ and $\mathbf{F}$, respectively to reveal its high degree of symmetry.

$$\mathbf{PQ}^{-1} = \begin{pmatrix} \mathbf{E} & \mathbf{F} \\ \mathbf{F} & \mathbf{E} \end{pmatrix} \tag{2.1-27}$$

The node average fluxes are solutions of the nodal balance equation in which the nodal leakage is represented by the difference between incoming and outgoing currents. If the outgoing currents are eliminated from the nodal balance equation, the node average fluxes can be calculated as functions of the incoming currents and the transverse leakages.

The corresponding nodal balance equation is written in matrix notation

$$\begin{pmatrix} \Sigma_{r1} & -\frac{\nu\Sigma_{f2}}{k} \\ -\Sigma_{21} & \Sigma_{a2} \end{pmatrix} \begin{pmatrix} \phi_1 \\ \phi_2 \end{pmatrix} = \left[\mathbf{I}_2 \quad \mathbf{I}_2\right] \sum_{u=x,y,z} \frac{1}{a_u}(\mathbf{J}_u^{in} - \mathbf{J}_u^{out}) \tag{2.1-28}$$

After the outgoing currents $\mathbf{J}_u^{out}$ are eliminated in this equation and some mathematical manipulations are performed, the nodal balance equation for the determination of the node average flux can be obtained :

$$\begin{bmatrix} \Sigma_{r1} - H_{11} & -\frac{\nu\Sigma_{f2}}{k} - H_{12} \\ -\Sigma_{21} - H_{21} & \Sigma_{a2} - H_{22} \end{bmatrix} \begin{bmatrix} \phi_1 \\ \phi_2 \end{bmatrix} = [\mathbf{I}_2 \quad \mathbf{I}_2] \sum_{u=x,y,z} \frac{1}{2a_u} \left[(\mathbf{P}_u \mathbf{Q}_u^{-1} - \mathbf{I}_4)(\mathbf{V}_u + \mathbf{W}_u - 4\mathbf{J}_u^{in}) + \mathbf{V}_u \right] \tag{2.1-29}$$

where $H_{11} = \sum_{u=x,y,z} \frac{1}{a_u}(E_{u11} + F_{u11} - 1)$, $H_{12} = \sum_{u=x,y,z} \frac{1}{a_u}(E_{u12} + F_{u12})$,

$H_{21} = \sum_{u=x,y,z} \frac{1}{a_u}(E_{u21} + F_{u21})$, $H_{22} = \sum_{u=x,y,z} \frac{1}{a_u}(E_{u22} + F_{u22} - 1)$.

2.1.3 AFEN/NEM Hybrid Method

Analytic Function Expansion Nodal Method (AFEN) [5,6] directly solves the multi-dimensional diffusion equation instead of the transverse-averaged one-dimensional one. It is based on analytic basis functions satisfying the diffusion equation at any points of the node. The flux expansion consisting of basis functions includes non-separable cross terms which are coupled to other spatial directions. AFEN determines all nodal unknowns such as node average, surface average and corner-point fluxes by means of the nodal coupling equations which comprise the nodal balance equation for node average flux, the interface current continuity condition for surface fluxes and Corner-Point Balance Method (CPB) [7] or Method of Successive Smoothing (MSS) [8] for corner fluxes. In the AFEN/NEM hybrid method [9], NEM is used for the axial direction where the neutronic coupling is relatively weak compared to the radial direction. For the application of coarse-mesh rebalancing (CMR) acceleration scheme [9] , a response matrix formulation of the AFEN/NEM hybrid method is derived.

In order to solve the two-group two-dimensional diffusion equation, λ_g^n is defined as

the eigenvalue of matrix $(\mathbf{D}^n)^{-1}[\mathbf{\Sigma}^n - (1/k_{eff})\ \boldsymbol{\nu}\mathbf{\Sigma}_f^n]$ and $\mathbf{R}^n$ as the 2x2 matrix with columns of the corresponding eigenvectors. In addition, ξ is introduced as:

$$\xi^n(x,y) = (\mathbf{R}^n)^{-1}\,\boldsymbol{\Phi}^n(x,y) \tag{2.1-30}$$

which satisfies the partial differential equation:

$$\nabla^2\xi_g^n(x,y) - \lambda_g^n\xi_g^n(x,y) = 0 \tag{2.1-31}$$

The general solution of the above equation can be expressed in the following form:

$$\xi_g^n(x,y) = \sum_{i=0}^{\infty}\{A_{gi}^n SN\kappa_g^n(\alpha_{gxi}^n x + \alpha_{gyi}^n y) + B_{gi}^n CS\kappa_g^n(\alpha_{gxi}^n x + \alpha_{gyi}^n y)\} \tag{2.1-32}$$

where $\kappa_g^n = \sqrt{|\lambda_g^n|}$,

$$(\alpha_{gxi}^n)^2 + (\alpha_{gyi}^n)^2 = 1,$$

$$SN\kappa_g^n(\alpha_{gxi}^n x + \alpha_{gyi}^n y) = \begin{cases}\sinh\kappa_g^n(\alpha_{gxi}^n x + \alpha_{gyi}^n y) & \lambda_g^n > 0\\ \sin\kappa_g^n(\alpha_{gxi}^n x + \alpha_{gyi}^n y) & \lambda_g^n < 0\end{cases},$$

$$CS\kappa_g^n(\alpha_{gxi}^n x + \alpha_{gyi}^n y) = \begin{cases}\cosh\kappa_g^n(\alpha_{gxi}^n x + \alpha_{gyi}^n y) & \lambda_g^n > 0\\ \cos\kappa_g^n(\alpha_{gxi}^n x + \alpha_{gyi}^n y) & \lambda_g^n < 0\end{cases}.$$

The sets of $(\alpha_{gxi}^n, \alpha_{gyi}^n)$ are chosen as (1, 0), (0, 1), ($\sqrt{2}/2$, $\sqrt{2}/2$) and (-$\sqrt{2}/2$, $\sqrt{2}/2$), which are distributed 45 degrees apart on a unit circle. Thus, the intranodal flux expansion consists of a set of eight basis functions:

$$\xi(x,y) = C_g^n + A_{g1}^n SN\kappa_g^n x + A_{g2}^n CS\kappa_g^n x + A_{g3}^n SN\kappa_g^n y + A_{g4}^n CS\kappa_g^n y$$
$$+ B_{g1}^n SN\frac{\sqrt{2}}{2}\kappa_g^n x SN\frac{\sqrt{2}}{2}\kappa_g^n y + B_{g2}^n SN\frac{\sqrt{2}}{2}\kappa_g^n x CS\frac{\sqrt{2}}{2}\kappa_g^n y \qquad (2.1\text{-}33)$$
$$+ B_{g3}^n CS\frac{\sqrt{2}}{2}\kappa_g^n x SN\frac{\sqrt{2}}{2}\kappa_g^n y + B_{g4}^n CS\frac{\sqrt{2}}{2}\kappa_g^n x CS\frac{\sqrt{2}}{2}\kappa_g^n y$$

In the response matrix formulation of this method, however, interface partial currents are used as the nodal unknowns instead of corresponding surface fluxes. Once all the coefficients in the flux expansion are expressed in terms of the nodal unknowns for the response matrix formulation, we build as many solvable nodal coupling equations as the number of these unknowns to be determined.

The first set of nodal coupling equations to be solved for the node-average flux can be obtained by integrating Eq. (2.1-2a) over a node volume:

$$\Sigma_{rg}\phi_g + \sum_{d=x,y,z}\frac{1}{a_d}\left[(j_{gdr}^{out} - j_{gdr}^{in}) + (j_{gdl}^{out} - j_{gdl}^{in})\right] = \sum_{g'<g}\Sigma_{g'g}\phi_{g'} + \frac{1}{k_{eff}}\sum_{g'}\chi_g\nu\Sigma_{fg'}\phi_{g'} \qquad (2.1\text{-}34)$$

The second set of nodal coupling equations for the surface average partial currents are derived by applying continuity condition of the net neutron currents across the node interface and the diffusion approximation relating partial currents with net currents and surface fluxes. The node outgoing partial current can then be expressed in terms of incoming partial currents, node average fluxes and corner fluxes. For example, the interface partial currents in x-direction on the right-hand side as illustrated in Fig. 2-2 is

$$\mathbf{J}_r^{out} = \frac{\mathbf{P}_1 + \mathbf{P}_2}{2}\mathbf{J}_r^{in} + \frac{\mathbf{P}_1 - \mathbf{P}_2}{2}\mathbf{J}_l^{in} + \frac{1}{4}(\mathbf{1} - \mathbf{P}_1)\overline{\boldsymbol{\Phi}} + \frac{\mathbf{P}_3 + \mathbf{P}_4}{2}\delta\boldsymbol{\Phi}_t + \frac{\mathbf{P}_3 - \mathbf{P}_4}{2}\delta\boldsymbol{\Phi}_t \qquad (2.1\text{-}35)$$

where $\mathbf{J}_s^{out}$ = outgoing partial current at surface s,

$\mathbf{J}_s^{in}$ = incoming partial current at surface s,

$\overline{\boldsymbol{\Phi}}$ = node average flux,

$\delta\Phi_s$ = difference between averaged corner flux and corner flux determined at each adjacent node (s = l, r),

$\mathbf{P}_i$ = coupling coefficient,

$\mathbf{1}$ = unity matrix,

subscript r, l = right and left surfaces.

In the above equation, the coupling coefficients $\mathbf{P}_i$'s are constant matrices whose elements depend on k_{eff} and the group constants of the node. The MSS or CPB can be used to solve the corner fluxes, which form the third set of nodal coupling equations. This will be described in details in Section 8.

The axial intranodal distribution in this method is determined by solving the transverse-integrated one-dimensional equivalent diffusion equation in the axial direction by the nodal expansion method (NEM), since the spatial coupling in the axial direction is relatively weak when compared to that for the radial direction.

$$-\frac{\partial}{\partial z}D_g^m\frac{\partial}{\partial z}\psi_g^m(z)+(\Sigma_{ag}^m+\sum_{g'>g}\Sigma_{gg'}^m)\psi_g^m(z)$$
$$=\sum_{g'<g}\Sigma_{g'g}^m\psi_{g'}^m(z)+\frac{1}{k}\sum_{g'}\sum_j\chi_{pg}^j\nu\Sigma_{fg'}^{jm}\psi_{g'}^m(z)-D_g^mL_g^m(z) \qquad (2.1\text{-}36)$$

The term $-D_gL_g(z)$ in Eq. (2.1-36) is the transverse leakage. The surface average flux $\psi_g(z)$ can be expanded into a quartic polynomial with orthogonal functions (see Eq. (2.1-4)). The outgoing partial currents on the left and right surfaces of a node in the axial direction are given by Eq. (2.1-7).

2.1.4 Non-linear Nodal Expansion Method

In the non-linear nodal expansion method (NNEM) [10], both the coarse-mesh finite difference (CMFD) method and the two-node NEM method are used for the solution of the multi-group diffusion equation. The node current of the CMFD method is given as follows:

$$J_{gu}^{m\pm} = \mp \tilde{D}_{gu}^{m\pm} \left(\phi_g^{m\pm1} - \phi_g^{m} \right) \tag{2.1-37}$$

where $\tilde{D}_{gu}^{m\pm} = \dfrac{2\, D_g^{m\pm1}\, D_g^{m}}{D_g^{m\pm1}\, a_{u,m} + D_g^{m}\, a_{u,m\pm1}}$.

The assumption of linear flux variation is not accurate for the large node size. Thus this method involves iterations between solutions of the CMFD problem and the two-node NEM problems. The CMFD problem incorporates the global coupling of the nodes while the two-node problems incorporates local higher order coupling. The method is nonlinear because the coefficient matrix for the CMFD problem contains the nodal coupling coefficients which need to be updated by the two-node calculations during the iteration.

In the two-node NEM calculation, the interface current is obtained by solving the NEM equations for the two-node problem in which the flux solution of the previous CMFD problem is used as the boundary condition. The two-node problem calculation is performed for every interface of all nodes and all directions to provide an improved estimate of the net current. The interface current is then used to determine a corrective nodal coupling coefficient, $\hat{D}_{gu}^{m+}$, such that the following expression can be reproduced for the NEM based interface current.

$$J_{gu}^{m\pm} = \mp \tilde{D}_{gu}^{m\pm} \left(\phi_g^{m\pm1} - \phi_g^{m} \right) \mp \hat{D}_{gu}^{m+} \left(\phi_g^{m\pm1} + \phi_g^{m} \right) \tag{2.1-38}$$

The next CMFD problem is formulated using the above relation for the current. The second term of RHS of Eq. (2.1-38) can be regarded as a correction term which corrects the error of the linear flux used to obtain the first term.

The two-node problem produces 8 unknowns per energy group which can be solved with 8 conditions: two nodal balance equations, one current continuity condition, one flux continuity condition and four moment equations. The definition and derivation of NEM are the same as in Section 2.1.1.

2.1.5 Non-linear Analytic Nodal Method

The non-linear nodal analytic method (NANM) [11] is basically the same as the NNEM described in the preceding section except for the main kernel to update the interface current. For correction of the interface current, it uses the analytic nodal method (ANM) instead of NEM.

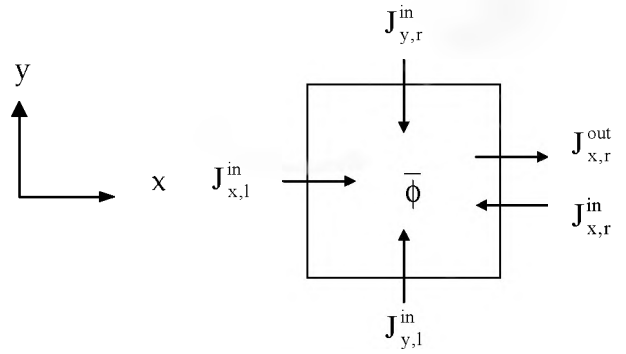

Figure 2-2 Indices of Partial Currents and Node Average Flux in a Rectangular Node

2.2 Hexagonal Geometry

2.2.1 AFEN/NEM Hybrid Method

The AFEN method [12] directly solves the multi-dimensional diffusion equation instead of the transverse-integrated one-dimensional diffusion equations by expanding the solution into non-separable analytic basis functions, which satisfy the diffusion equation at any points of the node. The flux expansion consisting of basis functions includes non-separable cross terms which are coupled to other spatial directions. The AFEN method determines all nodal unknowns such as node average, surface average and corner-point flux by means of the nodal coupling equations which comprise the nodal balance equation and the interface current continuity condition. In the AFEN/NEM hybrid method [13], NEM is used for the axial direction where the neutronic coupling is relatively weak compared to the radial direction. For the application of coarse-mesh rebalancing (CMR) acceleration scheme, a response matrix formulation of the AFEN/NEM hybrid method is derived.

AFEN for two-dimensional geometry is based on decoupling the multigroup diffusion equations for a node n into the "mode-group" partial differential equations

$$\nabla^2 \xi_g^n(x,y) - \lambda_g^n \xi_g^n(x,y) = 0 \qquad (2.2\text{-}1)$$

by defining $\xi^n(x,y) = (\mathbf{R}^n)^{-1}\phi^n(x,y)$. Here, λ_g^n 's are the eigenvalues of matrix $(\mathbf{D}^n)^{-1}[\mathbf{\Sigma}^n - (1/k_{eff})\ \boldsymbol{\nu}\boldsymbol{\Sigma}_f^n]$ and $\mathbf{R}^n$ is the matrix with columns of the corresponding eigenvectors. The general solution of the Eq. (2.2-1) can be expressed as:

$$\xi_g^n(x,y) = \sum_{i=0}^{\infty} \{A_{gi}^n SN\kappa_g^n(\alpha_{gxi}^n x + \alpha_{gyi}^n y) + B_{gi}^n CS\kappa_g^n(\alpha_{gxi}^n x + \alpha_{gyi}^n y)\} \qquad (2.2\text{-}2)$$

where $\kappa_g^n = \sqrt{|\lambda_g^n|}$,

$$(\alpha^n_{gxi})^2 + (\alpha^n_{gyi})^2 = 1,$$

$$SN\kappa^n_g(\alpha^n_{gxi}x + \alpha^n_{gyi}y) = \begin{cases} \sinh \kappa^n_g(\alpha^n_{gxi}x + \alpha^n_{gyi}y) & \lambda^n_g > 0 \\ \sin \kappa^n_g(\alpha^n_{gxi}x + \alpha^n_{gyi}y) & \lambda^n_g < 0 \end{cases},$$

$$CS\kappa^n_g(\alpha^n_{gxi}x + \alpha^n_{gyi}y) = \begin{cases} \cosh \kappa^n_g(\alpha^n_{gxi}x + \alpha^n_{gyi}y) & \lambda^n_g > 0 \\ \cos \kappa^n_g(\alpha^n_{gxi}x + \alpha^n_{gyi}y) & \lambda^n_g < 0 \end{cases}.$$

In the regular hexagonal node the AFEN method adopts one node-average flux, six interface fluxes, and six corner fluxes per group as the nodal unknowns and expands the intranodal flux distribution in the node into twelve analytic basis functions and one additional constant term. The sets of $(\alpha^n_{gxi}, \alpha^n_{gyi})$ in Eq. (2.2-1) are chosen with the same constraints applied to the rectangular geometry. They are (1, 0), (0, 1), ($\sqrt{3}$/2, 1/2), (-$\sqrt{3}$/2, 1/2), (1/2, $\sqrt{3}$/2) and (1/2, -$\sqrt{3}$/2), which are the coordinates evenly distributed 30 degrees apart on a unit circle. Introducing three Cartesian coordinate systems, (x,y), (u,v) and (p,q) for the convenience of handling the hexagonal node, the intranodal flux distribution of the node is expressed as:

$$\begin{aligned} \xi^n_g(x,y) = C_g &+ A^x_{g1}SN\kappa^n_g x + B^x_{g1}CS\kappa^n_g x + A^x_{g2}SN\kappa^n_g y + B^x_{g2}CS\kappa^n_g y \\ &+ A^p_{g1}SN\kappa^n_g p + B^p_{g1}CS\kappa^n_g p + A^p_{g2}SN\kappa^n_g q + B^p_{g2}CS\kappa^n_g q \\ &+ A^u_{g1}SN\kappa^n_g u + B^u_{g1}CS\kappa^n_g u + A^u_{g2}SN\kappa^n_g v + B^u_{g2}CS\kappa^n_g v \end{aligned} \qquad (2.2\text{-}3)$$

where $u = -\frac{1}{2}x - \frac{\sqrt{3}}{2}y$, $v = \frac{\sqrt{3}}{2}x - \frac{1}{2}y$, $p = -\frac{1}{2}x + \frac{\sqrt{3}}{2}y$, $q = -\frac{\sqrt{3}}{2}x - \frac{1}{2}y$.

In the response matrix formulation of this method [13], however, interface partial currents are used as the nodal unknowns instead of corresponding surface fluxes. Once all the coefficients in the flux expansion Eq. (2.2-3) are expressed in terms of the nodal unknowns for the response matrix formulation, we build as many solvable nodal coupling equations as the number of these unknowns to be determined. The first set of nodal coupling equations to be solved for the node-average flux can be obtained by integrating Eq.

(2.1-2a) over a node volume. The second set of nodal coupling equations for the surface average partial currents are derived by applying continuity condition of the net neutron currents across the node interface and the diffusion approximation relating partial currents with net currents and surface fluxes. The node outgoing partial current can then be expressed in terms of incoming partial currents, node average fluxes and corner fluxes. For example, the interface partial currents in x-direction on the right-hand side as illustrated in Fig. 2-3 is

$$\begin{aligned}\mathbf{J}^{out}_{x,r} = & \frac{\mathbf{P}_1+\mathbf{P}_2}{2}\mathbf{J}^{in}_{x,r} + \frac{\mathbf{P}_1-\mathbf{P}_2}{2}\mathbf{J}^{in}_{x,l} \\ & + (\mathbf{P}_3+\mathbf{P}_4)\frac{\mathbf{J}^{in}_{u,l}+\mathbf{J}^{in}_{p,l}}{2} + (\mathbf{P}_3-\mathbf{P}_4)\frac{\mathbf{J}^{in}_{u,r}+\mathbf{J}^{in}_{p,r}}{2} \\ & + (\mathbf{P}_5+\mathbf{P}_6)\frac{\boldsymbol{\Phi}_{u,r}+\boldsymbol{\Phi}_{p,l}}{2} + (\mathbf{P}_5-\mathbf{P}_6)\frac{\boldsymbol{\Phi}_{u,l}+\boldsymbol{\Phi}_{p,r}}{2} \\ & + \mathbf{P}_7\frac{\boldsymbol{\Phi}_{x,l}+\boldsymbol{\Phi}_{x,r}}{2} + \frac{1}{4}(\mathbf{I}+\mathbf{P}_1+2\mathbf{P}_3+8\mathbf{P}_5+4\mathbf{P}_7)\,\overline{\boldsymbol{\Phi}}\end{aligned} \tag{2.2-4}$$

where $\mathbf{J}^{out}_{d,s}$ = outgoing partial current vector in d- direction at surface s,

$\mathbf{J}^{in}_{d,s}$ = incoming partial current vector in d- direction at surface s,

$\boldsymbol{\Phi}_{d,s}$ = corner flux vector in d-direction at surface s,

$\overline{\boldsymbol{\Phi}}$ = node average flux vector,

$\mathbf{P}_i$ = coupling coefficient matrix.

In the above equation, the coupling coefficients are constant matrices whose elements depend on k_{eff} and the group constants of the node. By applying the corner point balance (CPB) scheme for the corner flux evaluation in hexagonal node, the set of nodal coupling equations for the corner-point fluxes can be derived in terms of surface average fluxes and node average fluxes. It forms the third set of nodal coupling equations and it will be described in details in Section 8.2.2.

The axial intranodal distribution is determined by solving the transverse-integrated one-

dimensional equivalent diffusion equation in the axial direction by the nodal expansion method (NEM). The definition and derivation of NEM are the same as in Section 2.1.3.

2.2.2 Non-linear Local Fine-mesh Method

The objective of the two-node problem to be solved for the application of the nonlinear iteration technique is to find the surface-averaged current at the interface of the two nodes, given the group constants, k_{eff}, current profiles at the transverse surfaces, and node average fluxes. To accomplish the objective, the intra-nodal flux distribution satisfying the constraint on the node average fluxes should be determined first. The intranodal flux distribution within the two hexagons can be represented in terms of mesh-averaged fluxes if the finite difference scheme is used. [14]

Suppose that a hexagon is divided into N thin trapezoids as shown in Fig. 2-4. The mesh spacing is rather desirable, in the aspect of computational efficiency, to have tightly spaced meshes only near the interface of the two hexagons since the current at the interface is the one to be evaluated with sufficient accuracy. For the i-th trapezoid, a mesh-averaged flux (ϕ_i) and surface-averaged normal neutron currents (J_i^R, J_i^L, J_i^T, J_i^B) can be defined. Then the neutron balance equation in a energy group is given as:

$$J_i^R h_{i+1} - J_i^L h_i + \Sigma \phi_i V_i = -(J_i^T - J_i^B) l_i \tag{2.2-5}$$

where J_i^S (with the superscript S being L, R, B, and T) and ϕ_i are two element vectors, h_i, l_i, and V_i are the height at the left side, the length of the top (and bottom) side and the volume of mesh i, respectively, and Σ is a 2x2 matrix consisting of two group constants as:

$$\Sigma \equiv \begin{bmatrix} \Sigma_{r1} - \lambda\nu\Sigma_{f1} & -\lambda\nu\Sigma_{f2} \\ -\Sigma_{12} & \Sigma_{r2} \end{bmatrix}, \quad \lambda = \frac{1}{k_{eff}} \tag{2.2-6}$$

By using the finite difference approximation, the currents at the left and right boundaries of a node can be obtained in a conventional way. The neutron balance equation given by Eq. (2.2-7) holds for all the interior meshes except the two meshes located at the left

and the right boundaries of the two-node problem in which no boundary condition is given. Thus there are only 2*(N-1) balance equations available per group for the 2N unknowns. The additional two equations needed for a unique solution come from the constraints on the node average flux.

$$\frac{1}{V_H}\sum_{i=1}^{N}\phi_i V_i=\bar{\phi}_L\,,\qquad \frac{1}{V_H}\sum_{i=N+1}^{2N}\phi_i V_i=\bar{\phi}_R \tag{2.2-9}$$

where V_H is the volume of the hexagon.

The linear system consisting of Eq. (2.2-5) for meshes 2 through 2N-1 and Eq. (2.2-9) is primarily a block tridiagonal system with nonzero off-diagonal elements mostly at the last two rows. The left-hand side of the linear system is shown schematically below:

$$A\phi=\begin{bmatrix} d_2 & \alpha_3 & & & & & & \\ \alpha_3 & \ddots & \ddots & & & & & \\ & \ddots & d_n & \alpha_{n+1} & & & & \\ & & \alpha_{n+1} & d_{n+1} & \ddots & & & \\ & & & \ddots & \ddots & \alpha_{2n-1} & & \\ & & & & \alpha_{2n-1} & d_{2n-1} & \alpha_{2n} & \\ & & & \beta_{n+1} & \cdots & \beta_{2n-1} & \beta_{2n} & \\ \beta_2 & \cdots & \beta_n & & & & & \end{bmatrix}\begin{bmatrix} \alpha_2\phi_2 \\ \vdots \\ \\ \alpha_n\phi_n \\ \\ \alpha_{n+1}\phi_{n+1} \\ \vdots \\ \\ \alpha_{2n-1}\phi_{2n-1} \\ \alpha_{2n}\phi_{2n} \\ \\ \beta_1\phi_1 \end{bmatrix} \tag{2.2-10}$$

Note that the basic element in the coefficient matrix is a 2x2 matrix.

It can be solved easily by using the Gauss Elimination technique because of the nearly tridiagonal structure. The fill-in problem will occur only at the last column and the last row during the Gauss Elimination and thus no significant computational burden will be encountered.

To obtain the currents at the external boundaries in which an albedo type of boundary condition is given, a set of one-node problems needs to be solved instead of the two-node problems. Similarly to the two-node problem, the one-dimensional one-node problem can

be solved by the fine-mesh finite difference method (FDM).

The accuracy of a transverse-integrated method is limited by the accuracy of the profile of transverse current approximated by a low order function as long as the one-dimensional problem is solved with sufficient accuracy. In order to obtain better profiles of transverse currents, two methods were applied. The first one is a simple vector addition scheme and is applied to the interior nodal interface. The other one is a more sophisticated method which utilizes a precalculated two-dimensional fine mesh solution for a hexagon located at the boundary when determining the current profile at an external surface as a superposition of the currents induced from the current sources placed at the other five surfaces. This method is used for the boundary surfaces in which the transverse leakage shape varies more drastically.

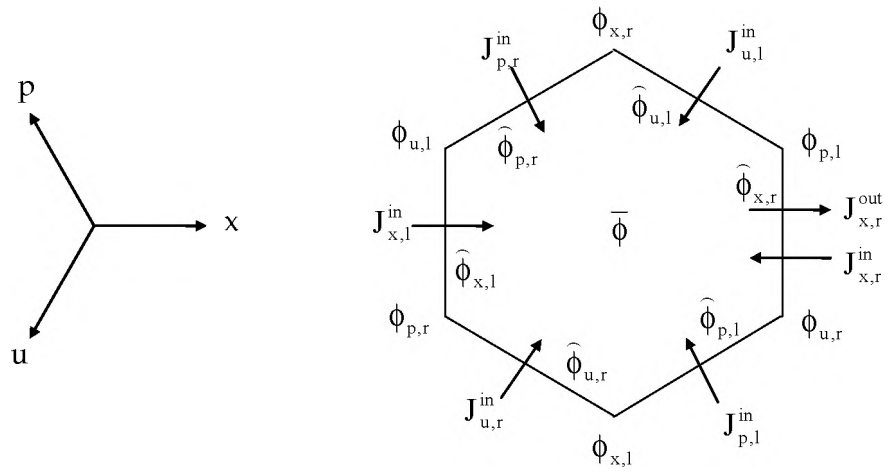

Figure 2-3 Indices of Currents and Fluxes in Hexagonal Geometry

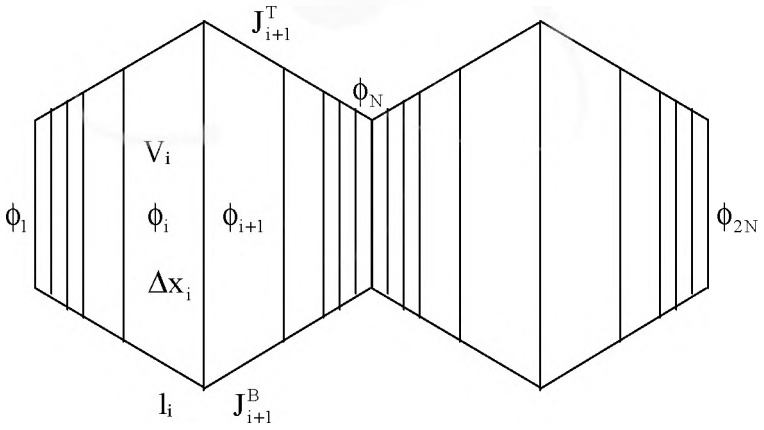

Figure 2-4 Fine Mesh Structure of a Two Hexagonal Node Problem

2.2.3 Non-linear Triangle-based Polynomial Expansion Nodal Method

In contrast with the non-linear local fine-mesh method that is based on two-node problem, the non-linear triangle-based polynomial expansion nodal (NTPEN) method [15,16] is based on one-node problem to find the outgoing partial currents and node average flux, given the group constants, k_{eff}, incoming partial currents, corner point fluxes. Instead of surface-based sweep of two-node problem, one-node problem sweeps the problem domain from node-base.

The non-linear triangle-based polynomial expansion nodal (NTPEN) method is a variation of the higher order polynomial expansion nodal (HOPEN) method [17] that solves the multi-group neutron diffusion equation in the hexagonal-z geometry. In contrast with the HOPEN method that represents the intranodal solution in a three-dimensional domain with a truncated polynomial expansion, only two-dimensional intranodal expansion is considered in the TPEN method for a triangular domain. The axial dependence of the intranodal flux is incorporated separately and it is determined by the nodal expansion method (NEM). For the consistency of node geometry of the other methods which are based on hexagon, TPEN solver is coded to solve one hexagonal node which is composed of 6 triangular nodes directly by Gauss elimination scheme.

Fig. 2-5 displays a triangular node and the nodal unknowns defined in the TPEN method. The nine unknowns are the volume average flux, first-order x- and y-moments, three surface average fluxes and three corner fluxes, respectively. A truncated polynomial expansion of the intranodal flux in the two-dimensional domain that is consistent with the nine unknowns can be set as:

$$\phi_g^m(x,y) = c_{g0}^m + a_{gx}^m x + a_{gy}^m y + b_{gx}^m x^2 + b_{gu}^m u^2 + b_{gp}^m p^2 + c_{gx}^m x^3 + c_{gu}^m u^3 + c_{gp}^m p^3 . \qquad (2.2\text{-}11)$$

Once the polynomial approximation of the intranodal flux distribution is made, the nine unknowns are uniquely determined from nine constraints, one nodal balance equation, two weighted residual equations, three surface current conditions and three corner point leakage conditions. For these equations, the following two-dimensional neutron diffusion equation

can be constructed:

$$-D_g^m\left(\frac{\partial^2}{\partial x^2}+\frac{\partial^2}{\partial y^2}\right)\phi_g^m(x,y)+\Sigma_{rg}^m\phi_g^m(x,y)$$
$$=\frac{\chi_g}{k_{eff}}\sum_{g'}\nu\Sigma_{fg'}^m\phi_{g'}^m(x,y)+\sum_{g'}\Sigma_{sgg'}^m\phi_{g'}^m(x,y)+S_{gz}^m(x,y), \qquad (2.2\text{-}12)$$

where $S_{gz}^m(x,y)$ is axial source distribution which comes from axial leakage.

The nine constraints to determine the nine nodal unknowns can be derived as the following form from the definitions of each constraint:

Nodal Balance Equation:

$$80\frac{D_g^m}{h^2}+\Sigma_{rg}^m\bar{\phi}_g^m=\frac{\chi_g}{k_{eff}}\sum_{g'}\nu\Sigma_{fg'}^m\bar{\phi}_{g'}^m+\sum_{g'}\Sigma_{sgg'}^m\bar{\phi}_{g'}^m+\bar{S}_{gz}^m$$
$$+32\frac{D_g^m}{h^2}\left(\bar{\phi}_{gx}^m+\bar{\phi}_{gu}^m+\bar{\phi}_{gp}^m\right)-\frac{16}{3}\frac{D_g^m}{h^2}\left(\phi_{gx}^m+\phi_{gu}^m+\phi_{gp}^m\right). \qquad (2.2\text{-}13)$$

Weighted residual equation using $w(x,y)=x$:

$$80\frac{D_g^m}{h^2}+\Sigma_{rg}^m\tilde{\phi}_{gx}^m=\frac{\chi_g}{k_{eff}}\sum_{g'}\nu\Sigma_{fg'}^m\tilde{\phi}_{g'x}^m+\sum_{g'}\Sigma_{sgg'}^m\tilde{\phi}_{g'x}^m+\tilde{S}_{gzx}^m$$
$$+\frac{8}{3}\frac{D_g^m}{h^2}\left(2\bar{\phi}_{gx}^m-\bar{\phi}_{gu}^m-\bar{\phi}_{gp}^m\right)-\frac{8}{9}\frac{D_g^m}{h^2}\left(2\phi_{gx}^m-\phi_{gu}^m-\phi_{gp}^m\right). \qquad (2.2\text{-}14)$$

Weighted residual equation using $w(x,y)=y$:

$$80\frac{D_g^m}{h^2}+\Sigma_{rg}^m\tilde{\phi}_{gy}^m=\frac{\chi_g}{k_{eff}}\sum_{g'}\nu\Sigma_{fg'}^m\tilde{\phi}_{g'y}^m+\sum_{g'}\Sigma_{sgg'}^m\tilde{\phi}_{g'y}^m+\tilde{S}_{gzy}^m$$
$$-8\frac{D_g^m}{h^2}\left(\bar{\phi}_{gu}^m-\bar{\phi}_{gp}^m\right)+\frac{8}{3}\frac{D_g^m}{h^2}\left(\phi_{gu}^m-\phi_{gp}^m\right). \qquad (2.2\text{-}15)$$

Net current condition at boundary surfaces:

$$\bar{J}^{m}_{gx} = \frac{\sqrt{3}}{3}\frac{D^{m}_{g}}{h}\left\{2\phi^{m}_{gx} + \phi^{m}_{gu} + \phi^{m}_{gp} - 24\bar{\phi}^{m}_{gx} + 20\bar{\phi}^{m}_{g} + 120\tilde{\phi}^{m}_{gx}\right\}. \tag{2.2-16}$$

Net leakage condition at corner points:

$$L^{m}_{gx} = 4\sqrt{3}\frac{D^{m}_{g}}{h}\left\{-\phi_{gc} + \bar{\phi}^{m}_{gx} - 15\tilde{\phi}^{m}_{gx}\right\} \ . \tag{2.2-17}$$

Fig. 2-6 shows 6 triangular nodes in a hexagonal node. For this hexagonal node, 6 incoming partial currents and 6 corner point fluxes are specified as the boundary conditions. Applying the TPEN to the six triangles yields 31 unknowns, 6 triangle node average fluxes, 6 x-moments, 6 y-moments, 6 inner surface fluxes, 6 outgoing partial currents and 1 center point flux. And Eqs. (2.2-13) through (2.2-17) are used to determine these unknowns. The resulting linear system to determine these unknowns is expressed as:

$$\begin{bmatrix} \mathbf{C}_0 & \mathbf{0} & \mathbf{0} & -32\mathbf{C}_1\mathbf{I}_0 & -64\mathbf{C}_1 & 16/3\,\mathbf{C}_1 \\ \mathbf{0} & \mathbf{C}_0 & \mathbf{0} & 8/3\,\mathbf{C}_1\mathbf{I}_0 & -32/3\,\mathbf{C}_1 & 16/9\,\mathbf{C}_1 \\ \mathbf{0} & \mathbf{0} & \mathbf{C}_0 & -8\mathbf{C}_1\mathbf{I}_1 & \mathbf{0} & \mathbf{0} \\ 20\mathbf{I}_2 & -60\mathbf{I}_2 & 60\mathbf{I}_3 & -48\mathbf{I} & \mathbf{0} & 2\mathbf{I} \\ 20\mathbf{I} & 120\mathbf{I} & \mathbf{0} & \mathbf{0} & -48\mathbf{I}-\boldsymbol{\gamma} & 2\mathbf{I} \\ \mathbf{0} & -15\mathbf{I}_4 & \mathbf{0} & \mathbf{0} & 2\mathbf{I}_4 & -6\mathbf{i} \end{bmatrix} \begin{bmatrix} \bar{\boldsymbol{\varphi}} \\ \tilde{\boldsymbol{\varphi}}_x \\ \tilde{\boldsymbol{\varphi}}_y \\ \boldsymbol{\varphi}_s \\ \mathbf{j}_o \\ \boldsymbol{\varphi}_p \end{bmatrix} = \begin{bmatrix} \bar{\mathbf{S}}_a \\ \tilde{\mathbf{S}}_x \\ \tilde{\mathbf{S}}_y \\ \mathbf{S}_s \\ \mathbf{S}_j \\ \mathbf{S}_p \end{bmatrix} \tag{2.2-18}$$

where

$$\mathbf{C}_0 = \text{diag.}\left[\mathbf{a}_0\ \mathbf{a}_0\ \mathbf{a}_0\ \mathbf{a}_0\ \mathbf{a}_0\ \mathbf{a}_0\right] + 80\mathbf{C}_1,\ \mathbf{C}_1 = \text{diag.}\left[\mathbf{a}_1\ \mathbf{a}_1\ \mathbf{a}_1\ \mathbf{a}_1\ \mathbf{a}_1\ \mathbf{a}_1\right],$$

$$\boldsymbol{\gamma} = \text{diag.}\left[\mathbf{a}_2\ \mathbf{a}_2\ \mathbf{a}_2\ \mathbf{a}_2\ \mathbf{a}_2\ \mathbf{a}_2\right],\ \mathbf{I} = \text{dia.}\left[\mathbf{i}\ \mathbf{i}\ \mathbf{i}\ \mathbf{i}\ \mathbf{i}\ \mathbf{i}\right],\ \mathbf{I}_0 = \begin{bmatrix} \mathbf{i} & \mathbf{i} & & & & \\ & \mathbf{i} & \mathbf{i} & & & \\ & & \mathbf{i} & \mathbf{i} & & \\ & & & \mathbf{i} & \mathbf{i} & \\ & & & & \mathbf{i} & \mathbf{i} \\ \mathbf{i} & & & & & \mathbf{i} \end{bmatrix}$$

$$\mathbf{I}_1 = \begin{bmatrix} \mathbf{i} & -\mathbf{i} & & & & \\ & \mathbf{i} & -\mathbf{i} & & & \\ & & \mathbf{i} & -\mathbf{i} & & \\ & & & \mathbf{i} & -\mathbf{i} & \\ & & & & \mathbf{i} & -\mathbf{i} \\ -\mathbf{i} & & & & & \mathbf{i} \end{bmatrix}\ \mathbf{I}_2 = \begin{bmatrix} \mathbf{i} & & & & & \mathbf{i} \\ \mathbf{i} & \mathbf{i} & & & & \\ & \mathbf{i} & \mathbf{i} & & & \\ & & \mathbf{i} & \mathbf{i} & & \\ & & & \mathbf{i} & \mathbf{i} & \\ & & & & \mathbf{i} & \mathbf{i} \end{bmatrix}\ \mathbf{I}_3 = \begin{bmatrix} \mathbf{i} & & & & & -\mathbf{i} \\ -\mathbf{i} & \mathbf{i} & & & & \\ & -\mathbf{i} & \mathbf{i} & & & \\ & & -\mathbf{i} & \mathbf{i} & & \\ & & & -\mathbf{i} & \mathbf{i} & \\ & & & & -\mathbf{i} & \mathbf{i} \end{bmatrix}$$

$$\mathbf{I}_4 = \begin{bmatrix} \mathbf{i} & \mathbf{i} & \mathbf{i} & \mathbf{i} & \mathbf{i} & \mathbf{i} \end{bmatrix},\ \bar{\boldsymbol{\varphi}} = \text{row}\left\{ \bar{\varphi}^1 \quad \bar{\varphi}^2 \quad \cdots \quad \bar{\varphi}^6 \right\},\ \tilde{\boldsymbol{\varphi}}_x = \text{row}\left\{ \tilde{\varphi}_x^1 \quad \tilde{\varphi}_x^2 \quad \cdots \quad \tilde{\varphi}_x^6 \right\},$$

$$\tilde{\boldsymbol{\varphi}}_y = \text{row}\left\{ \tilde{\varphi}_y^1 \quad \tilde{\varphi}_y^2 \quad \cdots \quad \tilde{\varphi}_y^6 \right\},\ \bar{\boldsymbol{\varphi}}_s = \text{row}\left\{ \bar{\varphi}_s^1 \quad \bar{\varphi}_s^2 \quad \cdots \quad \bar{\varphi}_s^6 \right\},$$

$$\mathbf{j}_o = \text{row}\left\{ \mathbf{j}_o^1 \quad \mathbf{j}_o^2 \quad \cdots \quad \mathbf{j}_o^6 \right\},\ \boldsymbol{\varphi}_p = \begin{bmatrix} \varphi_1^p \\ \varphi_2^p \end{bmatrix},$$

$$\mathbf{a_0} = \begin{bmatrix} \Sigma_{r1} - \dfrac{1}{k_{eff}}\nu\Sigma_{f1} & -\dfrac{1}{k_{eff}}\nu\Sigma_{f2} \\ -\Sigma_{s21} & \Sigma_{r2} \end{bmatrix},\ \mathbf{a_1} = \frac{1}{h^2}\begin{bmatrix} D_1 & 0 \\ 0 & D_2 \end{bmatrix},\ \mathbf{a_2} = \frac{\sqrt{3}h}{D_1 D_2}\begin{bmatrix} D_1 & 0 \\ 0 & D_2 \end{bmatrix}$$

$$\mathbf{i} = \begin{bmatrix} 1 & 0 \\ 0 & 1 \end{bmatrix},\ \bar{\boldsymbol{\varphi}}^m = \begin{bmatrix} \bar{\varphi}_1^m \\ \bar{\varphi}_2^m \end{bmatrix},\ \tilde{\boldsymbol{\varphi}}_x^m = \begin{bmatrix} \tilde{\varphi}_{1x}^m \\ \tilde{\varphi}_{2x}^m \end{bmatrix},\ \tilde{\boldsymbol{\varphi}}_y^m = \begin{bmatrix} \tilde{\varphi}_{1y}^m \\ \tilde{\varphi}_{2y}^m \end{bmatrix},\ \bar{\boldsymbol{\varphi}}_s^m = \begin{bmatrix} \bar{\varphi}_{1s}^m \\ \bar{\varphi}_{2s}^m \end{bmatrix},\ \mathbf{j}_o^m = \begin{bmatrix} \bar{J}_{1o}^m \\ \bar{J}_{2o}^m \end{bmatrix}$$

m=1,…,6.

The above linear system (2.2-18) can be solved directly by a block Gaussian Elimination scheme provided the aforementioned boundary conditions.

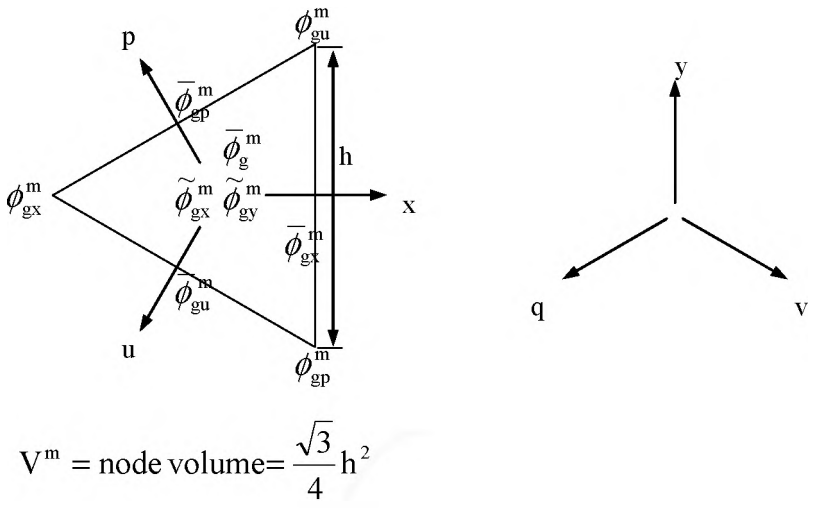

Figure 2-5. Unknowns and Coordinates for the TPEN method

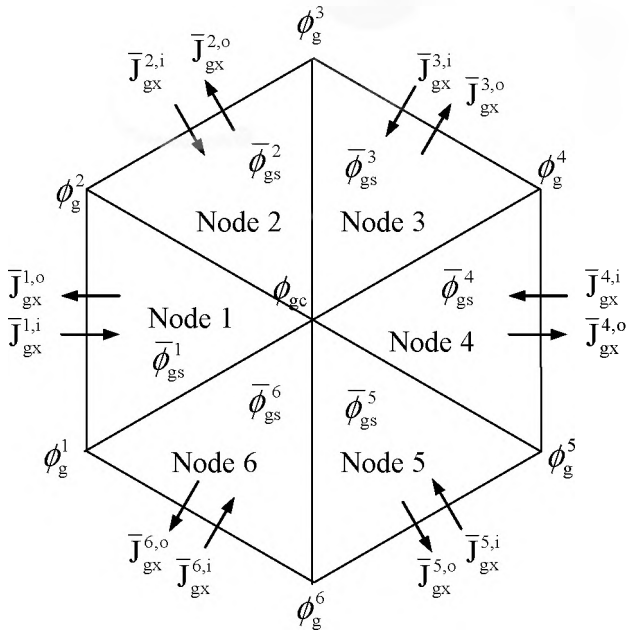

Figure 2-6. Boundary Conditions and Nodal Unknowns on a Hexagonal Node for TPEN

To use the TPEN method, first of all the axial leakage on hexagonal node must be known beforehand. The three-dimensional neutron diffusion equation can be reduced to a two-dimensional one by integrating over the axial direction as:

$$-D_g^m\left(\frac{\partial^2}{\partial x^2}+\frac{\partial^2}{\partial y^2}\right)\phi_g^m(x,y)+\Sigma_{rg}^m\phi_g^m(x,y) = \frac{\chi_g}{k_{eff}}\sum_{g'}\nu\Sigma_{fg'}^m\phi_{g'}^m(x,y)+\sum_{g'}\Sigma_{sgg'}^m\phi_{g'}^m(x,y)+S_{gz}^m(x,y), \tag{2.2-19}$$

where

$$\phi_g^m(x,y)=\frac{1}{h_z^m}\int\phi_g^m(x,y,z)\,dz,$$

$$S_{gz}^m(x,y)=-\frac{1}{h_z^m}\int-D_g^m\frac{\partial^2}{\partial z^2}\phi_g^m(x,y,z)\,dz$$

$$=-\frac{1}{h_z^m}\left(J_{gz}^{m,T}(x,y)-J_{gz}^{m,B}(x,y)\right).$$

The superscript 'T' and 'B' denote top and bottom surface of node m respectively, and S_{gz}^m is the axial leakage source which comes from the axial leakage term. Eq. (2.2-19) means that the radial distribution of the axial leakage source should be pre-determined to obtain a radial solution. In the MASTER code, a NEM solver generates the surface average axial currents that are fed into the TPEN solver as the axial leakage source. The radial shape of the axial leakage source is considered in the following.

Fig.2-7 shows the node average axial leakages for one center and 6 neighboring hexagons. The axial leakage source is defined as:

$$\bar{S}_{gz}^m=-\frac{1}{h_z^m}\left(\bar{J}_{gz}^{m,T}-\bar{J}_{gz}^{m,B}\right). \tag{2.2-20}$$

Using the 7 node average axial leakages shown in Fig. 2-7, the radial dependence of the axial leakage within the central hexagon can be approximated employing a two-dimensional polynomial consisting of 7 independent terms as:

$$S_{gz}(x,y) = d_{g0} + d_{g1}x + d_{g2}y + d_{g3}x^2 + d_{g4}u^2 + d_{g5}p^2 + d_{g6}xup. \quad (2.2\text{-}21)$$

The 7 coefficients of Eq.(2.2-21) can be determined by imposing 7 node average axial leakage constraints.

The TPEN solver requires three kinds of axial leakage source parameters on a triangle: triangular averaged axial sources, and *x*- and *y*- source moments. Fig. 2-8 shows these axial leakage source parameters of the 6 triangles of the central hexagon which are defined as:

$$\begin{aligned}
\bar{S}_{gz}^{c,n} &= \frac{1}{A^n} \int_{A^n} S_{gz}(x,y)\,dA \ , \\
\tilde{S}_{gzx}^{c,n} &= \frac{2}{\sqrt{3}h}\frac{1}{A^n} \int_{A^n} xS_{gz}(x,y)\,dA \ , \\
\tilde{S}_{gzy}^{c,n} &= \frac{2}{h}\frac{1}{A^n} \int_{A^n} yS_{gz}(x,y)\,dA \ .
\end{aligned} \quad (2.2\text{-}22)$$

By inserting Eq.(2.2-21) to (2.2-22), one can obtain axial sources which are expressed by 7 hexagon averaged axial leakage sources of Fig.2-7. For example, the axial sources of the 1st triangle of center hexagon are:

$$\begin{aligned}
\bar{S}_{gz}^{c,1} &= w_1 S_{gz}^c + w_2 S_{gz}^1 + w_3 \left(S_{gz}^2 + S_{gz}^6\right) + w_4 \left(S_{gz}^3 + S_{gz}^5\right) + w_5 S_{gz}^4, \\
\tilde{S}_{gzx}^{c,1} &= w_{x1} S_{gz}^c + w_{x2} S_{gz}^1 + w_{x3} \left(S_{gz}^2 + S_{gz}^6\right) + w_{x4} \left(S_{gz}^3 + S_{gz}^5\right) + w_{x5} S_{gz}^4, \\
\tilde{S}_{gzy}^{c,1} &= w_{y1} \left(S_{gz}^2 - S_{gz}^6\right) + w_{y2} \left(S_{gz}^3 - S_{gz}^5\right).
\end{aligned} \quad (2.2\text{-}23)$$

where

$$w_1 = 1, \quad w_2 = \frac{83}{540}, \quad w_3 = \frac{17}{540}, \quad w_4 = -\frac{37}{540}, \quad w_5 = -\frac{43}{540},$$

$$w_{x1} = -\frac{1}{54}, \quad w_{x2} = \frac{59}{3240}, \quad w_{x3} = \frac{7}{1620}, \quad w_{x4} = -\frac{1}{324}, \quad w_{x5} = -\frac{7}{3240},$$

$$w_{y1} = -\frac{1}{40}, \quad w_{y2} = -\frac{1}{360}.$$

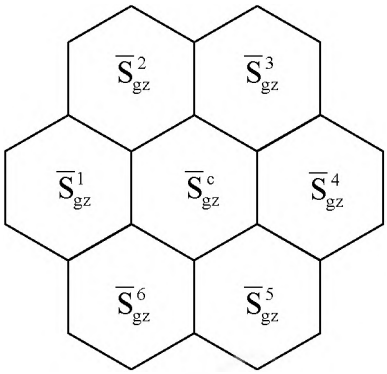

Figure 2-7. Notations for Axial Sources near Center Hexagon

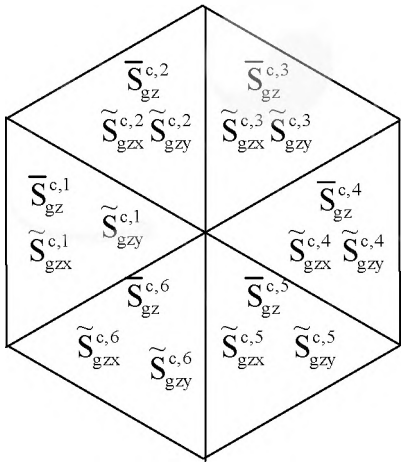

Figure 2-8. Triangular Axial Leakage Source Parameters

3. Transient Neutronics Methodology

The nodal expansion method (NEM) [1,2,3] starts with the multigroup neutron diffusion equation in P_1-form.

$$\frac{1}{v_g}\frac{\partial \varphi_g}{\partial t}(r,t) + \nabla \cdot J_g(r,t) + (\Sigma_{ag}(r,t) + \sum_{g'>g} \Sigma_{gg'}(r,t))\varphi_g(r,t)$$
$$= \sum_{g'<g} \Sigma_{g'g}(r,t)\varphi_{g'}(r,t) + \frac{1}{k}\sum_{g'}\sum_{j}(1-\beta^j)\chi^j_{pg}\nu\Sigma^j_{fg'}(r,t)\varphi_{g'}(r,t) \quad (3\text{-}1a)$$
$$+ \sum_{i} \chi^i_{dg}\lambda_i C_i(r,t) + \chi_{eg} S^{ext}_g(r,t)$$

$$J_g(r,t) + D_g(r,t)\nabla\varphi_g(r,t) = 0 \quad (3\text{-}1b)$$

$$\frac{\partial C_i(r,t)}{\partial t} + \lambda_i C_i(r,t) = \frac{1}{k}\sum_{g'}\sum_{j}\beta^j_i \nu\Sigma^j_{fg'}\varphi_{g'}(r,t) \quad (3\text{-}1c)$$

where v_g = neutron velocity in group g,

φ_g = neutron flux in group g,

J_g = neutron current in group g,

Σ_{ag} = absorption cross section in group g,

Σ_{gg} = scattering cross section from g′ to g,

$\nu\Sigma^j_{fg}$ = ν-fission cross section of fissionable isotope j in group g,

k = eigenvalue,

C_i = average precursor concentration in precursor group i,

β^j = total yield of delayed neutrons of fissionable isotope j ($= \sum_i \beta^j_i$),

χ^j_{pg} = prompt fission spectrum of fissionable isotope j in group g,

χ_{eg} = external source spectrum in group g,

χ_{dg}^{i} = delayed fission spectrum of precursor group i in group g,

λ_i = decay constant of precursor group i ,

S_g^{ext} = external source.

Integrating Eq. (3-1) over a node volume leads to the exact nodal balance equation as follows:

$$\frac{1}{v_g}\frac{d\phi_g^m}{dt}+\sum_{u=x,y,z}\frac{1}{a_u^m}\left[\left(j_{gul}^{-m}+j_{gur}^{+m}\right)-\left(j_{gul}^{+m}+j_{gur}^{-m}\right)\right]+\left(\Sigma_{ag}^{m}+\sum_{g'>g}\Sigma_{gg'}^{m}\right)\phi_g^m$$
$$=\sum_{g'<g}\Sigma_{g'g}^{m}\phi_{g'}^{m}+\frac{1}{k}\sum_{g'}\sum_{j}(1-\beta^j)\chi_{pg}^{j}\nu\Sigma_{fg'}^{jm}\phi_{g'}^{m}+\sum_{i}\chi_{dg}^{i}\lambda_i C_i^m+\chi_{eg}S_g^{ext,m} \quad (3\text{-}2a)$$

$$j_{gus}^{+m}-j_{gus}^{-m}+D_g^m\left.\frac{\partial\psi_{gu}^{m}}{\partial u}\right|_S=0 \quad (3\text{-}2b)$$

$$\frac{\partial C_i^m}{\partial t}+\lambda_i C_i^m=\frac{1}{k}\sum_{g'}\sum_{j}\beta_i^j\nu\Sigma_{fg'}^{jm}\phi_{g'}^{m} \quad (3\text{-}2c)$$

where a_u^m = mesh size in the direction u (=x,y,z) of node m,

$j_{gus}^{\pm m}$ = incoming and outgoing currents in group g at the surfaces s (=l, r) of node m.

The surface average fluxes are defined by

$$\psi_{gus}^{m}=\frac{1}{A_u^m}\int_0^{a_v^m}\int_0^{a_w^m}\varphi_g(r,t)\,dv\,dw \quad (3\text{-}3)$$

where A_u^m = transverse area to u-direction.

By integrating Eq. (3-1) over the transverse leakage directions, one can obtain the 1-

dimensional equivalent diffusion equations:

$$\frac{1}{v_g}\frac{d\psi^m_{gu}}{dt}-\frac{\partial}{\partial u}D^m_g\frac{\partial}{\partial u}\psi^m_{gu}+(\Sigma^m_{agu}+\sum_{g'>g}\Sigma^m_{gg'u})\psi^m_{gu}$$
$$=\sum_{g'<g}\Sigma^m_{g'gu}\psi^m_{g'u}+\frac{1}{k}\sum_{g'}\sum_{j}(1-\beta^j)\chi^j_{pg}\nu\Sigma^{jm}_{fg'}\psi^m_{g'u}+\sum_{i}\chi^i_{dg}\lambda_i\varsigma^m_{ju} \qquad (3\text{-}4a)$$
$$-D^m_gL^m_{gu}+\chi_{eq}S^{ext,m}_g$$

$$\frac{\partial\varsigma^m_{iu}}{\partial t}=-\lambda_i\varsigma^m_{iu}+\frac{1}{k}\sum_{g'}\sum_{j}\beta^j_i\nu\Sigma^{jm}_{fg'u}\psi^m_{g'u} \qquad (3\text{-}4b)$$

where $L^m_{gu}=-\frac{1}{A^m_u}\int_0^{a^m_v}\int_0^{a^m_w}(\frac{d^2}{dv^2}+\frac{d^2}{dw^2})\phi_g(r,t)dvdw$,

$$\varsigma^m_{iu}=\frac{1}{A^m_u}\int_0^{a^m_v}\int_0^{a^m_w}C_i(r,t)dvdw=\frac{\sum_{g'}\sum_{j}\beta^j_i\nu\Sigma^{jm}_{fg'u}\psi^m_{g'u}}{\sum_{g'}\sum_{j}\beta^j_i\nu\Sigma^{jm}_{fg'}\phi^m_{g'}}C^m_i.$$

To solve the equivalent 1-D diffusion equations, two additional approximations are needed. The first term of the left hand side of Eq. (3-4a) is approximated by

$$\frac{d\psi_{gu}}{dt}=\frac{1}{\phi_g}\frac{d\phi_g}{dt}\psi_{gu} \qquad (3\text{-}5)$$

The time-dependent flux $\phi_g(t)$ can be expressed as an exponential form

$$\phi_g(t)=e^{\omega(t-t_0)}T_g(t) \qquad (3\text{-}6)$$

where ω = frequency which can be calculated either during the iterative solution process or by using information from the previous time step.

Then, the derivation of $\phi_g(t)$ becomes

$$\frac{d\phi_g}{dt} = \omega\phi_g(t) + e^{\omega(t-t_0)}\frac{dT_g(t)}{dt} \tag{3-7}$$

Using the implicit first-order Euler formula we can rearrange Eq. (3-7) as follows:

$$\frac{d\phi_g}{dt} = \omega\phi_g(t) + \frac{(\phi_g(t) - e^{\omega\Delta t}\phi_g(t_0))}{\Delta t} \tag{3-8}$$

where $\Delta t = t - t_0$

Inserting Eq. (3-8) into Eq. (3-5) leads to the following expression.

$$\frac{d\psi_{gu}}{dt} = \frac{1}{\Delta t}(\omega\Delta t + 1 - \frac{\phi_g(t_0)}{\phi_g(t)}e^{\omega\Delta t})\psi_{gu} \tag{3-9}$$

In the same manner the partially integrated precursor concentrations are approximated by

$$\frac{d\varsigma_{iu}}{dt} = \frac{1}{C_i}\frac{dC_i}{dt}\varsigma_{iu} \tag{3-10}$$

which results in

$$\begin{aligned} C_i(t) &= C_i(t_0)e^{-\lambda_i(t-t_0)} + \frac{1}{k}\sum_{g'}\sum_j \beta_i^j \int_{t_0}^{t} \nu\Sigma_{fg'}^j\phi_{g'}(t')e^{\lambda_i(t'-t)}dt' \\ &= C_i(t_0)e^{-\lambda_i(t-t_0)} + \frac{1}{k}\sum_{g'}\sum_j \beta_i^j \int_{t_0}^{t} \nu\Sigma_{fg'}^j e^{\omega(t'-t_0)}e^{\lambda_i(t'-t)}T_{g'}(t')dt' \end{aligned} \tag{3-11}$$

By approximating $T_g(t)$ with its arithmetic average, the second term of the right-hand side of the equation above can be simplified:

$$\frac{1}{k}\sum_{g'}\sum_{j}\beta_i^j\int_{t_0}^{t}\nu\Sigma_{fg'}^j e^{\omega(t'-t_0)}e^{\lambda_i(t'-t)}T_{g'}(t')dt'$$
$$=\frac{1}{k}\sum_{g'}\sum_{j}\beta_i^j\nu\Sigma_{fg'}^j\frac{\left(\phi_{g'}(t)+\phi_{g'}(t_0)e^{\omega(t-t_0)}\right)}{2}\frac{1-e^{-(\omega+\lambda_i)(t-t_0)}}{\omega+\lambda_i} \qquad (3\text{-}12)$$
$$\cong\frac{1}{k}\sum_{g'}\sum_{j}\beta_i^j\nu\Sigma_{fg'}^j\phi_{g'}(t)\frac{1-e^{-(\omega+\lambda_i)(t-t_0)}}{\omega+\lambda_i}$$

Using Eqs. (3-8) and (3-11) , Eq. (3-2a) can be rewritten

$$\left(\frac{1+\omega\Delta t}{v_g\Delta t}+\Sigma_{ag}+\sum_{g>g}\Sigma_{gg}+\sum_{u=x,y,z}\frac{2c_{1gu}}{a_u}\right)\phi_g(t)$$
$$=\sum_{g'<g}\Sigma_{g\,g}\phi_{g'}(t)+\frac{1}{k}\sum_{g}\sum_{j}\chi_{tg}^j\nu\Sigma_{fg'}^j\phi_{g'}(t)$$
$$-\frac{1}{k}\sum_{i}\sum_{j}\sum_{g'}\chi_{dg}^i\beta_i^j\nu\Sigma_{fg'}^j\phi_{g'}(t)\frac{\omega+\lambda_i e^{-(\omega+\lambda_i)\Delta t}}{\omega+\lambda_i} \qquad (3\text{-}13)$$
$$+\sum_{i}\chi_{dg}^i\lambda_i C_i(t_0)e^{-\lambda_i\Delta t}+\frac{e^{\omega\Delta t}}{v_g\Delta t}\phi_g(t_0)$$
$$+\sum_{u=x,y,z}\frac{2c_{1gu}}{a_u}\left[2(j_{gul}^{+}+j_{gur}^{-})-a_{4gu}\right]+S_g^{ext}$$

where χ_{tg}^j = total fission spectrum ($(1-\beta^j)\chi_{pg}^j+\sum_i\beta_i^j\chi_{dg}^i$).

4 Adjoint Flux Solution

The adjoint nodal balance equation [18] starts with the similar form to the forward standard diffusion equation with a P_1-approximation.

$$\begin{aligned}\nabla\cdot -D(r,E)\nabla\varphi^*(r,E)+\Sigma_r(r,E)\varphi^*(r,E)\\ =\int_{E'}\Sigma_s(r,E\rightarrow E')\varphi^*(r,E')dE'\\ +\sum_j \nu\Sigma_f^j(r,E)\int_{E'}\frac{1}{k}\chi^j(E')\varphi^*(r,E')dE'+S^*(r,E)\end{aligned} \tag{4-1}$$

Discretizing the energy into groups in the 3-dimensional Cartesian geometry Eq. (4-1) can be rewritten as

$$\begin{aligned}\nabla\cdot -D(r)\nabla\varphi_g^*(r)+\Sigma_{rg}(r)\varphi_g^*(r)\\ =\sum_{g'}\Sigma_{gg'}(r)\varphi_{g'}^*(r)+\sum_j \nu\Sigma_{fg}^j(r)\sum_{g'}\frac{1}{k}\chi_{g'}^j\varphi_{g'}^*(r)+S_g^*(r)\end{aligned} \tag{4-2}$$

For simplicity the adjoint current is defined in the following form.

$$J_g^*(r)=-D_g(r)\nabla\varphi_g^*(r) \tag{4-3}$$

Integrating Eq. (4-2) over volume with the definition of the node average adjoint flux

$$\phi_g^{m*}=\frac{1}{V}\int_V\varphi_g^*(x,y,z)dV \tag{4-4}$$

leads to the standard adjoint nodal balance equation as follows:

$$\sum_{u=x,y,z} \frac{1}{a_u^m}\left[\left(j_{gul}^{-m^*} + j_{gur}^{+m^*}\right) - \left(j_{gul}^{+m^*} + j_{gur}^{-m^*}\right)\right] + \sum_{rg}^{m} \phi_g^{m^*}$$
$$= \sum_{g'} (\Sigma_{gg'}^{m} + \frac{1}{k} \sum_{j} \chi_{g'}^{j} \nu\Sigma_{fg'}^{jm}) \phi_{g'}^{m^*} + S_g^{m^*} \tag{4-5}$$

Now the transverse integrated adjoint flux is defined as

$$\psi_{gu}^{m^*} = \frac{1}{A_u^m} \int_0^{a_v^m} \int_0^{a_w^m} \varphi_g^*(r) dv dw \tag{4-6}$$

At the surface the equation fulfills the following conditions:

$$\psi_{gu}^{m^*}\Big|_{s=l,r} = \psi_{gus}^{m^*} \tag{4-7}$$

In addition it can be approximated by using the diffusion theory approximation.

$$\psi_{gu}^{m^*} = 2(j_{gus}^{+m^*} + j_{gus}^{-m^*}) \tag{4-8}$$

In the same manner as the forward equation the 1-dimensional flux is assumed as a quartic polynomial.

$$\psi_{gu}^{m^*}(u) = \sum_{i=0}^{4} a_{igu}^* \xi_i(u) \tag{4-9}$$

where $\xi_i(u)$'s are the same as in Section 2.1.1.

The first three coefficients of Eq. (4-9) can easily be found with the boundary conditions.

$$a_{0gu}^* = \phi_g^{m^*} \tag{4-10}$$

$$a^*_{1gu} = \frac{\psi^*_{gur} - \psi^*_{gul}}{2}$$

$$a^*_{2gu} = \phi_g{}^* - \frac{\psi^*_{gur} + \psi^*_{gul}}{2}$$

The last two coefficients a^*_{3gu} and a^*_{4gu} can be solved using the weighted residual method with 1-dimensional equivalent diffusion equations obtained by integrating Eq. (4-5) over the transverse direction.

$$\int_0^{a_u} w_i(-D^m_g \nabla^2 \psi^m_{gu}{}^*(u) + \Sigma^m_{rg}(r)\psi^m_{gu}{}^*(u) - Q^m_g{}^* + D^m_g L^m_{gu}{}^*(u))du = 0 \qquad (4\text{-}11)$$

where $w_i = \xi_i(u)$ (i = 1, 2),

$$Q^{m*}_g = \sum_{g'} (\Sigma_{gg'} + \sum_j \frac{\chi^j_{g'}}{k} \nu\Sigma^{jm}_{fg})\phi^{m*}_{g'} + S^{ext,m*}_g ,$$

$$L^m_{gu}{}^*(u) = -\frac{1}{A_u}\int_0^{a_v}\int_0^{a_w}(\frac{d^2}{dv^2} + \frac{d^2}{dw^2})\phi^*_g(r)dvdw .$$

The adjoint transverse leakage is also approximated by a quadratic polynomial in the same fashion as the forward case whose coefficients are found by applying the boundary conditions at surfaces. The resulting equation is

$$L^m_{gu}{}^* = b^*_{0gu} + b^*_{1gu}\xi_1(u) + b^*_{2gu}\xi_2(u) \qquad (4\text{-}12)$$

where $b^*_{0gu} = \int_0^1 L^{m*}_{gu}(u)du = \bar{L}^{m*}_{gu}$,

$$b^*_{1gu} = \frac{L^{m*}_{gur} - L^{m*}_{gul}}{2},$$

$$b^*_{2gu} = \bar{L}^{m*}_{gu} - \frac{L^{m*}_{gur} + L^{m*}_{gul}}{2}.$$

The relationship between outgoing and incoming currents and node average fluxes in the adjoint equation can be expressed by use of the diffusion equation approximation for the adjoint partial currents.

The adjoint nodal balance equation for AFEN method for both rectangular and hexagonal geometries is as follows:

$$\begin{aligned} \nabla^2 \phi_1 - c_1\phi_1 + c_2\phi_2 &= 0 \\ \nabla^2 \phi_2 + c_4\phi_1 - c_3\phi_2 &= 0 \end{aligned} \tag{4-13}$$

where $c_1 = \dfrac{\Sigma_{a1} + \Sigma_{12} - \nu\Sigma_{f1}/k}{D_1}$, $c_2 = \dfrac{\Sigma_{12}}{D_1}$, $c_3 = \dfrac{\Sigma_{a2}}{D_2}$, $c_4 = \dfrac{\nu\Sigma_{f2}}{D_2 k}$.

In the above equation c_2 and c_4 are different from those of forward calculation. The response matrix formulation of this method and the solution procedure are essentially the same as those of forward method.

5. Transverse Leakage Approximation

5.1 Axial Leakage Approximation of NEM/NIM Method

To solve the equivalent 1-D diffusion equation Eq. (2.1-5) using the weighted residual method, first of all the transverse leakage $D_g^m L_{gu}^m$ must be known beforehand. Therefore, L_{gu} is approximated as a quadratic polynomial whose coefficients can be obtained by using leakage information from adjacent nodes.

$$L_{gu} = b_{0gu} + b_{1gu}\xi_1(u) + b_{2gu}\xi_2(u) \tag{5-1}$$

where $b_{0gu} = \int_0^1 L_{gu}(u)du = \bar{L}_{gu}$,

$$b_{1gu} = \frac{L_{gur} - L_{gul}}{2},$$

$$b_{2gu} = \bar{L}_{gu} - \frac{L_{gur} + L_{gul}}{2}.$$

The first and second coefficients b_{1gu} and b_{2gu} are determined by continuity conditions at box interfaces m±1 adjacent to m.

$$\begin{aligned} L_{gur}^{m-1} &= L_{gu}^{m-1}(1) = L_{gu}^{m}(0) = L_{gul}^{m} \\ D_{gu}^{m-1}\frac{dL_{gu}^{m-1}}{du}(1) &= D_{gu}^{m}\frac{dL_{gu}^{m}}{du}(0) \end{aligned} \tag{5-2}$$

Inserting Eq. (5-1) into Eq. (5-2) yields a tridiagonal system for the determination of the unknown boundary values L_{gur} and L_{gul}. Another useful method to approximate the interface leakages is to use a linear equation in Eq. (5-2). The boundary values are then given by

$$L_{gul}^{m} = \frac{D_{gu}^{m}\bar{L}_{gu}^{m} + D_{gu}^{m-1}\bar{L}_{gu}^{m-1}}{D_{gu}^{m} + D_{gu}^{m-1}} \tag{5-3a}$$

$$L_{gur}^{m} = \frac{D_{gu}^{m}\bar{L}_{gu}^{m} + D_{gu}^{m+1}\bar{L}_{gu}^{m+1}}{D_{gu}^{m} + D_{gu}^{m+1}} \tag{5-3b}$$

$$D_{g}^{m}\bar{L}_{gx}^{m} = \sum_{u=y,z} \frac{1}{a_u}\left[\left(j_{gur}^{+} - j_{gur}^{-}\right) + \left(j_{gul}^{-} - j_{gul}^{+}\right)\right] \tag{5-3c}$$

Eq. (5-3) describes the simplified leakage approximation. The derivation of Eqs. (5-2) and (5-3) shows that the leakage approximation is the natural choice in transverse-integrated nodal schemes like NEM. Other methods which rely on intranodal flux expansions are only practical in two dimensions and must be combined with either the M_2B^2-variant or the assumption of separability in z-direction. This can easily be seen by splitting L_{gu} into two parts

$$L_{gu}(u) = L_{gu}^{v}(u) + L_{gu}^{w}(u) \tag{5-4}$$

$$L_{gu}^{v}(u) = -\frac{1}{A_u}\int_0^{a_v}\int_0^{a_w} \frac{d^2}{dv^2}\phi_g(r)\,dv\,dw$$

$$L_{gu}^{w}(u) = -\frac{1}{A_u}\int_0^{a_v}\int_0^{a_w} \frac{d^2}{dw^2}\phi_g(r)\,dv\,dw$$

If u = z and (v, w) = (x, y), then the formalism (5-2) or (5-3) can be used to determine the parabolic z-dependence of transverse leakage. In the separable case the following relations hold

$$D_g L_{gz}(z) = D_g B_{gz}^2 \psi_g(z) \tag{5-5}$$

where $D_g B_{gz}^2 = \frac{1}{\phi_g}\sum_{u=x,y}\frac{1}{a_u}\left[\left(j_{gur}^{+} - j_{gur}^{-}\right) + \left(j_{gul}^{-} - j_{gul}^{+}\right)\right]$

If u = x and (v,w) = (y,z), the integration over z can be formally performed to yield

$$L^{y}_{gx}(x) = -\frac{1}{a_y}\int_0^{a_y} \frac{d^2}{dy^2}\phi_g(x/a_x, y/a_y)dy \tag{5-6}$$

If the z-integrated flux $\phi_g(x/a_x, y/a_y)$ can be approximated by a non-separable function the above integral can be evaluated. A parabolic approximation leads to

$$\begin{aligned}\phi_g(x,y) &= \sum_{i,j}^{2} c_{ijg}\xi_i(x)\xi_j(y) \\ D_g L^{y}_{gx}(x) &= 12\frac{D_{gy}}{a_y}\left(c_{02g} + c_{12g}\xi_1(x) + c_{22g}\xi_2(x)\right)\end{aligned} \tag{5-7}$$

with

$$D_g b_{1gx} = 3\frac{D_{gy}}{a_y}\left(\phi_g(0,0) - \phi_g(1,0) + \phi_g(0,1) - \phi_g(1,1) + 2(\psi_{gxr} - \psi_{gxl})\right)$$

$$\begin{aligned}D_g b_{2gx} = 3\frac{D_{gy}}{a_y}\big(&\phi_g(0,0) + \phi_g(1,0) + \phi_g(0,1) + \phi_g(1,1) + 4\phi_g \\ &- 2(\psi_{gxr} + \psi_{gxl}) - 2(\psi_{gyr} + \psi_{gyl})\big)\end{aligned}$$

where the time-dependence of ϕ has been suppressed.

Replacing x by y the corresponding formulae for the y-direction are obtained. The contribution of the z-direction

$$L^{z}_{gx}(x) = -\frac{1}{A_x}\int_0^{a_y}\int_0^{a_z} \frac{d^2}{dz^2}\phi_g(r)dydz \tag{5-8}$$

is again given by Eqs. (5-2) and (5-3) or under the assumption of separability of the flux in z-direction by

$$D_g L^{z}_{gx}(x) = \frac{1}{\phi_g}\frac{1}{a_z}\left[\left(j^{+}_{gzr} - j^{-}_{gzr}\right) + \left(j^{-}_{gzl} - j^{+}_{gzl}\right)\right]\psi_{gx}(x) \tag{5-9}$$

5.2 Axial Leakage Approximation of TPEN

The three-dimensional neutron diffusion equation can be reduced to a two-dimensional one by integrating over the axial direction as:

$$-D_g^m\left(\frac{\partial^2}{\partial x^2}+\frac{\partial^2}{\partial y^2}\right)\phi_g^m(x,y)+\Sigma_{rg}^m\phi_g^m(x,y) = \frac{\chi_g}{k_{eff}}\sum_{g'}\nu\Sigma_{fg'}^m\phi_{g'}^m(x,y)+\sum_{g'}\Sigma_{sgg'}^m\phi_{g'}^m(x,y)+S_{gz}^m(x,y), \tag{5.2-1}$$

where

$$\phi_g^m(x,y)=\frac{1}{h_z^m}\int\phi_g^m(x,y,z)\,dz,$$

$$S_{gz}^m(x,y)=-\frac{1}{h_z^m}\int-D_g^m\frac{\partial^2}{\partial z^2}\phi_g^m(x,y,z)\,dz$$

$$=-\frac{1}{h_z^m}\left(J_{gz}^{m,T}(x,y)-J_{gz}^{m,B}(x,y)\right).$$

The superscript 'T' and 'B' denote top and bottom surface of node m respectively, and S_{gz}^m is the axial leakage source which comes from the axial leakage term. Eq. (5.2-1) means that the radial distribution of the axial leakage source should be pre-determined to obtain a radial solution. In the MASTER-3.0 code, a NEM solver generates the surface average axial currents that are fed into the TPEN solver as the axial leakage source. The radial shape of the axial leakage source is considered in the following.

Fig.5-1 shows the node average axial leakages for one center and 6 neighboring hexagons. The axial leakage source is defined as:

$$\bar{S}_{gz}^m=-\frac{1}{h_z^m}\left(\bar{J}_{gz}^{m,T}-\bar{J}_{gz}^{m,B}\right). \tag{5.2-2}$$

Using the 7 node average axial leakages shown in Fig. 5-1, the radial dependence of the axial leakage within the central hexagon can be approximated employing a two-dimensional

polynomial consisting of 7 independent terms as:

$$S_{gz}(x,y) = d_{g0} + d_{g1}x + d_{g2}y + d_{g3}x^2 + d_{g4}u^2 + d_{g5}p^2 + d_{g6}xup. \quad (5.2\text{-}3)$$

The 7 coefficients of Eq. (5.2-3) can be determined by imposing 7 node average axial leakage constraints.

The TPEN solver requires three kinds of axial leakage source parameters on a triangle: triangular averaged axial sources, and *x*- and *y*- source moments. Fig. 5-2 shows these axial leakage source parameters of the 6 triangles of the central hexagon which are defined as:

$$\begin{aligned}
\overline{S}_{gz}^{c,n} &= \frac{1}{A^n} \int_{A^n} S_{gz}(x,y)\,dA \ , \\
\widetilde{S}_{gzx}^{c,n} &= \frac{2}{\sqrt{3}h}\frac{1}{A^n} \int_{A^n} xS_{gz}(x,y)\,dA \ , \\
\widetilde{S}_{gzy}^{c,n} &= \frac{2}{h}\frac{1}{A^n} \int_{A^n} yS_{gz}(x,y)\,dA \ .
\end{aligned} \quad (5.2\text{-}4)$$

By inserting Eq. (5.2-3) to (5.2-4), one can obtain axial sources which are expressed by 7 hexagon averaged axial leakage sources of Fig.5.1. For example, the axial sources of the 1st triangle of center hexagon are:

$$\begin{aligned}
\overline{S}_{gz}^{c,1} &= w_1 S_{gz}^c + w_2 S_{gz}^1 + w_3 \left(S_{gz}^2 + S_{gz}^6\right) + w_4 \left(S_{gz}^3 + S_{gz}^5\right) + w_5 S_{gz}^4, \\
\widetilde{S}_{gzx}^{c,1} &= w_{x1} S_{gz}^c + w_{x2} S_{gz}^1 + w_{x3} \left(S_{gz}^2 + S_{gz}^6\right) + w_{x4} \left(S_{gz}^3 + S_{gz}^5\right) + w_{x5} S_{gz}^4, \\
\widetilde{S}_{gzy}^{c,1} &= w_{y1} \left(S_{gz}^2 - S_{gz}^6\right) + w_{y2} \left(S_{gz}^3 - S_{gz}^5\right).
\end{aligned} \quad (3.4\text{-}5)$$

where

$$w_1 = 1, \quad w_2 = \frac{83}{540}, \quad w_3 = \frac{17}{540}, \quad w_4 = -\frac{37}{540}, \quad w_5 = -\frac{43}{540},$$

$$w_{x1} = -\frac{1}{54}, \quad w_{x2} = \frac{59}{3240}, \quad w_{x3} = \frac{7}{1620}, \quad w_{x4} = -\frac{1}{324}, \quad w_{x5} = -\frac{7}{3240},$$

$$w_{y1} = -\frac{1}{40}, \qquad w_{y2} = -\frac{1}{360}.$$

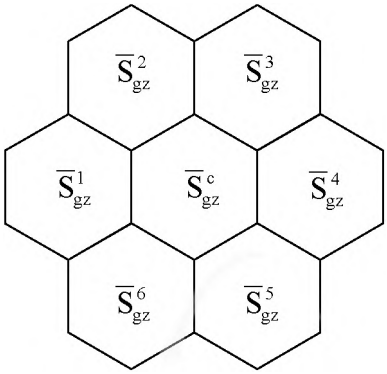

Figure 5-1 Notations for Axial Sources near Center Hexagon

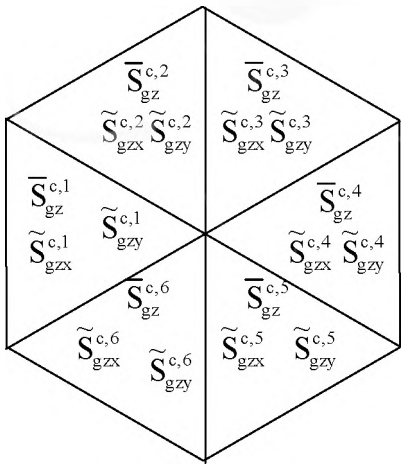

Figure 5-2 Triangular Axial Leakage Source Parameters

6. Assembly Homogenization

6.1 Simplified Equivalence Theory

Since the nodal methods treat large nodes as homogenized regions, it is needed to determine the equivalent diffusion parameters. In the lattice codes, flux and volume weighted few group cross sections are determined with zero current boundary conditions. However, it is known that the use of these cross sections does not allow preserving any of conservation quantities such as reaction rates, currents and fluxes of the heterogeneous cell calculations, which leads to large errors. Consequently, additional degrees of freedom must be introduced such that all conservation conditions can be met. The "equivalence theory" [19,20,21] has been turned out to be very effective to meet the purpose.

The equivalence theory starts with the continuity condition of the corresponding surface average heterogeneous fluxes at the interface of two adjacent nodes k and k':

$$\phi_{gu}^{het,k}(u_s) = \phi_{gu}^{het,k'}(u_s) \tag{6.1-1}$$

Since there is no longer physical reason to assume that the homogenized flux should be continuous at the interfaces between two different homogenized assemblies, Eq. (6.1-1) can be rewritten using the discontinuity factor f_{gu}.

$$f_{gu}^{k}\phi_{gu}^{hom,k}(u_s) = f_{gu}^{k'}\phi_{gu}^{hom,k'}(u_s) \tag{6.1-2}$$

where the discontinuity factor is defined as the ratios of the heterogeneous flux to the corresponding homogenized surface flux.

If the multigroup reference solution for the heterogeneous node is known, the two equivalence parameters, D_{gu} and f_{gu} can be determined by solving the following equivalent equation system for the homogenized flux:

$$-D_g \frac{d^2\phi_g(u)}{du^2} + \Sigma_{tg}\phi_g(u) - \sum_{g'} (\Sigma_{g'g} + \frac{\chi_g}{k}\nu\Sigma_{fg'})\phi_{g'}(u) = -D_g L_g(u) \qquad (6.1\text{-}3)$$

where $L_g(u)$ = transverse leakage for group g. The quantities such as the eigenvalue, flux weighted cross sections and surface average currents on the two adjacent faces can be obtained from heterogeneous multigroup solution, and the transverse leakage can be approximated from the heterogeneous pointwise leakage distribution.

According to the conservation principles it is required that the solution of the equivalent equation system for the inhomogeneous boundary value problem must reproduce the surface average heterogeneous fluxes at both boundaries. To meet this requirement the resulting homogeneous equivalent solution is adjusted by introducing the discontinuity factor as defined by Eq. (6.1-2)

MASTER-3.0 uses the "simplified equivalence theory" (SET) for assembly homogenization by default. The simplifying assumption is made so that the interaction of assemblies can be described in terms of only a single pair of direction-independent D_g and f_g.

$$\begin{aligned} D_{gx} &= D_{gy} = D_{gz} = D_g \\ f_{gx} &= f_{gy} = f_{gz} = f_g \end{aligned} \qquad (6.1\text{-}4)$$

One of the advantages of this theory is that the existing nodal diffusion equation can be used without any modification. The equivalent cross sections and diffusion coefficient are redefined in SET.

$$\Sigma_g^{SET} = \frac{\Sigma_g}{f_g}, D_g^{SET} = \frac{D_g}{f_g} \qquad (6.1\text{-}5)$$

The solution of the conventional diffusion theory using these refined cross sections and

diffusion coefficients becomes the modified "SET-flux" $f_g \phi_g(r)$ which is continuous at the assemblies boundaries.

The SET homogenization scheme is very convenient to implement and achieves good accuracy in calculating average assembly powers and reconstructed local pin powers for unrodded and rodded cores. However, it is limited to the analysis of the interior symmetric fuel assemblies because it is not able to consider the direction dependency of equivalent parameters by nature.

6.2 Assembly Discontinuity Factor

The SET has very simple to consider with good accuracy whereas it is valid only when a fuel assembly is symmetric. In case of asymmetric fuel assemblies, however, the same heterogeneity factors cannot be applied to all the sides. Therefore, we need to provide sidewise discontinuity factors (DFs, or f_{gus}) [21] different from side to side. In the actual calculation, we do not know the true heterogeneous flux which must be known to determine the value of DFs. This problem is solved by referring to the Assembly discontinuity factors (ADFs) coming from isolated assembly spectrum calculations with reflective boundary conditions. Thus, DFs are approximated by ADFs directly computed from single assembly calculations without knowing the heterogeneous reactor solution.

MASTER-3.0 can use DFs for asymmetric fuel assemblies. The neuronics solution with DFs can be easily obtained. For example, it is only necessary to divide the surface-averaged fluxes of the partial current equations by their corresponding DFs. The a_{igu} (i = 1, ..,4) of NEM flux expansion coefficients are given as

$$
\begin{aligned}
a_{1gu} &= \frac{1}{2}\left(\frac{\psi_{gur}}{f_{gur}} - \frac{\psi_{gul}}{f_{gul}}\right), \quad a_{2gu} = \phi_g - \frac{1}{2}\left(\frac{\psi_{gur}}{f_{gur}} + \frac{\psi_{gul}}{f_{gul}}\right) \\
a_{3gu} &= \frac{(j^+_{gur} - j^-_{gur}) + (j^+_{gul} - j^-_{gul})}{12 D_{gu}} + \frac{1}{6}\left(\frac{\psi_{gur}}{f_{gur}} - \frac{\psi_{gul}}{f_{gul}}\right) \\
a_{4gu} &= \frac{(j^+_{gur} - j^-_{gur}) - (j^+_{gul} - j^-_{gul})}{12 D_{gu}} - \left(\phi_g - \frac{1}{2}\left(\frac{\psi_{gur}}{f_{gur}} + \frac{\psi_{gul}}{f_{gul}}\right)\right)
\end{aligned}
\tag{6.2-1}
$$

where $D_{gu} = D^m_g / a_u$.

The partial current equations for node m be then represented as

$$
\begin{aligned}
j^{-m}_{gul} &= c^m_{1gul}(\phi^m_g + a^m_{4gu}) + c^m_{2gul} j^{+m}_{gul} + c^m_{3gul} j^{-m}_{gur} - c^m_{4gul} a^m_{3gu} \\
j^{+m}_{gur} &= c^m_{1gur}(\phi^m_g + a^m_{4gu}) + c^m_{3gur} j^{+m}_{gul} + c^m_{2gur} j^{-m}_{gur} + c^m_{4gur} a^m_{3gu}
\end{aligned}
\tag{6.2-2}
$$

where

$$
\begin{aligned}
c_{1gul} &= 6 D_{gu}\left(1 + \frac{4 D_{gu}}{f_{gur}}\right) / F_{gu}, \quad c_{1gur} = 6 D_{gu}\left(1 + \frac{4 D_{gu}}{f_{gul}}\right) / F_{gu}, \\
c_{2gul} &= \left(1 + 8 D_{gu}\left(\frac{1}{f_{gur}} - \frac{1}{f_{gul}}\right) - \frac{48 D^2_{gu}}{f_{gur} f_{gul}}\right) / F_{gu}, \\
c_{2gur} &= \left(1 - 8 D_{gu}\left(\frac{1}{f_{gur}} - \frac{1}{f_{gul}}\right) - \frac{48 D^2_{gu}}{f_{gur} f_{gul}}\right) / F_{gu}, \\
c_{3gul} &= -\frac{8 D_{gu}}{f_{gur}} / F_{gu}, \quad c_{3gur} = -\frac{8 D_{gu}}{f_{gul}} / F_{gu}, \\
c_{4gul} &= 6 D_{gu}\left(1 + \frac{12 D_{gu}}{f_{gur}}\right) / F_{gu}, \quad c_{4gul} = 6 D_{gu}\left(1 + \frac{12 D_{gu}}{f_{gul}}\right) / F_{gu}, \\
F_{gu} &= 1 + 8 D_{gu}\left(\frac{1}{f_{gur}} + \frac{1}{f_{gul}}\right) + \frac{48 D^2_{gu}}{f_{gur} f_{gul}}.
\end{aligned}
\tag{6.2-3}
$$

For the AFEN method and the TPEN method, we can also obtain the relationship between the homogeneous and heterogeneous partial currents. The homogeneous and heterogeneous surface fluxes are related as

$$\psi_{gus} = \frac{\psi_{gus}^{het}}{f_{gus}}. \tag{6.2-4}$$

Also recall that the homogeneous and heterogeneous net currents at a node interface are identical and each surface flux is expressed by its partial currents:

$$\begin{aligned} J_{gus}^{net} &= j_{gus}^{+} - j_{gus}^{-} = j_{gus}^{het,+} - j_{gus}^{het,-}, \\ \psi_{gus} &= 2\,(j_{gus}^{+} + j_{gus}^{-}),\ \psi_{gus}^{het} = 2\,(j_{gus}^{het,+} + j_{gus}^{het,-}). \end{aligned} \tag{6.2-5}$$

Then, we can derive the relationship between the homogeneous and heterogeneous partial currents:

$$\begin{aligned} j_{gul}^{-m} &= \left(\frac{1}{f_{gul}} + 1\right) j_{gul}^{-m,het} + \left(\frac{1}{f_{gul}} - 1\right) j_{gul}^{+m,het} \Big/ 2, \\ j_{gul}^{+m} &= \left(\frac{1}{f_{gul}} - 1\right) j_{gul}^{-m,het} + \left(\frac{1}{f_{gul}} + 1\right) j_{gul}^{+m,het} \Big/ 2. \end{aligned} \tag{6.2-6}$$

6.3 Cross Section Representation

The two-group assembly homogenized cross sections are generated from single fuel assembly calculations based on the multi-group neutron transport theory. To make use of these cross sections in a dimensional code, they need to be functionalized with some variation parameters. In MASTER-3.0, microscopic cross sections at a certain burnup are determined by the following formula:

$$\begin{aligned}\sigma(ppm, T_f, T_m, \rho_m) = \sigma(ppm_0, T_{f0}, T_{m0}, \rho_{m0}) \\ + \frac{\partial\sigma}{\partial ppm}(ppm - ppm_0) + \frac{\partial\sigma}{\partial\sqrt{T_f}}(\sqrt{T_f} - \sqrt{T_{f0}}) \\ + \frac{\partial\sigma}{\partial T_m}(T_m - T_{m0}) + \frac{\partial\sigma}{\partial\rho_m}(\rho_m - \rho_{m0})\end{aligned} \qquad (6.3\text{-}1)$$

where $\sigma(ppm_0, T_{f0}, T_{m0}, \rho_{m0})$ = microscopic cross section at the reference state,

ppm_0 = boron concentration at the reference conditions,

T_{f0} = fuel temperature at the reference conditions,

T_{m0} = moderator temperature at the reference conditions,

ρ_{m0} = moderator density at the reference conditions.

The macroscopic group constants used in the flux calculation are obtained by combining the number densities, microscopic cross sections and feedback terms. The cross sections are assumed to vary linearly with boron concentration, moderator temperature, moderator density, the square root of the fuel temperature. In case of the moderator temperature variation, however, more than two variation points can be established to cover a wide range of moderator temperature from room temperature to the maximum temperature in a core because it is known that the change of microscopic cross sections with moderator temperature variations are not linear.

7. Reflector Representation

7.1 Equivalent Reflector Cross Sections

MASTER-3.0 uses the equivalent homogenized reflector cross sections [22,23,24,25] based on the simplified equivalence theory (SET). The homogenized reflector cross sections are generated to preserve the response matrix of the heterogeneous geometry at the interface of core and reflector.

The reflector homogenization problem can be simplified to the 1-dimensional 2-group spectral geometry as shown in Fig. 7-1. Since the transverse leakages are zero in the 1-dimensional geometry, the 2-group diffusion equation at the interface of core and reflector can be written as

$$\begin{aligned} \frac{D_1^{het}}{f_1}\frac{\partial^2\phi_1(x)}{\partial x^2} - \frac{\Sigma_{a1}^{het}+\Sigma_{12}^{het}}{f_1}\phi_1(x) &= 0 \\ \frac{D_2^{het}}{f_2}\frac{\partial^2\phi_2(x)}{\partial x^2} - \frac{\Sigma_{a2}^{het}}{f_2}\phi_2(x) + \frac{\Sigma_{12}^{het}}{f_1}\phi_1(x) &= 0 \end{aligned} \qquad (7.1\text{-}1)$$

where f_g = heterogeneity factor of group g using the boundary condition at $x = x_b$,

$$\left.\frac{\partial\phi_g}{\partial x}\right|_{x=x_b} = 0 \qquad (7.1\text{-}2)$$

The analytic solution of Eq. (7.1-1) can easily be achieved as follows:

$$\begin{aligned} \phi_1(x) &= A_1(\sinh w_1 x - \coth w_1 x_b \cosh w_1 x) \\ \phi_2(x) &= K A_1(\sinh w_1 x - \coth w_1 x_b \cosh w_1 x) \\ &\quad + A_2(\sinh w_2 x - \coth w_2 x_b \cosh w_2 x) \end{aligned} \qquad (7.1\text{-}3)$$

where $w_1 = \sqrt{\frac{\Sigma_{a1}^{het} + \Sigma_{12}^{het}}{D_1^{het}}}$, $w_2 = \sqrt{\frac{\Sigma_{a2}^{het}}{D_2^{het}}}$, $K \equiv \frac{(\Sigma_{12}^{het}/f_1)/(D_2^{het}/f_2)}{w_2^2 - w_1^2}$

The response matrix ($R_{gg'}$) between fluxes and net currents can be defined at two different heterogeneous regions, fuel and shroud.

$$\phi_g^{het,n}(x) = \sum_{g'} R_{gg'}^{het} J_{g'}^{het,n}(x) \tag{7.1-4}$$

where the superscript n (= 1,2) denotes the two different calculations performed with different fuel characteristics such as an enrichment variation.

Using the net current definition at the interface

$$J_g(0) = -\frac{D_g}{f_g}\frac{\partial \phi_g}{\partial x}\bigg|_{x=0} \tag{7.1-5}$$

and Eq. (7.1-4) we can get the response matrix coefficients which are composed of 4 unknowns, f_g and D_g (g = 1,2). In order to derive a homogenized representation for the heterogeneous reflector, the equivalent flux solutions has the same reflector response matrix coefficients as those in the heterogeneous reflector geometry.

$$R_{gg'} = R_{gg'}^{het} \tag{7.1-6}$$

If f_1 is set to be unity due to no source term, we can compute f_2 and D_g (g=1,2) and determine the equivalent cross section for the reflector.

$$D_1^{eq} = D_1, \quad D_2^{eq} = D_2/f_2 \tag{7.1-7}$$
$$\Sigma_{a1}^{eq} = \Sigma_{a1}, \quad \Sigma_{a2}^{eq} = \Sigma_{a2}/f_2, \quad \Sigma_{12}^{eq} = \Sigma_{12}$$

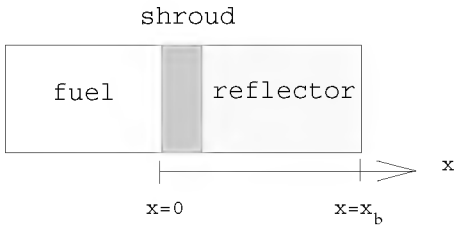

Figure 7-1 One-Dimensional Spectral Geometry of Reflector

7.2 Radial Reflector Constants

The equivalent reflector cross sections are not dependent on coolant temperature and density, but on boron concentration dissolved and shroud thickness. It is known that the reflector thickness has little influence on the equivalent cross sections if it is large enough. To avoid the frequent preparation of the equivalent reflector cross sections, the correlation is established through the variation calculations with the boron concentration dissolved in the reflector and the steel shroud thickness

$$f(x) = a_0 + a_1 x + a_2 x^2 \qquad (7.2\text{-}1)$$

where x = steel shroud thickness (cm).

However, this correlation is not valid for the corner reflector region faced with two fuel assemblies. Even though the 2-dimensional spectral geometry is investigated in the same manner as the 1-dimensional case, only the removal cross sections is simply corrected to account for the change of steel-to-water ratio

$$c = \frac{\ell_{FA} - t_s}{\ell_{FA}} \tag{7.2-2}$$

where ℓ_{FA} = side length of a fuel assembly,

t_s = shroud thickness.

According to the analyses, the fast absorption, thermal transport and absorption cross section have a linear relationship to the boron concentration, whereas the fast transport and scattering cross sections show no dependence on it. Thus the constant boron derivative is used to describe the variation of reflector cross sections.

7.3 Axial reflector Cross Sections

The generation of the axial reflector cross sections is basically the same as that of the radial reflector except that they are expressed with microscopic cross sections. If only the quantities and properties of structure materials within the top and bottom axial reflector regions are known, one can easily calculate the microscopic cross sections representing the axial reflectors using CASMO-3 [26,27] or HELIOS [28] in the similar manner to an edge-type of radial reflector. As a result, the axial reflector cross sections are composed of H_20, B-10 and a structure material. The difference of cross sections between top and bottom due to the contents of structure materials can be neglected and has little effect on the axial and radial quantities as well as the core average ones. The volume fraction of the water and the dissolved boron concentration are the same as in the interior core region.

8. Corner flux Evaluation

8.1 Method of Successive Smoothing

8.1.1 Cartesian Geometry

In order to construct flux corner values, a rough estimate for the corner flux ϕ_{00}^{i} is made by linear extrapolation from each of the nodes surrounding the corner concerned. These estimates are then averaged with weighting factors to be chosen appropriately. Using the Method of Successive Smoothing (MSS) method [8] in the Cartesian geometry as show in Fig. 8-1, ϕ_{00} is determined as:

$$\phi_{00} = \sum_{i=1}^{4} w_i \phi_{00}^{i} \tag{8.1-1}$$

where $\phi_{00}^{1} = \psi_A + \psi_B - \overline{\phi^{1}}$, $\phi_{00}^{2} = \psi_B + \psi_C - \overline{\phi^{2}}$,

$\phi_{00}^{3} = \psi_C + \psi_D - \overline{\phi^{3}}$, $\phi_{00}^{4} = \psi_D + \psi_A - \overline{\phi^{4}}$,

ψ_X = surface average flux at face X,

$\overline{\phi^{n}}$ = node average flux in node n.

Another way to construct the corner fluxes is as follows:

$$\phi_{00}^{1} = \psi_A \psi_B / \overline{\phi^{1}}, \quad \phi_{00}^{2} = \psi_B \psi_C / \overline{\phi^{2}} \tag{8.1-2}$$

$$\phi_{00}^{3} = \psi_C \psi_D / \overline{\phi^{3}}, \quad \phi_{00}^{4} = \psi_D \psi_A / \overline{\phi^{4}}$$

In practice, an arithmetic weighting with w_i = 0.25 in the fast group and weighting with diffusion constants $w_i = D_i / \sum_i D_i$ in the thermal group have proved to be the best choice for quadratic geometry. [29]

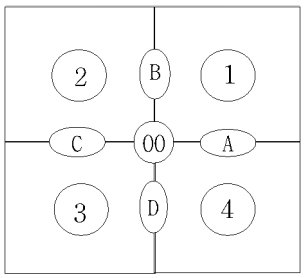

Figure 8-1 Four Adjacent Nodes in Cartesian Geometry

8.1.2 Hexagonal Geometry

The calculation of flux values at the vertices of the hexagonal fuel assemblies [30] is similar to that of rectangular fuel assemblies. The corner flux of a node, ϕ_{00}, in the Hexagonal geometry is derived by appropriate linear combinations of surface fluxes and node average flux

$$\phi_{00} = \sum_{i=1}^{3} w_i \phi_{00}^i \qquad (8.1\text{-}3)$$

where $\phi_{00}^1 = \frac{17}{26}\psi_A + \frac{17}{26}\psi_B - \frac{8}{26}\overline{\phi^1}$, $\phi_{00}^2 = \frac{17}{26}\psi_B + \frac{17}{26}\psi_C - \frac{8}{26}\overline{\phi^2}$,

$\phi_{00}^3 = \frac{17}{26}\psi_C + \frac{17}{26}\psi_D - \frac{8}{26}\overline{\phi^3}$,

ψ_X = surface average flux at face X,

$\overline{\phi^n}$ = node average flux in node n,

with $w_i = D_i / \sum_i D_i$.

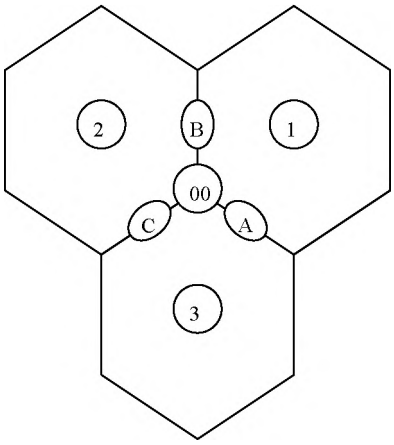

Figure 8-2 Three Adjacent Nodes in Hexagonal Geometry

8.2 Corner-Point Balance Method

8.2.1 Cartesian Geometry

The vertex flux of a node must be known ahead of the determination of cross terms of the flux expansion. MSS having been employed in MASTER-3.0 approximates the node vertex flux by a linear extrapolation of the surface-averaged and node-averaged fluxes. It then determines the common vertex flux of four adjacent nodes by taking the arithmetic average of the vertex fluxes. This approach is not accurate enough in the cases where neutron flux varies very rapidly around the vertex because the arithmetically averaged value is quite different from the vertex values resulting from the adjacent nodes by MSS. This deficiency can be overcome by using the multi-dimensional flux expansion and then evaluating the vertex flux based on the neutron balance within a small box around the vertex which is shared by four adjacent nodes [7]. The neutron balance in the small box is fairly equivalent to the leakage balance at its surfaces if it is quite small without any singular source. The leakage balance is expressed as:

$$L_g^1 + L_g^2 + L_g^3 + L_g^4 = 0 \qquad (8.2\text{-}1)$$

where L_g^i = the net neutron leakage out of the node i.

The multi-dimensional flux expansion can be expressed by the spatially nonseparable quartic polynomial or more complicated expansion used in AFEN. In this study, the following quartic polynomial is used for all the solution options: NEM, NIM and AFEN.

$$\phi_g(x,y) = \sum_{i,j=0}^{i+j\le 4} C_{gij}\,\xi_i\left(\frac{x}{a_x}\right)\xi_j\left(\frac{y}{a_y}\right) \tag{8.2-2}$$

where $\xi(x)$ is the same function as in Eq. (2.1-4). The coefficients for both i and j > 0 are referred to as the cross terms which can be approximated using neutron fluxes at the four vertices of the node. Once all expansion coefficients of the above equation are known, the transverse leakage is obtained in a straightforward manner. Therefore, the net neutron leakage out of the node i in a small box can finally be written as:

$$\begin{aligned} L_g^i = & -4\,D_g^i\left[\frac{dy^i}{a_x^i}+\frac{dx^i}{a_y^i}\right]\phi_{g00}^i - 2D_g^i\frac{dy^i}{a_x^i}\phi_{g10}^i - 2D_g^i\frac{dx^i}{a_y^i}\phi_{g01}^i \\ & -6\,D_g^i\left[\frac{dy^i}{a_x^i}+\frac{dx^i}{a_y^i}\right]\bar{\phi}_g^i \\ & +2\,D_g^i\left[3\frac{dy^i}{a_x^i}+2\frac{dx^i}{a_y^i}\right]\psi_{gxl}^i + 2\,D_g^i\left[2\frac{dy^i}{a_x^i}+3\frac{dx^i}{a_y^i}\right]\psi_{gyl}^i \\ & +2D_g^i\frac{dy^i}{a_x^i}\psi_{gxr}^i + 2D_g^i\frac{dx^i}{a_y^i}\psi_{gyr}^i \end{aligned} \tag{8.2-3}$$

The substitution of Eq. (8.2-3) into Eq. (8.2-1) yields exact set of equations for the vertex fluxes in terms of node-averaged and surface-averaged fluxes, diffusion coefficients and node sizes of four adjacent nodes. The resulting vertex fluxes are used to solve the transverse leakage profile more accurately for NIM and NEM and to complete the nodal coupling equation at corner points for AFEN.

8.2.2 Hexagonal Geometry

The multi-dimensional flux expansion can be expressed by the spatially nonseparable quartic polynomial or more complicated expansion used in AFEN. In MASTER-3.0, the following quartic polynomial is used for hexagonal geometry [13]. The basis polynomials are chosen such that they are even or odd in the directions and are linearly independent to their 120 degree symmetric functions.

$$\begin{aligned}\phi(x,y) = C_g &+ A^x_{g1}\xi_{10}(x) + B^x_{g1}\xi_{20}(x) + A^x_{g2}\xi_{01}(y) + B^x_{g2}\xi_{02}(y) \\ &+ A^p_{g1}\xi_{10}(p) + B^p_{g1}\xi_{20}(p) + A^p_{g2}\xi_{01}(q) + B^p_{g2}\xi_{02}(q) \\ &+ A^u_{g1}\xi_{10}(u) + B^u_{g1}\xi_{20}(u) + A^u_{g2}\xi_{01}(v) + B^u_{g2}\xi_{02}(v)\end{aligned} \tag{8.2-4}$$

where $\xi_{10}(x) = x^3 + x$, $\xi_{20}(x) = x^4 + x^2$, $\xi_{01}(x) = x^3 - x$, $\xi_{02}(x) = x^4 - x^2$.

The thirteen coefficients are easily determined by one node-average flux, six surface average fluxes and six corner-point fluxes. It is based on the neutron leakage balance within a very small triangle around the corner point without any singular source.

$$L^1_g + L^2_g + L^3_g = 0 \tag{8.2-5}$$

where L^n_g = net neutron leakage out of the node n. For example, the corner-point flux at the top-most location perpendicular to x-direction is

$$\begin{aligned}\phi_{x,r} = {} & w_1\bar{\phi} + w_2\phi_{x,l} + w_3(\phi_{p,l} + \phi_{u,l}) + w_4(\phi_{p,r} + \phi_{u,r}) \\ & + w_5(\hat{\phi}_{p,r} + \hat{\phi}_{u,l}) + w_6(\hat{\phi}_{p,l} + \hat{\phi}_{u,r}) + w_7(\hat{\phi}_{x,l} + \hat{\phi}_{x,r})\end{aligned} \tag{8.2-6}$$

where $\phi_{d,s}$ = corner-point flux at the top(bottom)-most location (s = r (l)) perpendicular to d-direction,

$\hat{\phi}_{d,s}$ = surface flux in d-direction at surface s,

$\bar{\phi}$ = node average flux,

w_i = coupling coefficient.

9. Reconstruction of Pin Information

The interpolation techniques for the reconstruction of local pin fluxes and power from a coarse mesh nodal solution are described in this section. Knowledge of detailed pin information is essential for accurate calculations of peaking factors and detector reaction rates for tracking of individual pins and for Departure from Nucleate Boiling (DNB) evaluation.

The reconstruction is based on the following procedure [31] : First, the global node average flux distribution is found. Second, the local homogeneous flux shape within each node is computed by solving the diffusion equation assuming homogeneous material properties. The boundary conditions to the local problem are provided by the global solution. Finally, the node heterogeneity is then accounted for by modulating the local homogeneous flux with form functions describing the fine structure of the assembly. This procedure is directly applied to the local heterogeneous flux and power distribution. The heterogeneous pin burnup is accumulated using integration of the calculated heterogeneous pin power over time.

9.1 Local Homogeneous Information

9.1.1 Cartesian Geometry

Most of those methods are accurate enough in cases where the flux gradients are not steep, but they lead to intolerable errors in case of the rodded fuel assemblies and especially the loading pattern of Mixed Oxide (MOX) fuel assemblies showing very large thermal flux gradients at the node edges.

The analytic solution method (AS) by use of corner flux evaluation with MSS [29] or CPB [7] is based on analytical functions which fulfill the diffusion equation in each interior point of a node. They are referred as MSS-AS and CPB-AS, respectively. Its interpolation

function requires 8 coefficients per energy group which are constructed from the 4 corner flux values and the 4 node surface average flux values. The local interpolation is in principle a 3-dimensional problem. However, the expenditure of solving the 3-dimensional problem can be reduced by assuming that the radial (x,y)-direction and the axial(z)-direction are separable. Then we can reduce a 3-dimensional problem to a 2-dimensional one.

The stationary diffusion equation with the assumption of constant material properties within a node is

$$\begin{aligned} \Delta\phi_1 - c_1\phi_1 + c_2\phi_2 &= 0 \\ \Delta\phi_2 + c_4\phi_1 - c_3\phi_2 &= 0 \end{aligned} \tag{9.1-1}$$

where $c_1 = \dfrac{\Sigma_{a1} + \Sigma_{12} - \nu\Sigma_{f1}/k + (1/\bar{\phi}_1)\sum_{s=l,r}(j_{1zs}^{out} - j_{1zs}^{in})/a_z}{D_1}$, $\quad c_2 = \dfrac{\nu\Sigma_{f2}/k}{D_1}$,

$c_3 = \dfrac{\Sigma_{a2} + (1/\bar{\phi}_2)\sum_{s=l,r}(j_{2zs}^{out} - j_{2zs}^{in})/a_z}{D_2}$, $\quad c_4 = \dfrac{\Sigma_{12}}{D_2}$.

The $\bar{\phi}_g$ is the node average flux and j_{gzs}^{out} and j_{gzs}^{in} are the outgoing and incoming partial currents in z-direction at the left (s=l) and right (s=r) node boundaries, respectively. The nodal coarse mesh methods provide the nodal flux functions for each calculated node.

$$r(x) = \frac{1}{a}\int_{-\frac{a}{2}}^{\frac{a}{2}} \phi(x,y)\,dy \tag{9.1-2}$$

$$s(y) = \frac{1}{a}\int_{-\frac{a}{2}}^{\frac{a}{2}} \phi(x,y)\,dx$$

Using the information derived from $r(x)$ and $s(y)$, we can construct an interpolation

function $\phi(x, y)$ within a node.

Using the functions

$$\phi_1 = \eta_1 + \alpha\eta_2 \qquad (9.1\text{-}3)$$
$$\phi_2 = \beta\ \eta_1 + \eta_2$$

where $\alpha = \frac{c_2}{c_1 - \kappa_2{}^2}$, $\beta = \frac{c_4}{c_3 - \kappa_1{}^2}$.

Eq. (9.1-1) can be simplified as

$$\Delta\eta_1 = \kappa_1{}^2\eta_1 \qquad (9.1\text{-}4)$$
$$\Delta\eta_2 = \kappa_2{}^2\eta_2$$

where $\kappa_1{}^2 = \frac{c_1 + c_3}{2} - \sqrt{(\frac{c_1 - c_3}{2})^2 + c_2c_4}$, $\kappa_2{}^2 = \frac{c_1 + c_3}{2} + \sqrt{(\frac{c_1 - c_3}{2})^2 + c_2c_4}$.

The basic functions of Eq. (9.1-4) are given by

$$w_1 = \sinh\kappa_g\xi_i \qquad \text{for} \quad \kappa_g^2 > 0, \kappa_g = \sqrt{\kappa_g^2} \qquad (9.1\text{-}5a)$$
$$w_2 = \cosh\kappa_g\xi_i$$

or

$$w_1 = \sin\kappa_g\xi_i \qquad \text{for} \quad \kappa_g^2 < 0, \kappa_g = \sqrt{-\kappa_g^2} \qquad (9.1\text{-}5b)$$
$$w_2 = \cos\kappa_g\xi_i$$

where $\xi_i = x\cos\alpha_i + y\sin\alpha_i$, $i = 1, 2, ...$

The functions η_g can be approximated in the following form

$$\eta_g^{2n} = \sum_{i=1}^{n} \sum_{k=1}^{2} c_{ik} w_k(\alpha_i, \kappa_g, x, y) \tag{9.1-6}$$

The coefficients of Eq. (9.1-6) are determined by boundary conditions. For a Cartesian geometry α_i is recommended by the symmetry of the node.

$$\alpha_1 = 0^\circ$$
$$\alpha_i = \alpha_{i-1} + 45^\circ, \quad i = 2, 3, 4$$

Since Eq. (9.1-6) does not reproduce exactly the average nodal flux value resulting from the nodal calculation such as NEM, NIM and ANM, the equation is transformed with a constant so that the average nodal flux value can be preserved. This is called as the improved analytic solution method (IAS) [32].

$$\eta_g = c_{0g} + \sum_{i=1}^{4} \sum_{k=1}^{2} d_{ik} w_k(\alpha_i, \kappa_g, x, y) \tag{9.1-7}$$

Using the addition theorem of sine, cosine and hyperbolic functions Eq. (9.1-7) can be rewritten as

$$\begin{aligned} \eta_g = {} & c_{0g} + c_{1g}SN\kappa_g x + c_{2g}CS\kappa_g x + c_{3g}SN\kappa_g y + c_{4g}CS\kappa_g y \\ & + c_{5g}SN\frac{\sqrt{2}}{2}\kappa_g x SN\frac{\sqrt{2}}{2}\kappa_g y + c_{6g}SN\frac{\sqrt{2}}{2}\kappa_g x CS\frac{\sqrt{2}}{2}\kappa_g y \\ & + c_{7g}CS\frac{\sqrt{2}}{2}\kappa_g x\ SN\frac{\sqrt{2}}{2}\kappa_g y + c_{8g}CS\frac{\sqrt{2}}{2}\kappa_g x\ CS\frac{\sqrt{2}}{2}\kappa_g y \end{aligned} \tag{9.1-8}$$

where SN and CS are trigonometric functions for $\kappa_g^2 < 0$ and they are hyperbolic functions for $\kappa_g^2 > 0$.

The nine unknown expansion coefficients per energy group c_{ig} are determined by using the boundary conditions such as node average, four edge average and four corner values which in turn can be calculated by means of the corresponding fluxes.

In order to construct flux corner values, a rough estimate for the corner flux ϕ^{i}_{00} is made by either linear extrapolation (MSS) or CPB method from each of the nodes surrounding the corner concerned. With the notation of the corner fluxes ϕ_{ij} (i,j = 0,1) and the edge fluxes ψ_{us} (u = x,y; s = r,l) as defined in Fig. 9-1 the coefficients in Eq. (9.1-8) for the case $\kappa_g^2 > 0$ becomes

$$
\begin{aligned}
c_{0g} &= \bar{\eta}_g - (c_{2g} + c_{4g})\frac{\sinh A}{A} - c_{8g}\frac{\sinh^2 B}{B^2} \\
c_{1g} &= \frac{\frac{\sinh B}{B}(\eta_{00} + \eta_{01} - \eta_{10} - \eta_{11}) + 2\cosh B(\eta_{xr} - \eta_{xl})}{4\sinh A(\cosh B - \frac{\sinh B}{B})} \\
c_{2g} &= \frac{\frac{\sinh B}{B}Q_1 - (\cosh B + \frac{\sinh B}{B})Q_2 + 4\cosh B\bar{\eta}_g}{4(\cosh A - \frac{\sinh A}{A})(-\cosh B + \frac{\sinh B}{B})} + \frac{\eta_{xr} + \eta_{xl} - \eta_{yr} - \eta_{yl}}{4(\cosh A - \frac{\sinh A}{A})} \\
c_{3g} &= \frac{\frac{\sinh B}{B}(\eta_{00} + \eta_{10} - \eta_{01} - \eta_{11}) + 2\cosh B(\eta_{yr} - \eta_{yl})}{4\sinh A(\cosh B - \frac{\sinh B}{B})} \\
c_{4g} &= \frac{\frac{\sinh B}{B}Q_1 - (\cosh B + \frac{\sinh B}{B})Q_2 + 4\cosh B\bar{\eta}_g}{4(\cosh A - \frac{\sinh A}{A})(-\cosh B + \frac{\sinh B}{B})} - \frac{\eta_{xr} + \eta_{xl} - \eta_{yr} - \eta_{yl}}{4(\cosh A - \frac{\sinh A}{A})} \qquad (9.1\text{-}9) \\
c_{5g} &= \frac{\eta_{00} + \eta_{11} - \eta_{10} - \eta_{01}}{4\sinh^2 B} \\
c_{6g} &= \frac{\eta_{11} - \eta_{00} + \eta_{10} - \eta_{01} - 2(\eta_{xr} - \eta_{xl})}{4\sinh B(\cosh B - \frac{\sinh B}{B})}
\end{aligned}
$$

$$c_{7g} = \frac{\eta_{11} + \eta_{01} - \eta_{00} - \eta_{10} - 2(\eta_{yr} - \eta_{yl})}{4\sinh B(\cosh B - \frac{\sinh B}{B})}$$

$$c_{8g} = \frac{Q_1 - 2Q_2 + 4\bar{\eta}_g}{4(\cosh B - \frac{\sinh B}{B})^2}$$

where $A = \frac{a}{2}\kappa_g$, $B = \frac{\sqrt{2}}{2}\frac{a}{2}\kappa_g$,

$Q_1 = \eta_{11} + \eta_{01} + \eta_{00} + \eta_{10}$, $Q_2 = \eta_{xr} + \eta_{xl} + \eta_{yr} + \eta_{yl}$.

The results for the case $\kappa_g^2 > 0$ are obtained from the above equations by replacing sinh and cosh by sin and cos, respectively.

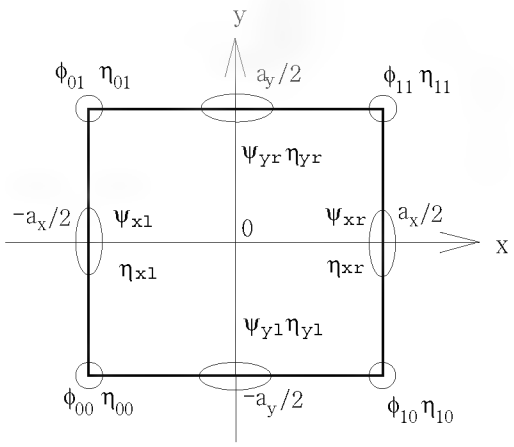

Figure 9-1 Corner and Edge Fluxes in Cartesian Geometry

9.1.2 Hexagonal Geometry

For the intra-nodal flux and power reconstruction for hexagonal fuel assemblies are basically the same as that of rectangular fuel assemblies. This method is AFEN method, which is equivalent to IAS [32] and uses MSS or CPB method for the corner flux evaluation. Since the corner fluxes are resulted from the AFEN nodal solution, the intra-nodal flux and power reconstruction is consistent to AFEN nodal solution as described in section 2.1.3.

9.2 Local Heterogeneous Information

The local heterogeneous flux shapes are not directly provided from the nodal solution, but obtained by the modulation method. The fine-mesh form functions for fuel assemblies are precalculated with zero net current boundary conditions.

$$f_g^{\phi,het}(x,y) = \phi_g^{het}(x,y)/\phi_g^{hom}(x,y) \tag{9.2-1}$$

Therefore, an approximation of the reconstructed flux distribution of the assembly in the global problem is obtained by the product of a global homogenized flux distribution and a local heterogeneous form function:

$$\phi_g^{het}(x,y) = f_g^{\phi,het}(x,y)\phi_g^{hom}(x,y) \tag{9.2-2}$$

The form function accounts for the assembly heterogeneity caused by water holes, burnable absorbers, enrichment variations, etc.. The power form functions are precomputed from single assembly calculations in the same manner as the flux form functions.

$$f^{p,het}(x,y) = \frac{P^{het}(x,y)}{P^{hom}(x,y)} \tag{9.2-3}$$

where $p^{hom}(x,y) = \sum_g \kappa\Sigma_{fg}^{hom}(x,y)\phi_g^{hom}(x,y)$.

On the contrary, however, the heterogeneous burnup distributions are calculated directly using the heterogeneous power distribution obtained.

Since cross sections and formfunctions are generated with idealized boundary conditions such as a zero net current boundary condition, the influence of neighboring assemblies is not considered. Even though the spectral influence between assemblies is not

so large in the core composing of UO_2 fuel only, it becomes serious in the cores including MOX fuels or the cores having loading patterns with large heterogeneity among assemblies. Therefore, the method accounting for the spectral history effect [33] should be implemented to enhance the accuracy of local information for those cores when reconstructing.

9.3 Pin Burnup Calculation

The local heterogeneous burnup within an assembly is not estimated by the modulation of the burnup form function, but is accumulated using the local heterogeneous power. The increase of local heterogeneous burnup at the position (x,y) is expressed as

$$\Delta B^{het}(x,y) = \frac{\bar{P}^{het}(x,y)}{\bar{P}} \overline{\Delta B} \qquad (9.3\text{-}1)$$

where $\bar{P}^{het}(x,y)$ = local heterogeneous power averaged over Δt at (x,y),

$\bar{P}$ = node average power over Δt,

$\overline{\Delta B}$ = increase of node average burnup corresponding to $\bar{P}$ $(= c\bar{P}P_{th}\Delta t)$,

P_{th} = thermal power (MWt),

Δt = depletion time interval (sec),

c = burnup conversion factor (MWD/kgU) $\left(= A_0 / \sum_i (M_i N_i)_{initial}\right)$,

A_0 = Avogadro's number,

M_i = atomic weight of heavy nuclide i,

N_i = number density of heavy nuclide i.

In order to get more accurate power during depletion, the pinwise power from the previous depletion step is averaged with that from the current one.

$$\overline{P}^{het}(x,y) = \frac{P_{n-1}^{het}(x,y) + P_{n}^{het}(x,y)}{2} \quad (9.3\text{-}2)$$

where the subscripts n-1 and n denote previous and current depletion steps, respectively.

10. Depletion

MASTER-3.0 has the microscopic depletion module consistent to CASMO-3 [26,27]. It contains depletion models for fuel, burnable poison, xenon, and samarium. The inventories of fuel and fission product nuclides can be obtained by solving their depletion chain equations.

The depletion equations are solved using the semi weighted predictor-corrector method (SWPC) or fully weighted predictor-corrector method (FWPC). FWPC consists of two steps of calculation stages: the predictor stage and the corrector stage. Both stages include a steady-state flux calculation and a depletion calculation. It should be noted that because σ and ϕ are varying during depletion, the average σ and ϕ over a time step must be accurately calculated.

As shown in Fig. 10-1, the predictor stage nuclide number density N_n corresponding to the burnup point B_n at time t_n are depleted to yield the predicted number density N^p_{n+1} with the microscopic cross section σ_n and the flux ϕ_n assumed to be constant during Δt. At time t_{n+1}, the predicted nuclide number density N^p_{n+1} leads to the determination of the predicted microscopic cross section σ^p_{n+1} and the flux ϕ^p_{n+1}. Since the constant cross section and flux during a given time interval is a rough assumption, the corrector flux ϕ^c_n and cross section σ^c_n for depletion are evaluated by weighting ϕ_n and σ_n at time t_n, and ϕ^p_{n+1} and σ^p_{n+1} at a predictor stage.

$$\phi^c_n = \omega\phi_n + (1-\omega)\phi^p_{n+1} \qquad (10\text{-}1)$$
$$\sigma^c_n = \omega\sigma_n + (1-\omega)\sigma^p_{n+1}$$

where the subscripts p, c = predictor, corrector,

ω = weighting factor.

Consequently the nuclide number density N_{n+1} and burnup B_{n+1} for the next time point t_{n+1} is determined with the present nuclide number densities and corrector microscopic cross sections together with corrector fluxes. The fixed weighting factor is used for most nuclides. However, for burnable poisons whose absorption cross sections vary significantly with time, the depletion is performed with less than 5-day time step size instead of using weighting factor.

SWPC is basically the same as FWPC except that the corrected fluxes ϕ_n^c are not estimated since flux variation during a depletion period are relatively small. MASTER-3.0 uses the SWPC by default to reduce the computing time with maintaining computation accuracy or the FWPC by option.

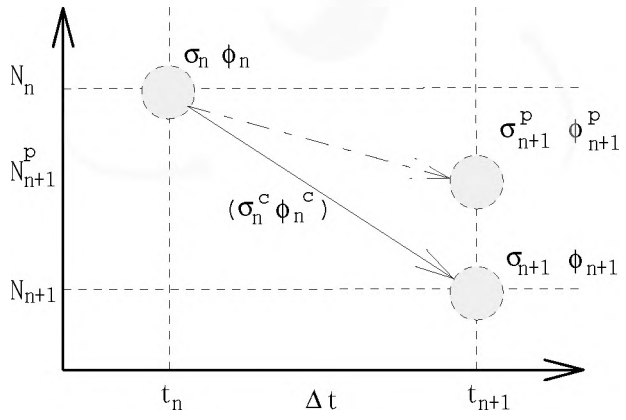

Figure 10-1 Predictor-Corrector Scheme

10.1 Heavy Nuclide Depletion

The heavy nuclide chain is largely composed of the U-235 chain and the U-238 chain [34]. The U-235 chain is coupled to the U-238 chain through Np-237 and Pu-238. The heavy nuclide chain, consisting of 11 nuclides as shown in Fig. 10-2.

Time dependent nuclide number densities are determined by the first order differential equation,

$$\frac{dN_i}{dt} = P_{i-1} N_{i-1} - R_i N_i \qquad (10.1\text{-}1)$$

where P_i = production rate of nuclide i $\left(\lambda_{i-1} + \sum_{i'} y_{ii'} \sum_g \sigma_{cgi'} \phi_g \right)$,

$y_{ii'}$ = yield fraction of nuclide i from nuclide i',

R_i = removal rate of nuclide i $\left(\lambda_i + \sum_g \sigma_{agi} \phi_g \right)$,

N_i = number density of nuclide i,

λ_i = decay constant of nuclide i,

σ_{cgi} = microscopic capture cross section of nuclide i in group g,

σ_{agi} = microscopic absorption cross section of nuclide i in group g.

The decay constants and fission product yields of nuclides are listed in Tables 10-1 and 10-2, respectively.

The analytic solution of the above equation can be expressed as

$$N_i = \sum_{j=1}^{i} a_{ij} \exp(-R_j \Delta t) \qquad (10.1\text{-}2)$$

where $a_{ij} = \frac{P_{i-1} a_{i-1j}}{R_i - R_j}$ when j < i,

$$a_{ii} = N_i \Delta t - \sum_{j=1}^{i-1} a_{ij} .$$

The decay constant and fission product yields of nuclides are listed in Tables 10-1 and 10-2, respectively.

Table 10-1 Decay Constants of Nuclides

Nuclide	Decay Constant	Nuclide	Decay Constant	Nuclide	Decay Constant
Pa-233	.2975E-6	Cm-242	.4922E-7	Xe-135	.2100E-4
Np-239	.3441E-5	Cm-244	.1213E-8	Pm-149	.3626E-5
Pu-241	.1536E-8	I-135	.2924E-4		

Table 10-2 Fission Product Yields of Nuclides

Nuclide	Pm-149	Sm-149	I-135	Xe-135	FP*
Th-232	.00882	.0	.05314	.00031	1.0
Pa-233	.00882	.0	.05314	.00031	1.0
U-233	.00777	.0	.04913	.01283	1.0
U-234	.01067	.0	.06298	.00242	1.0
U-235	.01067	.0	.06298	.00242	1.0
U-236	.01067	.0	.06298	.00242	1.0
Np-237	.01067	.0	.06298	.00242	1.0
U-238	.01608	.0	.06827	.00028	1.0
Pu-239	.01239	.0	.06447	.01152	1.0
Pu-240	.01239	.0	.06447	.01152	1.0
Pu-241	.01524	.0	.07068	.00231	1.0
Pu-242	.01524	.0	.07068	.00231	1.0

FP : Fission Product

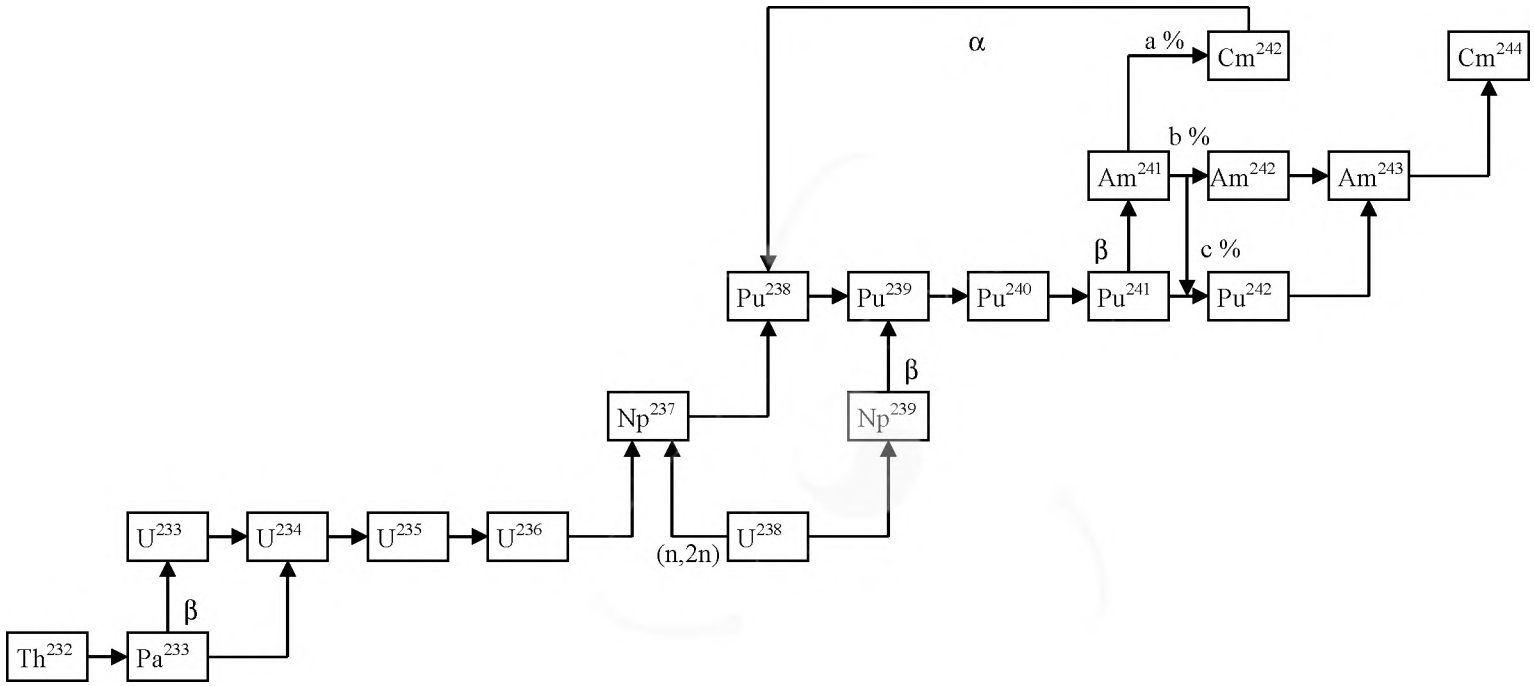

Figure 10-2. Chain Reaction of Heavy Nuclides

10.2 Burnable Absorber Depletion

Basically, the burnable absorber depletion equation is the same as that of the heavy nuclide chain. The burnable absorber such as a gadolinium having rapid change of their number densities during depletion would cause large error for large time step unless the thermal absorption cross section within a given depletion interval is well estimated. Therefore, the effective microscopic cross section versus number density table is more useful than macroscopic cross section versus burnup. The detailed Gadolinium isotopes chains are as follows:

$$\frac{\partial N^i}{\partial t} = -N^i \sigma_a^i \phi + N^{i-1} \sigma_a^{i-1} \phi \qquad (10.2\text{-}1)$$

where N^i = number density of nuclide Gd^i (i = 154 ~ 158),

σ_a^i = microscopic absorption cross section of nuclide Gd^i.

These five equations can be rearranged using the effective number density and cross section as

$$\frac{\partial N^{eff}}{\partial t} = -N^{eff} \sigma_a^{eff} \phi \qquad (10.2\text{-}2)$$

where $N^{eff} = \sum_{i=1}^{5} iN^i$, $\sigma_a^{eff} = (\sum_{i=1}^{5} N^i \sigma_a^i)/N^{eff}$.

In spite of using the effective quantities, a large error occurs in estimating gadolinium number densities around the burnout time. For this reason, MASTER-3.0 treats specially the microscopic cross section and depletion behaviors of burnable absorber in order to reduce the error coming from large time step.

10.3 Fission Product Chain

10.3.1 Xenon and Iodine Depletion

The differential equations of the fission product poison Xe^{135} and its precursor I^{135} are defined by the following:

$$\frac{dI(t)}{dt} = -\lambda_I I(t) + Y_I \Sigma_f \phi \tag{10.3-1}$$

$$\frac{dX(t)}{dt} = \lambda_I I(t) + Y_X \Sigma_f \phi - \lambda_X X(t) - \sigma_X^a \phi\ X(t)$$

where $I(t)$ = number density of I^{135},

$X(t)$ = number density of X^{135},

λ_I = decay constant of I^{135},

λ_X = decay constant of X^{135},

Y_I = yield fraction of I^{135},

Y_X = yield fraction of X^{135},

Σ_f = macroscopic fission cross section,

σ_X^a = xenon microscopic absorption cross section.

For equilibrium conditions, the number densities are calculated by

$$I_\infty = \frac{Y_I \Sigma_f \phi_0}{\lambda_I} \tag{10.3-2}$$

$$X_\infty = \frac{\lambda_I I_\infty + Y_X \Sigma_f \phi_0}{\lambda_X + \sigma_X^a \phi_0}$$

where I_∞ = number density of I^{135} at equilibrium state,

X_∞ = number density of X^{135} at equilibrium state,

$\phi_0 = \phi(t_0)$.

For transient conditions, the number densities at time t are determined by the following equations:

$$I(t) = I(t_0)e^{-\lambda_I \Delta t} + \frac{Y_I \Sigma_f \phi_0}{\lambda_I}\left[1 - e^{-\lambda_I \Delta t}\right] \tag{10.3-3}$$

$$X(t) = X(t_0)e^{-(\lambda_X + \sigma_X^a \phi_0)\Delta t} + \frac{(Y_I + Y_X)\Sigma_f \phi_0}{\lambda_X + \sigma_X^a \phi_0}\left[1 - e^{-(\lambda_X + \sigma_X^a \phi_0)\Delta t}\right]$$
$$+ \frac{(\lambda_I I(t_0) - Y_I \Sigma_f \phi_0)}{(\lambda_X + \sigma_X^a \phi_0 - \lambda_I)}\left[e^{-\lambda_I \Delta t} - e^{-(\lambda_X + \sigma_X^a \phi_0)\Delta t}\right]$$

where Δt = time interval.

10.3.2 Samarium and Promethium Depletion

The differential equations of the fission product Sm^{149} and its precursor Pm^{149} have the same form as those of Xe^{135} and I^{135}.

$$\frac{dP(t)}{dt} = -\lambda_P P(t) + Y_P \Sigma_f \phi \tag{10.3-4}$$

$$\frac{dS(t)}{dt} = \lambda_P P(t) - \sigma_S^a \phi\, S(t)$$

where $P(t)$ = number density of P^{149},

$S(t)$ = number density of S^{149},

λ_P = decay constant of P^{149},

Y_P = yield fraction of P^{149},

σ_S^a = samarium microscopic absorption cross section.

For equilibrium conditions, the solutions of the above equations simply become

$$P_{\infty} = \frac{Y_P \Sigma_f \phi_0}{\lambda_P}, \qquad (10.3\text{-}5)$$

$$S_{\infty} = \frac{\lambda_P P_{\infty}}{\sigma_S^a \phi_0} = \frac{Y_P \Sigma_f}{\sigma_S^a}$$

where P_{∞} = number density of P^{149} at equilibrium state,

S_{∞} = number density of S^{149} at equilibrium state.

For transient conditions, the number densities at time t are determined by the following equations:

$$P(t) = P(t_0)e^{-\lambda_P \Delta t} + \frac{Y_P \Sigma_f \phi_0}{\lambda_P}\left[1 - e^{-\lambda_P \Delta t}\right] \qquad (10.3\text{-}6)$$

$$S(t) = S(t_0)\, e^{-\sigma_S^a \phi_0 \Delta t} + \frac{Y_P \Sigma_f}{\sigma_S^a}\left[1 - e^{-\sigma_S^a \phi_0 \Delta t}\right]$$
$$+ \frac{(\lambda_P P(t_0) - Y_P \Sigma_f \phi_0)}{(\sigma_S^a \phi_0 - \lambda_P)}\left[e^{-\lambda_P \Delta t} - e^{-\sigma_S^a \phi_0 \Delta t}\right]$$

11. Burnup Correction Model

11.1 Cartesian Geometry

The modern coarse-mesh and nodal methods allow solving 3-dimensional global few-group LWR problems on an assembly-size mesh with an accuracy of the order of 1 % in the average assembly power densities. Since, however, this degree of accuracy is limited to fresh initial core conditions, appropriate corrections are introduced to account for the nonlinear effects resulting from depletion and neutronic feedback in higher cycles.

The burnup correction model [35] is essential for the accuracy of nodal methods. Calculations based on 4 nodes per FA without burnup correction model showed an errors in FA average power of up to 3% while the 1 node per FA calculations with burnup correction model reduce the errors to a level of about 1%. Especially the burnup correction is very effective in the large spatial nodes which have significant burnup gradients.

The burnup correction model considers the absorption and fission macroscopic cross sections not to be homogenous within the node but to vary due to local burnup effects. The flux and cross section functions are the 2nd order of polynomial expansions:

$$\begin{aligned}\phi(x,y,z) &= \bar{\phi} + a_{100}\xi_1(x) + a_{200}\xi_2(x) + a_{010}\xi_1(y) + a_{020}\xi_2(y) \\ &\quad + a_{001}\xi_1(z) + a_{002}\xi_2(z) \\ \Sigma(x,y,z) &= \bar{\Sigma} + s_{100}\xi_1(x) + s_{200}\xi_2(x) + s_{010}\xi_1(y) + s_{020}\xi_2(y) \\ &\quad + s_{001}\xi_1(z) + s_{002}\xi_2(z)\end{aligned} \qquad (11.1\text{-}1)$$

where $\bar{\phi}$ = volume average flux,

$\bar{\Sigma}$ = volume average macroscopic cross section,

$\xi_i(x)$ = the same function as described in Eq. (2.1-4),

a_{ijk} ,s_{ijk} = expansion coefficients.

The expansion coefficients of flux and macroscopic cross section in Eq. (11.1-1) can easily be obtained from the known values at node surfaces. In the nodal balance equation the reaction rate is expressed as

$$\frac{1}{V}\int_V \Sigma(x,y,z)\phi(x,y,z)dV = \bar{\Sigma}\bar{\phi} + \frac{1}{3}(s_{100}a_{100} + s_{010}a_{010} + s_{001}a_{001}) + \frac{1}{5}(s_{200}a_{200} + s_{020}a_{020} + s_{002}a_{002}) \quad (11.1\text{-}2)$$

Dividing Eq. (11.1-2) by the average flux leads to the definition of an effective flux-volume homogenized cross section which is used instead of the normal cross section in the nodal balance equation:

$$\Sigma^{eff} = \bar{\Sigma} + \frac{1}{\bar{\phi}}\left[\frac{1}{3}(s_{100}a_{100} + s_{010}a_{010} + s_{001}a_{001}) + \frac{1}{5}(s_{200}a_{200} + s_{020}a_{020} + s_{002}a_{002})\right] \quad (11.1\text{-}3)$$

Meanwhile, for the solution of the 1-dimensional equivalent diffusion equations the transverse integrated reaction rate is approximated by

$$M_u(u) = \frac{1}{a_v a_w}\int_0^{a_v}\int_0^{a_w}\Sigma(u,v,w)\phi(u,v,w)dvdw = \Sigma^{eff}\psi_u(u) + \delta_{1u}\xi_1(u) + \delta_{2u}\xi_2(u) \quad (11.1\text{-}4)$$

where $\psi_u(u) = \frac{1}{a_v a_w}\int_0^{a_v}\int_0^{a_w}\phi(u,v,w)dvdw$.

$\Sigma^{eff}\psi_u(u)$ is used in the momentum equations instead of $\bar{\Sigma}\psi_u(u)$ and the correction term of Eq. (11.1-4) is transferred to the right hand side of the momentum equations. The coefficients δ_{1u} and δ_{2u} can be determined by the boundary conditions at 0 and a_u.

$$M_x(0) = (\bar{\phi} - a_{100} - a_{200})(\bar{\Sigma} - s_{100} - s_{200}) + \frac{1}{3}(s_{010}a_{010} + s_{001}a_{001}) + \frac{1}{5}(s_{020}a_{020} + s_{002}a_{002}) \quad (11.1\text{-}5)$$

$$M_x(a_x) = (\bar{\phi} + a_{100} - a_{200})(\bar{\Sigma} + s_{100} - s_{200}) + \frac{1}{3}(s_{010}a_{010} + s_{001}a_{001}) + \frac{1}{5}(s_{020}a_{020} + s_{002}a_{002})$$

$$\delta_{1x} = s_{100}(\bar{\phi} - a_{200}) - (\Delta\Sigma + s_{200})a_{100} \quad (11.1\text{-}6)$$

$$\delta_{2x} = s_{200}(\bar{\phi} - \frac{4}{5}a_{200}) - \frac{2}{3}s_{100}a_{100} - \Delta\Sigma a_{200}$$

where $\Delta\Sigma = \Sigma^{eff} - \bar{\Sigma}$.

In the same manner, $M_u(0)$ and $M_u(a_u)$ can be obtained for u = y, z.

11.2 Hexagonal Geometry

The burnup correction model considers the absorption and fission macroscopic cross sections not to be homogenous within the node but to vary due to local burnup effects. To make the problem simple, flux and cross section functions are approximated with six terms as follows:

$$\phi(x,p,u,z) = \bar{\phi} + a_{1000}\zeta_1(x) + a_{2000}\zeta_2(x) + a_{0100}\zeta_1(p) + a_{0200}\zeta_2(p) + a_{0010}\zeta_1(u) + a_{0020}\zeta_2(u) + a_{0001}\zeta_1(z) + a_{0002}\zeta_2(z) \quad (11.2\text{-}1)$$

$$\Sigma(x,p,u,z) = \bar{\Sigma} + s_{1000}\zeta_1(x) + s_{2000}\zeta_2(x) + s_{0100}\zeta_1(p) + s_{0200}\zeta_2(p) + s_{0010}\zeta_1(u) + s_{0020}\zeta_2(u) + s_{0001}\zeta_1(z) + s_{0002}\zeta_2(z)$$

where $\zeta_1(x) = \sinh(\frac{2}{h_x}x)$, $\zeta_2(x) = \cosh(\frac{2}{h_x}x) - \frac{2}{3}(1-e)$,

$$u = -\frac{1}{2}x - \frac{\sqrt{3}}{2}y,\quad v = \frac{\sqrt{3}}{2}x - \frac{1}{2}y,\quad p = -\frac{1}{2}x + \frac{\sqrt{3}}{2}y,\quad q = -\frac{\sqrt{3}}{2}x - \frac{1}{2}y.$$

The expansion coefficients of flux and cross section can easily be obtained from the known values such as node-average and surface-average values. The reaction rate for the nodal balance equation is expressed in the same way as Cartesian geometry. The effective flux-volume homogenized cross section finally can be simply written as:

$$\Sigma^{eff} = \bar{\Sigma} + \frac{1}{\bar{\phi}} \sum_{i,j,k,m=0}^{1\le i+j+k+m\le 2} C_{ijkm} a_{ijkm} s_{ijkm} \qquad (11.2\text{-}2)$$

which is actually used in the nodal balance equation.

11.3 Adjoint Burnup Correction

11.3.1 Cartesian Geometry

In adjoint case the effective cross section are calculated using the forward flux expansion coefficients. The function $M_u^*(u)$ for the 1-dimensional equivalent adjoint diffusion equation is defined as

$$M_u^*(u) = \frac{1}{a_v a_w} \int_0^{a_v} \int_0^{a_w} \Sigma(u, v, w)\phi^*(u, v, w)\,dv\,dw \qquad (11.3\text{-}1)$$

where

$$\phi^*(x, y, z) = \bar{\phi}^* + a_{100}^* h_1(x) + a_{200}^* h_2(x) + a_{010}^* h_1(y) + a_{020}^* h_2(y) + a_{001}^* h_1(z) + a_{002}^* h_2(z).$$

In the same manner as the forward equation this function is approximated by

$$M_u^*(u) = \Sigma^{eff}\psi_u^*(u) + \delta_{1u}^* h_1(u) + \delta_{2u}^* h_2(u) \qquad (11.3\text{-}2)$$

where $\psi_u^*(u) = \frac{1}{a_v a_w} \int_0^{a_v} \int_0^{a_w} \phi^*(u,v,w)\,dv\,dw$.

The coefficients δ_{1u}^* and δ_{2u}^* are determined fulfilling the following boundary conditions.

$$M_u^*(0) = \Sigma^{eff}\psi_u^*(0) - \delta_{1u}^* - \delta_{2u}^* \qquad (11.3\text{-}3)$$
$$M_u^*(a_u) = \Sigma^{eff}\psi_u^*(a_u) + \delta_{1u}^* - \delta_{2u}^*$$

The final equations are similar to Eq. (11.1-6) of the forward case.

$$\delta_{1x}^* = s_{100}(\bar{\phi}^* - a_{200}^*) - (\Delta\Sigma + s_{200})a_{100}^* \qquad (11.3\text{-}4)$$
$$\delta_{2x}^* = s_{200}(\bar{\phi}^* - \frac{4}{5}a_{200}^*) - \frac{2}{3}s_{100}a_{100}^* - \Delta\Sigma a_{200}^*$$

where $\Delta\Sigma = \Sigma^{eff} - \bar{\Sigma}$.

11.3.2 Hexagonal Geometry

In the adjoint burnup correction model for the hexagonal geometry is basically the same as that of forward case. The effective flux-volume homogenized cross section can be obtained as Eq. (11-2.2) with the corresponding adjoint values.

12. Thermal Hydraulic Calculation

In MASTER-3.0 each radial node corresponds to an individual flow channel which is axially segmented at each plane. Thus, the thermal-hydraulic calculation is performed for each node in the active core as an outer iteration. The thermal-hydraulic calculation is composed of a heat balance calculation for moderator enthalpy and a calculation for average fuel temperature using a burnup versus linear power dependent correlation. MASTER-3.0 has an additional capability of calculating moderator and fuel temperature distributions using COBRA3-C/P [36,37,38] or MATRA [ ] which allows transient calculations considering cross flow effects between channels as well as subchannel analyses.

12.1 Enthalpy Calculation

The enthalpy rise is computed from the bottom of each channel to the top. (See Figure 12-1) To calculate the average enthalpy increment in each axial node the following equation can be defined.

$$h_i = h_0 + \sum_{k=1}^{i-1} \frac{P_k}{\dot{m}} \Delta Z_k + \frac{1}{2} \frac{P_i}{\dot{m}} \Delta Z_i \qquad (12.1\text{-}1)$$

where h_0 = inlet enthalpy (J/kg),

P_i = linear power density at node i (w/cm),

$\dot{m}$ = mass flow rate (kg/sec),

ΔZ_i = axial height of node i (cm).

The calculated enthalpy in a node is converted to the moderator state properties such as moderator temperature and density based on the ASME steam table.

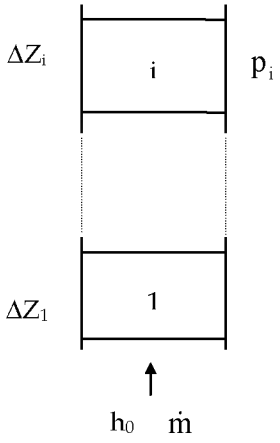

Figure 12-1 One-Dimensional Description for Enthalpy Calculation

12.2 Fuel Temperature Calculation

The fuel temperature is calculated with a burnup versus power dependent correlation prepared by a fuel performance analysis code which accounts for exposure and linear heat rate-dependent physical changes in the fuel pellet, clad and pellet-to-clad gap. The fuel temperature correlation has the polynomial form or the table form.

$$T_f = T_m + f(P, E) \tag{12.2-1a}$$

$$T_f = T_m + (\sum_{i=0}^{3} b_i E^i)P + (\sum_{i=0}^{3} c_i E^i)P^2 + (\sum_{i=0}^{3} d_i E^i)P^3 \tag{12.2-1b}$$

where T_m = moderator temperature (°C),

T_f = fuel temperature (°C),

$P = P_0 h_{gf}$ (KW/cm),

P_0 = linear power density (KW/cm),

h_{gf} = fraction of heat generated in the fuel,

E = fuel exposure (MWD/KgU),

b_i, c_i, d_i = precalculated polynomial coefficients specific to fuel type.

12.3 Feedback Model

Prior to the first neutronics calculation, the initial moderator and fuel thermal properties are determined based on the input values or the initial power distribution. The thermal feedback calculations follow each neutronics calculation whenever feedbacks are required. New moderator temperatures and densities are calculated from the heat generation rate of the fuel. Then, new fuel temperatures are determined using the fuel temperature correlation which is a function of power and burnup. Meanwhile, the cross section table contains microscopic cross sections evaluated at a reference state and their derivatives with respect to boron concentration, fuel temperature, and moderator temperature and density. The cross sections are assumed to vary linearly with those quantities for small changes about any given point. The dependence of the cross sections on the thermal-hydraulic parameters is approximated by the inclusion of the first derivative of the cross section (see section 6.3).

The update of moderator density leads to change of water and boron number densities.

$$N^{H_2O} = N_0^{H_2O} \frac{\rho_m}{\rho_{m0}} (1 + c(T_m - T_{m0})) \qquad (12.3\text{-}1a)$$

$$N^{B^{10}} = \frac{ppm}{10^6} * M_{H_20} * N^{H_20} * \frac{f_{B^{10}}}{f_{B^{10}} M_{B^{10}} + (1 - f_{B^{10}}) M_{B^{11}}} \qquad (12.3\text{-}1b)$$

where c = correction factor for thermal expansion,

ppm = boron concentration,

f_{B10} = natural abundance of B^{10} (19.80 a/o by default),

M_{H_20} = molecular weight of H_2O (=18.016 g),

$M_{B^{10}}$ = atomic weight of B^{10} (=10.0129 g),

$M_{B^{11}}$ = atomic weight of B^{11} (=11.0093 g).

12.4 COBRA3-C/P and MATRA Implementation

MASTER-3.0 has a capability of calculating the thermal-hydraulic quantities using COBRA3-C/P [36,37,38] or MATRA [39] by option. It allows three-dimensional transient calculations as well as subchannel analyses without any help of other codes and enables to keep the consistency between steady-state and transient results.

The conservation equations of the two-phase flow are expressed for the mixture quantities in 1-dimensional time-dependent form. The separated slip flow is assumed in each subchannel, and the void fraction distribution is evaluated as a function of enthalpy, heat flux and pressure. The fuel pin temperatures are calculated from the radial heat conduction equation, and their couplings to the coolant temperatures determining heat transfer dynamics are realized by appropriate models. The conservation equations for mass, momentum and energy are one-dimensional in axial direction. In COBRA3-C/P the basic conservation equation is simply described for a subchannel i connected to only one adjacent subchannel j.

The continuity equation can be written as

$$A_i \frac{\partial \rho_i}{\partial t} + \frac{\partial m_i}{\partial x} = -w_{ij} \qquad (12.4\text{-}1)$$

where A_i = cross flow area of subchannel i,

ρ_i = moderator density of subchannel i,

m_i = mass flow rate of subchannel i,

w_{ij} = diversion crossflow coming to subchannel i from neighboring subchannel j.

to express the mass balance taking into account the diversion crossflow w_{ij} per unit length. Since the turbulent crossflow doesn't contribute to net mass exchange, it is not included in this equation.

The energy equation is

$$\frac{1}{u_{eff}}\frac{\partial h_i}{\partial t}+\frac{\partial h_i}{\partial x}=\frac{q_i'}{m_i}-(h_i-h_j)\frac{w_{ij}^t}{m_i}-(T_i-T_j)\frac{c_{ij}}{m_i}+(h_i-h^*)\frac{w_{ij}}{m_i} \qquad (12.4\text{-}2)$$

where u_{eff} = effective velocity for energy transport,

w_{ij}^t = turbulent cross flow coming from neighboring subchannel j,

h = enthalpy,

T = temperature,

q′ = linear heat flux on the surface,

c_{ij} = thermal conduction coefficient,

h^* = enthalpy carried by diversion cross flow.

The axial momentum equation

$$\frac{1}{A_i}\frac{\partial m_i}{\partial t}-2u_i\frac{\partial \rho_i}{\partial t}+\frac{\partial p_i}{\partial x}=-\left(\frac{m_i}{A_i}\right)^2\left[\frac{\alpha v_i f_i \Phi_i}{2D_i}\right]+\frac{k_i v_i'}{2\Delta x}+A_i\frac{\partial}{\partial x}\left(\frac{v_i}{A_i}\right)''_{A\to B} \qquad (12.4\text{-}3)$$
$$-\rho_i g_c\cos\Theta-\frac{f_T}{A_i}(u_i-u_j)w_{ij}+\frac{1}{A_i}(2u_i-u^*)w_{ij}$$

where u = subchannel flow velocity,

u* = crossflow velocity,

ρ = two-phase density,

p = pressure,

k = grid-loss coefficient,

v = liquid specific volume,

v' = effective specific volume for momentum,

Φ = two-phase friction multiplier,

g_c = gravitational constant,

Θ = orientation of channel with respect to vertical,

f_T = turbulent momentum factor.

It includes the axial pressure gradient, its transient components, friction, spatial acceleration

and elevation pressure drop terms.

The transverse momentum equation

$$\frac{\partial w_{ij}}{\partial t} + \frac{\partial (u^{*} w_{ij})}{\partial x} + \left(\frac{s}{\ell}\right) C_{ij} w_{ij} = \left(\frac{s}{\ell}\right)(P_i - P_j) \qquad (12.4\text{-}4)$$

where $\frac{s}{\ell}$ = transverse momentum parameter,

P = pressure,

C_{ij} = loss of friction for transverse cross flow,

takes into account the momentum coupling between two adjacent subchannels. Setting the transverse momentum parameter to zero neglects the crossflow. This is equivalent to a conventional parallel channel model. To complete the system of conservation equations, included are correlations for single-phase friction factor and corresponding two-phase multiplier, spacer loss coefficients, and bulk and subcooled boiling void fraction. As for the crossflow calculation, the empirical models serve for determining forced and turbulent single- and two-phase mixing, and for specifying the parameters appearing in the transverse momentum equation.

For the detailed steady-state and transient thermal-hydraulic analysis of hexagonal geometry MATRA is used instead. MATRA is improved on the basis of COBRA-IV-I [40]. MATRA has been provided with an improved structure, various functions, and models to give more convenient user environment and to enhance the code accuracy. Among them, the pressure drop model has been improved to be applied to non-square-lattice rod arrays, and the models for the lateral transport between adjacent subchannels have been improved to enhance the accuracy in predicting two-phase flow phenomena. The applicability of MATRA code to rod bundles has been examined for various experimental data including flow blockage test, enthalpy and flow distribution tests under single-phase and two-phase conditions, and so on. One can refer the detailed methodologies of MATRA from the reference [39].

13. Iteration Strategy

13.1 Multi-level Coarse-mesh Rebalancing

The coarse-mesh rebalancing (CMR) is known as a very useful technique to accelerate an iterative convergence. The nodal balance equation with the leakage term is rewritten as

$$\begin{aligned}\Sigma_{rg}\phi_g(t)+\sum_u \frac{1}{a_u}\left[(j^+_{gur}-j^-_{gur})+(j^-_{gul}-j^+_{gul})\right]\\ =\sum_{g'<g}\Sigma_{g'g}\phi_{g'}(t)+\frac{1}{k}\sum_{g'}\Sigma_{pg'g}\phi_{g'}(t)+\sum_i \chi^i_{dg}\lambda_i C_i(t_0)e^{-\lambda_i\Delta t}\\ +\frac{e^{\omega\Delta t}}{v_g\Delta t}\phi_g(t_0)+S^{ext}_g\end{aligned} \qquad (13.1\text{-}1)$$

The iterative process to gain neutronics solution of Eq. (13.1-1) is based on the vectorized red-black Gauss-Seidel procedure. This solution procedure is applied only on the fine-mesh grid with usually a FA-mesh size. CMR is the simplest form of multi-level techniques. The CMR equations are obtained by introducing a coarse space-energy grid. Integrating Eq. (13.1-1) over mesh m and group g belonging to coarse-mesh block k, the CMR equations can be written

$$(R_k+\sum_u\sum_{s=l,r} j^{out}_{kus}-\frac{1}{k}P_k)d_k=\sum_{k'}\sum_u\sum_{s=l,r} j^{out}_{k'us}d_{k'}+S_k \qquad (13.1\text{-}2)$$

where $R_k=\sum_m\sum_g[(\Sigma_{ag}+\frac{1+\omega\Delta t}{v_g\Delta t})\phi_g(t)V]_m$, $m\in k$,

$P_k=\sum_m\sum_g\sum_{g'}(\Sigma_{pg'g}\phi_{g'}(t)V)_m$,

$S_k=\sum_m\{\sum_g\sum_i[\chi^i_{dg}\lambda_i C_i(t_0)e^{-\lambda_i\Delta t}+\frac{e^{\omega\Delta t}}{v_g\Delta t}\phi_g(t_0)+S^{ext}_g]V\}_m$,

$j^{out}_{kul}=\sum_m\sum_g(\frac{1}{a_u}j^-_{gul}V)_m$ for m boxes on left surface of box k,

$$j_{kur}^{out} = \sum_{m} \sum_{g} \left(\frac{1}{a_u} j_{gur}^{+} V\right)_m \quad \text{for m boxes on right surface of box k.}$$

The incoming currents of block k become the outgoing currents of block k' adjacent to k. They are multiplied by the driving factor $d_{k'}$ of these blocks which are the solutions of Eq. (13.1-2). Only a few interactions are performed on each level, but Eq. (13.1-2) on the coarsest grid should be solved exactly. If the coarsest grid becomes one-dimensional one, the eigenvalue is calculated by the Wielandt's method. Through repeating the restriction to coarser levels and the prolongation to finer levels the overall solution process is accelerated. The CMR acceleration is used for the nodal solution methods such as NEM, NIM and AFEN.

13.2 Asymptotic Extrapolation

The asymptotic extrapolation serves optionally for an additional acceleration of the neutronics iterative solution procedure. It is carried out on the finest-mesh and performed for partial currents, transverse leakages and average neutron fluxes. The asymptotic solution is approximated by three successive solutions on the finest-mesh if the asymptotic behavior of the flux convergence is achieved. This can be applied for the NEM, NIM and AFEN nodal solution methods.

14. Kinetic Parameters

MASTER-3.0 calculates effective delayed neutron fractions, delayed neutron precursor decay constants by solving forward and adjoint diffusion equations. The delayed neutron yields are given by

$$\beta_i = \frac{\int_V \sum_j \sum_g \beta_{ig}^j \nu\Sigma_{fg}^j \phi_g \, dV}{\int_V \sum_j \sum_g \nu\Sigma_{fg}^j \phi_g \, dV} \tag{14-1}$$

where β_{ig}^j = fraction of fission neutrons from the j-th nuclide in precursor group i from group g,

$\nu\Sigma_{fg}^j$ = macroscopic fission cross section for the j-th nuclide in group g.

The effective delayed neutron fraction is then

$$\beta_{eff,\,i} = \frac{\int_V \sum_j \sum_g \phi_g^* \chi_{ig} \beta_{ig}^j \nu\Sigma_{fg}^j \phi_g \, dV}{\int_V ((1 - \sum_i \beta_i) \sum_g \phi_g^* \chi_g + \sum_i \beta_i \sum_j \sum_g \phi_g^* \chi_{ig}) \nu\Sigma_{fg}^j \phi_g \, dV} \tag{14-2}$$

where ϕ_g^* = adjoint average flux for group g,

χ_{ig} = neutron spectrum for delayed group i from group g,

χ_g = prompt neutron fission spectrum from group g.

The total effective delayed neutron fraction is then

$$\beta_{eff} = \sum_i \beta_{eff,i} \tag{14-3}$$

The corresponding precursor decay constant is calculated by

$$\lambda_i = \frac{\int_V \sum_j \sum_g \beta_{ig}^j \nu\Sigma_{fg}^j \phi_g \, dV}{\int_V \sum_j \sum_g (\beta_{ig}^j \nu\Sigma_{fg}^j \phi_g)/\lambda_i^j \, dV} \tag{14-4}$$

where λ_i^j = precursor decay constant of the j-th nuclide in precursor group i.

The average inverse neutron velocity (sec/cm) can be obtained by using the following formula:

$$\frac{1}{v_g} = \frac{\int_V \phi_g^* \frac{\sigma_g}{\sigma(v')} \phi_g \, dV}{\int_V \phi_g^* \phi_g \, dV} \frac{1}{v_0} \tag{14-5}$$

where v_0 = 2200 m/sec.

The prompt neutron lifetime, ℓ, is given by

$$\ell = \frac{\int_V \sum_g \phi_g^* \frac{\sigma_g}{\sigma(v')} \phi_g \, dV}{\int_V \sum_j \sum_g \phi_g^* \chi_g \nu\Sigma_f^j \phi_g \, dV} \frac{1}{v_0} \tag{14-6}$$

Delayed neutron yields and decay constants listed in Tables 14-1 and 14-2 are taken from ENDF/B-V.

Table 14-1 Delayed Neutron Yields

Group	Th-232	U-233	U-234	U-235	U-236	U-238	Pu-239	Pu-240	Pu-241	Pu-242
1	.034	.086	.013	.038	.013	.013	.038	.028	.010	.028
2	.150	.274	.137	.213	.137	.137	.280	.273	.229	.273
3	.155	.227	.162	.188	.162	.162	.216	.192	.173	.192
4	.446	.317	.388	.407	.388	.388	.328	.350	.390	.350
5	.172	.073	.225	.128	.225	.225	.103	.128	.182	.128
6	.043	.023	.075	.026	.075	.075	.035	.029	.016	.029
total			.0151	.00685	.0151	.0151	.00223	.00321	.00549	.00321

Table 14-2 Delayed Constants (sec^{-1}) for delayed neutron groups

Grou	Th-232	U-233	U-234	U-235	U-236	U-238	Pu-239	Pu-240	Pu-241	Pu-242
1	.01237	.01258	.01323	.01272	.01323	.01323	.0129	.01294	.0128	.01294
2	.0334	.03342	.03212	.03174	.03212	.03212	.0311	.03131	.0299	.03131
3	.121	.131	.139	.116	.139	.139	.134	.135	.124	.135
4	.321	.303	.359	.311	.359	.359	.332	.333	.352	.333
5	1.21	1.27	1.41	1.40	1.41	1.41	1.26	1.36	1.61	1.36
6	3.29	3.14	4.03	3.87	4.03	4.03	3.21	4.03	3.47	4.03

15. Control Rod Model

15.1 Control Rod Cross Section

The control rod worth is treated using the delta macroscopic cross section concept. The insertion of control rods is described by adding burnup-dependent delta macroscopic cross sections of control rod to those of the unrodded assembly.

$$\Sigma_{\text{with cr}} = \Sigma_{\text{without cr}} + \Delta\Sigma_{\text{cr}} \tag{15.1-1}$$

The rodded assemblies are also treated according to the simplified equivalence theory. When the control rod cross sections are provided from single assembly calculations, the heterogeneity factors f of unrodded and rodded fuel assemblies are considered as follows:

$$\Delta\Sigma_{\text{cr}} = \frac{\Sigma_{\text{c}}}{f_{\text{c}}} - \frac{\Sigma_{\text{u}}}{f_{\text{u}}} \tag{15.1-2}$$

where the subscripts c and u denote rodded and unrodded assembly, respectively.

15.2 Heterogeneous Control Rod Model

To calculate the worth of control rods partially inserted in the axial direction, the control rod cross sections are weighted with flux and volume [41]. If the control rod is partially inserted in the axial direction in a given node in shown in Fig. 15-1, we can express the macroscopic cross section of the node as

$$\Sigma(z) = \Sigma_0 + \delta\Sigma(z) \tag{15.2-1}$$

where Σ_0 = macroscopic cross section of unrodded node,

$\delta\Sigma(z) = 0 \qquad (0 \le z \le z_1)$

$= \Delta\Sigma_{cr}$ ($z_1 \le z \le 1$).

The flux solution is assumed as a quartic polynomial according to NEM.

$$\varphi(x,y,z) = \sum_{i,j,k=0}^{4} a_{ijk}\xi_i(x)\xi_j(y)\xi_k(z) \tag{15.2-2}$$

Integrating the cross sections with flux over the xy-direction which is denoted by $\psi(u)$ leads to the following balance equation:

$$\frac{1}{V}\int_V \Sigma(z)\varphi(x,y,z)dxdydz = \int_0^1 \Sigma_0\psi(u)du + \int_{z_1}^1 \Delta\Sigma\psi(u)du \tag{15.2-3}$$

The right hand side of the above equation can be written as

$$RHS = (\Sigma_0 + \Delta\Sigma(1-z_1))\phi + RHS_0 \tag{15.2-4}$$

where

$$\begin{aligned} RHS_0 = \Delta\Sigma\Big[& a_{001}\left((1-z_1^{\,2})-(1-z_1)\right) \\ & + a_{002}\left(-2(1-z_1^{\,3})+3(1-z_1^{\,2})-(1-z_1)\right) \\ & + a_{003}\left(-3(1-z_1^{\,4})+6(1-z_1^{\,3})-3(1-z_1^{\,2})\right) \\ & + a_{004}\left(-6(1-z_1^{\,5})+15(1-z_1^{\,4})-12(1-z_1^{\,3})+3(1-z_1^{\,2})\right)\Big], \end{aligned}$$

$$a_{001} = \frac{\psi_{rz}-\psi_{lz}}{2},$$

$$a_{002} = \phi - \frac{\psi_{rz}+\psi_{lz}}{2},$$

$$a_{003} = \frac{j^+_{rz}-j^-_{rz}+j^+_{lz}-j^-_{lz}}{12D/z_1} + \frac{1}{3}a_{001},$$

$$a_{004} = \frac{j^+_{rz}-j^-_{rz}-j^+_{lz}+j^-_{lz}}{12D/z_1} - a_{002},$$

$$\phi = \int_0^1 \psi(u)du .$$

and a_{00i} represents the expansion coefficient of $\psi(z)$ which is known during iteration. By dividing the result of Eq. (15.2-4) by the node average flux we can get the flux volume homogenized cross section.

$$\Sigma^{hom} = \Sigma_0 + \Delta\Sigma(1-z_1) + \frac{RHS_0}{\phi} \tag{15.2-5}$$

where $\Sigma_0 + \Delta\Sigma(1-z_1)$ is the volume-averaged cross section and the additive term, RHS_0, represents the contribution of higher-order flux momentums. For the correction of the momentum equations, the weighted residual method is introduced.

$$\frac{1}{V}\int_V w_i(u)\Sigma(z)\varphi(x,y,z)dxdydz \tag{15.2-6}$$

where $w_i(u)$ = weighting function .

If we let $w_i(u)$ be $\xi_1(z)$, the resulting solution becomes

$$\begin{aligned}\int_0^1 h_1(z)\Sigma(z)\psi(z)dz &= \int_0^1 h_1(z)\Sigma_0\psi(z)dz + \Delta\Sigma\int_{z_1}^1 (2z-1)\psi(z)dz \\ &= \int_0^1 h_i(z)\Sigma_0\psi(z)dz - \Delta\Sigma\int_{z_1}^1 \psi(z)dz + 2\Delta\Sigma\int_{z_1}^1 z\psi(z)dz\end{aligned} \tag{15.2-7}$$

where

$$2\Delta\Sigma\int_{z_1}^{1} z\psi(z)dz = RHS_1$$

$$= \Delta\Sigma\Big[\phi(1-z_1^{\,2}) + a_{001}\frac{4}{3}((1-z_1^{\,3})-(1-z_1^{\,2}))$$
$$+ a_{002}(-3(1-z_1^{\,4})+4(1-z_1^{\,3})-(1-z_1^{\,2}))$$
$$+ a_{003}(-\frac{24}{5}(1-z_1^{\,5})+9(1-z_1^{\,4})-4(1-z_1^{\,3}))$$
$$+ a_{004}(-10(1-z_1^{\,6})+24(1-z_1^{\,5})-18(1-z_1^{\,4})+4(1-z_1^{\,3}))\Big]$$

Using the flux volume homogenized cross section Σ^{hom} Eq. (15.2-7) can be rewritten as

$$\int_0^1 h_1(z)\Sigma(z)\psi(z)dz$$

$$= \int_0^1 h_1(z)\Sigma_0\psi(z)dz - \Delta\Sigma(1-z_1)\phi - RHS_0 + RHS_1 \qquad (15.2\text{-}8)$$

$$= \int_0^1 h_1(z)\Sigma^{hom}\psi(z)dz - (\Delta\Sigma(1-z_1)+\frac{RHS_0}{\phi})(\phi+\frac{a_{001}}{3}+\frac{a_{003}}{5})+RHS_1$$

In the same manner, letting $w_i(u)$ be $\xi_2(u)$ yields the correction term of the 2nd momentum equation.

$$\int_0^1 h_2(z)\Sigma(z)\psi(z)dz = \int_0^1 h_2(z)\Sigma_0\psi(z)dz + \Delta\Sigma\int_{z_1}^{1}(6z(1-z)-1)\psi(z)dz$$

$$= \int_0^1 h_2(z)\Sigma_0\psi(z)dz - \Delta\Sigma\int_{z_1}^{1}\psi(z)dz + \Delta\Sigma\int_{z_1}^{1}(6z-6z^2)\psi(z)dz \qquad (15.2\text{-}9)$$

where

$$-6\Delta\Sigma\int_{z_1}^{1} z^2\psi(z)dz$$

$$= RHS_2$$

$$= -\Delta\Sigma\Big[2\phi(1-z_1^{\,3}) + a_{001}(3(1-z_1^{\,4}) - 2(1-z_1^{\,3}))$$

$$+ a_{002}(-\frac{36}{5}(1-z_1^{\,5}) + 9(1-z_1^{\,4}) - 2(1-z_1^{\,3}))$$

$$+ a_{003}(-12(1-z_1^{\,6}) + \frac{108}{5}(1-z_1^{\,5}) - 9(1-z_1^{\,4}))$$

$$+ a_{004}(-\frac{180}{7}(1-z_1^{\,7}) + 60(1-z_1^{\,6}) - \frac{216}{5}(1-z_1^{\,5}) + 9(1-z_1^{\,4}))\Big]$$

It can be rearranged as

$$\int_0^1 h_2(z)\Sigma(z)\psi(z)dz$$

$$= \int_0^1 h_2(z)\Sigma_0\psi(z)dz - \Delta\Sigma(1-z_1)\phi - RHS_0 + 3RHS_1 + RHS_2 \qquad (15.2\text{-}10)$$

$$= \int_0^1 h_2(z)\Sigma^{hom}\psi(z)dz - (\Delta\Sigma(1-z_1) + \frac{RHS_0}{\phi})(\phi + \frac{a_{002}}{5} - \frac{3}{35}a_{004}) + 3RHS_1 + RHS_2$$

Therefore, for the node with control rod partially inserted the volume homogenized cross section is replaced by the flux volume homogenized one in all equations as expressed in Eq. (15.2-5), and then the 1st and 2nd momentum equations are corrected using Eq. (15.2-8) and Eq. (15.2-10).

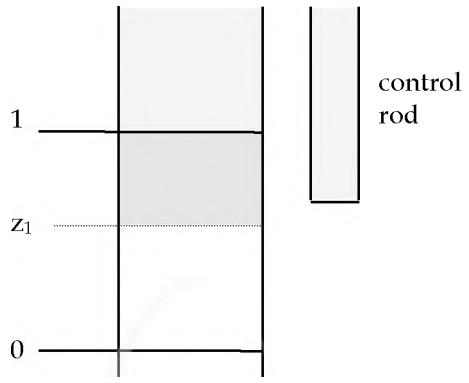

Figure 15-1 Control Rod Partially Inserted in the Axial Direction

MASTER has another heterogeneous control rod model [42] to correct for the rod cusping effect. In this model the flux redistribution should be properly reflected in the homogenized nodal cross section. In addition, the correctional nodal coupling coefficients (CNCC) which are normally obtained from a two-node calculation should be determined such that the intranodal cross section variation can be considered during the determination process. For NANM and NNEM the intranodal flux distribution in a partially rodded node is obtained by solving a three-node problem by the fine mesh finite difference scheme. The flux weighting factor and the interface currents used to determine the CNCC can be readily obtained from the intranodal flux solution.

Consider an axial three-node domain as shown in Figure 15-2. The middle node is partially rodded and it is adjacent to a fully rodded and an unrodded node. For the three-node problem, a transverse-integrated neutron balance equation can be obtained in the same way as the two-node nodal problem. Since the transverse-integrated equation is one-dimensional and there are only a few partially rodded nodes in a reactor, it is feasible to

employ a fine mesh finite difference scheme to solve the transverse-integrated equation, instead of employing the analytic nodal method for the three-node problem. For the finite-differenced one-dimensional problem, the coefficient matrix becomes primarily tridiagonal and the Gauss elimination can be applied efficiently to solve the linear system.

To solve a one-dimensional second-order differential equation, two boundary or constraint conditions must be specified. In a three-node problem, the boundary conditions may be specified at the two boundaries in terms of the neutron current. Another possibility is to use the node average fluxes of the rodded and unrodded nodes as the two constraints. Both the current and the node average flux are available from the previous CMFD calculation when the nonlinear nodal method is employed. The node average flux constraint is then used because it assures the fine mesh solution is consistent with the coarse mesh solution as far as the node average fluxes are concerned.

The intranodal flux distribution determined from the three-node problem is used to determine the currents at the upper and lower interfaces of the middle node. The interface currents can then be used to determine the CNCC. The solution of the three-node problem is performed every time when a nodal update is performed, resulting in the new flux weighting factors and the CNCC to be used in the subsequent CMFD calculations.

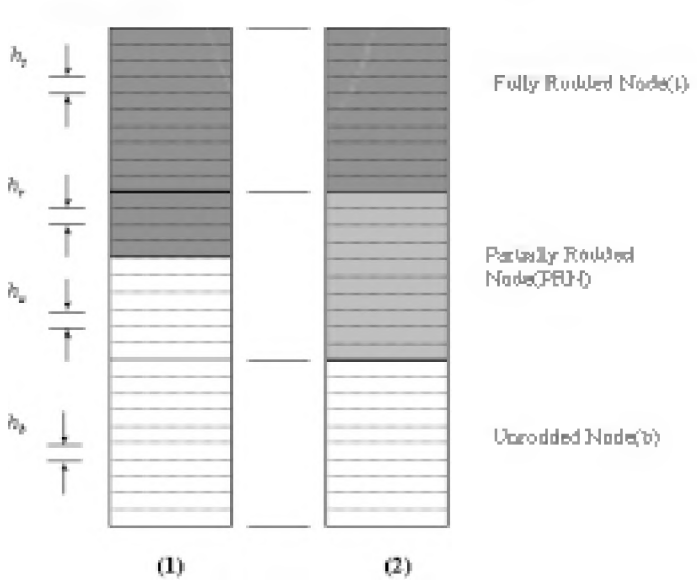

Figure 15-2 Three-Node Fine Mesh Problem

16. Detector Model

16.1 Detector Reaction Rate

The predicted reaction rates in in-core detectors are calculated for each thimble in an axial region as:

$$R(r) = \sum_{g} \Sigma_{ag}^{det} \phi_{g}^{het}(r) \qquad (16.1\text{-}1)$$

where Σ_{ag}^{det} = absorption cross section of a detector for group g,

$\phi_{g}^{het}(r)$ = heterogeneous flux for group g at the position r where a detector exists.

In the movable detector the number densities of detectors are assumed to be constant with burnup, but those of the fixed in-core detectors are depleted in a core.

The depletion of fixed in-core detectors is performed as follows:

$$N^{det}(t) = N^{det}(0) e^{-\sum_{g} \sigma_{ag}^{det} \phi_{g}^{het} t} \qquad (16.1\text{-}2)$$

where $N^{det}(t)$ = detector number density at time t,

σ_{ag}^{det} = detector microscopic absorption cross section for group g.

Since detectors are in most cases positioned into instrument thimbles which have no burnup values, the number density versus microscopic cross section table is prepared unlikely to other cross sections.

16.2 Analytic Constants for Flux Mapping

16.2.1 Detector Signal-to-Power Factor

In the CE-type plant the signal-to-power factor (W') for the cores where the instrumented assemblies are modeled is needed in order to convert the signals from detector into corresponding powers in CECOR [43]. The value W' is defined as:

$$W'(r) = \frac{P(r)}{R^{det}(r)} \tag{16.2-1}$$

where $p(r)$ = assembly power integrated over the detector length,

$R^{det}(r)$ = average activation rate per unit detector length.

16.2.2 Detector Coefficient

The detector coefficients required are determined depending on what flux mapping system they are used for. The followings show coefficients for CECOR and INCORE [44], respectively.

$$\text{CECOR coupling coefficient} = \frac{P_{ijk}}{\frac{1}{N}\sum_{n=1}^{N} P_n} \tag{16.2-2}$$

where P_{ijk} = power in the assembly located at (i, j, k),

P_n = power in an assembly which has a common surface with the assembly at (i, j, k),

N = the number of assemblies which have a common surface with the assembly at (i, j, k).

$$\text{INCORE constant} = \frac{P_{ijk}}{\sum_g \kappa \sigma_g^{det} \phi_g^{het}} \qquad (16.2\text{-}3)$$

where κ = energy release per fission,

σ_g^{det} = detector cross section for group g,

ϕ_g^{het} = heterogeneous flux for group g in the position where the detector exists.

17. Xenon Dynamics

The xenon dynamics module solves the time-dependent iodine/xenon and promethium/samarium differential equation described in section 10.3. The time discretization is performed by use of Hermite polynomials. The nodal flux shapes are approximated by linear functions within each time interval considered.

The iodine and promethium equations among Eq. (10.3-1) and Eq. (10.3-4) can be written again with linear approximation of the flux shape in a time interval as

$$\frac{dI}{dt} = a_0 + a_1(t - t_0) - \lambda_I I \qquad (17\text{-}1)$$

$$\frac{dP}{dt} = b_0 + b_1(t - t_0) - \lambda_P P$$

where $a_0 = y_I \Sigma_f \phi(t_0)$, $a_1 = y_I \Sigma_f \frac{\phi(t_1) - \phi(t_0)}{\Delta t}$,

$b_0 = y_P \Sigma_f \phi(t_0)$, $b_1 = y_P \Sigma_f \frac{\phi(t) - \phi(t_0)}{\Delta t}$.

These equations can be solved analytically by

$$I(t) = c_0 + c_1(t - t_0) + c_2 e^{-\lambda_I (t - t_0)} \qquad (17\text{-}2)$$

$$P(t) = d_0 + d_1(t - t_0) + d_2 e^{-\lambda_P (t - t_0)}$$

where $c_0 = \frac{\lambda_I a_0 - a_1}{\lambda_I^2}$, $c_1 = \frac{a_1}{\lambda_I}$, $c_2 = I(t_0) - c_0$,

$d_0 = \frac{\lambda_P b_0 - b_1}{\lambda_P^2}$, $d_1 = \frac{b_1}{\lambda_P}$, $d_2 = P(t_0) - d_0$.

If the concentration I_{n+1} and P_{n+1} for a considered time t_{n+1} are known, the time

discretization of the xenon and samarium equations among Eq. (10.3-1) and Eq. (10.3-4) is performed using Hermite polynomials. The general form of those equations can be expressed as

$$\dot{y} = g(y, t) \tag{17-3}$$

Then, the time discrete equations with Hermite polynomials read

$$y_{n+1} = y_n + \frac{\Delta t_n}{2}(g_{n+1} + g_n) + \frac{\Delta t_n^{\,2}}{12}(g_{n+1} - g_n) + R \tag{17-4}$$

where Δt_n = time interval,

R = remaining error of 4th order.

For each time step the calculation of the iodine/xenon and the promethium/samarium concentrations is performed iteratively together with the steady-state flux solution process.

18. Power Shape Matching

In this section a nodal method is presented how a given (target) power distribution can be generated. This is accomplished by adjusting the absorption cross sections (Σ_{a1}, Σ_{a2}) which are free parameters of the system model. The system parameters are then coincided with the core conditions of the core eigenvalue and flux distributions. This kind of nodal method is called the backward nodal solution method in the sense that cross sections are determined for given fluxes and eigenvalue. The results of this method are the absorption cross sections which form a consistent set of eigenvalue, currents and fluxes of the forward(normal) nodal solution. The adjusted cross sections are obtained by solving forward nodal equation iteratively.

The starting point for the derivation of the backward nodal solution is the two-group neutron diffusion equation in P_1 form.

$$\nabla \cdot J_g(r) + (\Sigma_{ag}(r) + \sum_{g'>g} \Sigma_{gg'}(r))\varphi_g(r) = \sum_{g'<g} \Sigma_{g'g}(r)\varphi_{g'}(r) + \frac{1}{\lambda}\sum_{g'}\sum_{j} \chi_{pg}^{j}\, \nu\Sigma_{fg'}^{j}(r)\varphi_{g'}(r) \tag{2.1-1a}$$

$$J_g(r) = -D_g(r)\nabla\varphi_g(r) \tag{2.1-1b}$$

Integrating Eq. (2.1-1) over a node volume leads to the exact nodal balance equation as follows:

$$\sum_{u=x,y,z}\frac{1}{a_u^m}\left[\left(j_{gul}^{-m} + j_{gur}^{+m}\right) - \left(j_{gul}^{+m} + j_{gur}^{-m}\right)\right] + \left(\Sigma_{ag}^{m} + \sum_{g'>g}\Sigma_{gg'}^{m}\right)\phi_g^m = \sum_{g'<g}\Sigma_{g'g}^{m}\phi_{g'}^{m} + \frac{1}{\lambda}\sum_{g'}\chi_g\,\nu\Sigma_{fg'}^{m}\phi_{g'}^{m} \tag{2.1-2a}$$

$$j_{gus}^{+m} - j_{gus}^{-m} = -D_g^m \left.\frac{\partial\psi_{gu}^m}{\partial u}\right|_S \tag{2.1-2b}$$

In the backward nodal expansion method (NEM), the surface average fluxes can be expanded into a quartic polynomial with orthogonal functions, which is exactly the same as normal NEM.

$$\psi_{gu}^{m}(u) = \sum_{i=0}^{4} a_{igu}\, h_i(u) \tag{2.1-4}$$

The first three coefficients of the right hand side of Eq. (2.1-4) can be expressed by nodal balance equations and continuity conditions, and the third and fourth order coefficients a_{3gu} and a_{4gu} can be determined by solving the one-dimensional equivalent diffusion equations with weighted residual method.

The equations for the outgoing currents on the left and right surfaces are given as functions of the diffusion coefficients, the incoming currents, the one-dimensional flux expansion coefficients (a_{3gu}, a_{4gu}) and the given nodal extrapolated fluxes.

$$\begin{aligned} j_{gul}^{-m} &= c_{1gu}^{m}\ (\phi_g^m + a_{4gu}^{m}) + c_{2gu}^{m}\ j_{gul}^{+m} + c_{3gu}^{m}\ j_{gur}^{-m} - c_{4gu}^{m}\ a_{3gu}^{m} \\ j_{gur}^{+m} &= c_{1gu}^{m}\ (\phi_g^m + a_{4gu}^{m}) + c_{3gu}^{m}\ j_{gul}^{+m} + c_{2gu}^{m}\ j_{gur}^{-m} + c_{4gu}^{m}\ a_{3gu}^{m} \end{aligned} \tag{2.1-7}$$

where ϕ_g^m = target flux,

$$c_{1gu} = \frac{D_{gu}}{1/6 + 2D_{gu}},$$

$$c_{2gu} = 1 - 4\,c_{1gu} - c_{3gu},$$

$$c_{3gu} = \frac{-c_{1gu}}{3/4 + 3D_{gu}},$$

$$c_{4gu} = c_{1gu} - 6D_{gu}\,c_{3gu},$$

$$D_{gu} = D_g^m / a_u.$$

With the partial currents, the target fluxes and cross sections, the model free parameters

$(\Sigma_{a1}, \Sigma_{a2})$ can be determined from the node neutron balance equation:

$$\Sigma_{a1}^{m} = (-L_1^m - \Sigma_{21}^{m} \phi_1^m + \frac{1}{\lambda} \sum_{g'} \chi_{pg} \nu\Sigma_{fg'}^{m} \phi_{g'}^{m}) / \phi_1^m$$
$$\Sigma_{a2}^{m} = (-L_2^m + \Sigma_{21}^{m} \phi_1^m) / \phi_2^m \qquad (18\text{-}1)$$

where

$$L_g^m = \sum_{u=x,y,z} \frac{1}{a_u^m} \left[\left(j_{gul}^{-m} + j_{gur}^{+m} \right) - \left(j_{gul}^{+m} + j_{gur}^{-m} \right) \right] \qquad (18\text{-}2)$$

Eq. (18-1) is solved only for the fuel region in the core. For the reflector region forward nodal calculation is performed.

19. One-dimensional Model

A 3-D neutronics code can be considered as the ultimate means of achieving high fidelity in the neutronic reactor core design and simulation. Nonetheless the 1-D neutronics model is often needed to replace the 3-D model in many practical circumstances. In the case that a 3-D model is avail, it is possible to generate the 1-D model through a consistent radial collapsing procedure. The 1-D kinetics equation can be derived by integrating the 3-D time-dependent neutron diffusion equation over the radial domain. The solution of the 1-D kinetics equation is relatively simple because it involves only a block tridiagonal linear system which can be solved directly by the Gaussian elimination scheme. However, it is important in the 1-D calculation to conserve the axial currents which ensure reproducing the reference 3-D results. This is realized in the HAMOCE code [45]. MASTER-3.0 is then implemented to calculate the 3-D consistent 1-D cross sections for the HAMOCE and 1-D model of MASTER-3.0 itself. The 1-D cross sections are created by calculating the following quantities for each axial region k.

$$
\begin{aligned}
&\phi_g^k = \sum_{ij} \phi_g^{ijk} V^{ijk} / \sum_{ij} V^{ijk}, \quad V^{ijk} = \text{volume of node } (i, j, k) \\
&\Sigma_{trg}^k = \sum_{ij} \Sigma_{trg}^{ijk} \phi_g^{ijk} V^{ijk} / \sum_{ij} \phi_g^{ijk} V^{ijk}, \\
&\Sigma_{ag}^k = \sum_{ij} \Sigma_{ag}^{ijk} \phi_g^{ijk} V^{ijk} / \sum_{ij} \phi_g^{ijk} V^{ijk}, \\
&\Sigma_{fg}^k = \sum_{ij} \Sigma_{fg}^{ijk} \phi_g^{ijk} V^{ijk} / \sum_{ij} \phi_g^{ijk} V^{ijk}, \\
&\kappa\Sigma_{fg}^k = \sum_{ij} \kappa\Sigma_{fg}^{ijk} \phi_g^{ijk} V^{ijk} / \sum_{ij} \phi_g^{ijk} V^{ijk}, \\
&\nu\Sigma_{fg}^k = \sum_{ij} \nu\Sigma_{fg}^{ijk} \phi_g^{ijk} V^{ijk} / \sum_{ij} \phi_g^{ijk} V^{ijk}, \\
&\Sigma_{21}^k = \sum_{ij} \Sigma_{21}^{ijk} \phi_g^{ijk} V^{ijk} / \sum_{ij} \phi_g^{ijk} V^{ijk}, \\
&\sigma_{ag,B10}^k = \sum_{ij} \sigma_{ag,B10}^{ijk} \phi_g^{ijk} V^{ijk} / \sum_{ij} \phi_g^{ijk} V^{ijk}, \\
&\sigma_{ag,iso}^k = \sum_{ij} \sigma_{ag,iso}^{ijk} \phi_g^{ijk} V^{ijk} / \sum_{ij} \phi_g^{ijk} V^{ijk}, \quad iso = Xe^{135}, Sm^{149},
\end{aligned}
\tag{19-1}
$$

$$Y^{iso,k} = \sum_{ij} Y^{iso,ijk} N_{fis}^{ijk} V^{ijk} / \sum_{ij} N_{fis}^{ijk} V^{ijk}, \quad Y = \text{fission yield},$$

$$iso = Pm^{149}, I^{135}, Xe^{135}, \quad fis = \text{fissile material},$$

$$T_m^k = \sum_{ij} T_m^{ijk} V^{ijk} / \sum_{ij} N_{fis}^{ijk} V^{ijk}, \quad T_m = \text{moderator temperature}$$

$$D_m^k = \sum_{ij} D_m^{ijk} V^{ijk} / \sum_{ij} V^{ijk}, \quad D_m^k = \text{moderator density}$$

$$T_f^k = \sum_{ij} T_f^{ijk} V^{ijk} / \sum_{ij} V^{ijk}, \quad T_f^k = \text{fuel temperature}$$

$$DB_g^{2,k} = \sum_{ij} \left[(J_{gxr}^{net} - J_{gxl}^{net}) V^{jk} + (J_{gyr}^{net} - J_{gyl}^{net}) V^{ik} \right] / \sum_{ij} \phi_g^{ijk} V^{ijk},$$

$$DB_g^2 = \text{radial buckling}, \quad V^{jk} = a_y a_z, \quad V^{ik} = a_x a_z$$

References

1. H. Finnemann *et al.*, "Interface Nodal Current Techniques for Multidimensional Reactor Calculations," Atomkernenergie, **30**, 123, 1977.

2. H. Finnemann and H. Raum, "Nodal Expansion Method for the Analysis of Space-time Effects in LWRs," Proceedings of a Specialists' Meeting on Calculation of 3-Dimensional Rating Distributions in Operating Reactors, Paris, November, 1979.

3. H. Finnemann, "Basic Equations of the FLUXT Module of the Neutron Diffusion Code NEMBOX," Siemens/KWU Work-Report B3/313/89/E385, November 15, 1989.

4. H. D. Fischer and H. Finnemann, "The Nodal Integration Method - A Diverse Solver for Neutron Diffusion Problems," Atomkernenergie, **39**, 229, 1981.

5 J. M. Noh and N. Z. Cho, "A New Diffusion Nodal Method Based on Analytic Basis Function Expansion," Trans. Am. Nucl. Soc., 69, 462, 1993.

6 J. M. Noh and N. Z. Cho, "A New Approach of Analytic Basis Function Expansion to Neutron Diffusion Nodal Calculation," Nucl. Sci. Eng., 116, 165, 1994.

7 M. H. Chang, K. S. Moon, J. M. Noh and S. H. Kim, "A Nodal Expansion Method with Spatially Coupled Effects Incorporated into the Transverse Leakage Approximation," Nucl. Sci. Eng., 103, 343, 1989.

8. H. Finnemann, R. Boer and J. Huesken, "Finite Difference Solution of the Flux Reconstruction Problem in Nodal Reactor Analysis," Proc. of Joint Int. Conf. on Mathematical Methods and Supercomputing in Nuclear Applications, Karlsruhe, Germany, April 19-23, 1, 533, 1993.

9. B. O. Cho *et al.*, "AFEN/NEM Hybrid Method for Reactor Core Analysis," KAERI/TR-1150/98, 1998.

10. H. G. Joo *et al.*, "Methods and Performance of Parallel Reactor Kinetics Code PARCS, " proc. of Int. Reac. Physics Conf., Mitto, Japan, 42, 1996.

11. T. J. Downar, H. G. Joo, and G. Jiang, "A Hybrid ANM/NEM Interface Current Technique for the Nonlinear Nodal Calculation," Proc. of Joint Int. Conf. Mathematical Methods and Supercomputing for Nuclear Applications, 1, 124, Saratoga, Oct. 5-9, 1997.

12. N. Z. Cho and J. M. Noh, "The AFEN Method for Hexagonal Nodal Calculation and Reconstruction," Trans. Am. Nucl. Soc., 71, 466, 1994.

13. B. O. Cho *et al.*, "Partial Current Based AFEN Formulation for Hexagonal-z Neutronics Solver in MASTER," Int. Conf. on the Physics of Nuclear Science and Technology, Long Island, Oct. 5-8, 1998.

14. H. G. Joo, C. H. Lee, B. O. Cho, K. B. Lee and S. Q. Zee, "Local Fine-mesh Solution Based Transverse-Integrated Nodal Method for Hexagonal Geometry," Int. Conf. on the Physics of Nuclear Science and Technology, Long Island, Oct. 5-8, 1998.

15. J. Y. Cho *et al.*, "Non-Linear Triangle-Based Polynomial Expansion Nodal Method for Hexagonal Core Analysis, " KAERI/TR-1652/2000.

16. J. Y. Cho *et al.*, "Hexagonal CMFD Formulation Employing Triangle-Based Polynomial Expansion Nodal Kernel," M&C 2001, Salt Lake City, Utah, USA.

17. J. Y. Cho *et al.* "Higher-Order Polynomial Expansion Nodal Method for Hexagonal Core Neutronics Analysis," Ann. Nucl. Energy, Vol.25, No.13, p1021, 1998.

18. Philip Delmolino, "Specification of the Adjoint Module FLUXA of PANBOX2," SIEMENS/KWU Work-Report BT25/92/E288, September, 1992.

19. K. Koebke, "A New Approach to Homogenization and Group Condensation," IAEA Technical Committee Meeting on Homogenization Methods in Reactors Physics, IAEA-

TECDOC-231, Lugano, 1978.

20. K. Koebke, "Advances in Homogenization and Dehomogenization," International Topical Meeting On Advances in Mathematical Methods for the Solution of Nuclear Engineering Problems, **2**, 60, Munich, 1981.

21. K. S. Smith, "Assembly Homogenization Techniques for Light Water Reactor Analysis," Prog. Nucl. Energy, **17**, No.3, 1986.

22. H. J. Winter, K. Koebke, "Effective Cross Sections for the Radial and Axial Reflector in the Standard 79A Design Method," Siemens/KWU Technical Report R121-339/80, December, 1980.

23. K. Koebke and H. Winter, "The Equivalent Reflector Model," Siemens/KWU Technical-Report U6/521/82/E307, November 3, 1982.

24. K. B. Lee, "Generation of Equivalent Homogenized Reflector Constants using CASMO-3," SPC Work-Report KBL:94:001, November 21, 1994.

25. K. B. Lee *et al.*, "Verification of Equivalent Radial Reflector Cross Sections by Using CASMO-3 for PWR Core Design," CASMO User's Meeting, February 22-24, 1995.

26. M. Edenius and B. Forssen, "CASMO-3: A Fuel Assembly Burnup Program Methodology Version 4.4, " STUDSVIK/NFA-89/2, November, 1989.

27. M. Edenius and B. Forssen, "CASMO-3 User's Manual," STUDSVIK/NFA-89/3, November, 1989.

28. HELIOS Users' Manual, 15 Dec. 1995.

29. R. Boeer and H. Finnemann, "Fast Analytical Flux Reconstruction Method for Nodal

Space-time Nuclear Reactor Analysis," Ann. Nucl. Energy, **19**, No.10-12, 617-628, 1992.

30. H. Finnemann *et al.*, "Finite Difference Solution of the Flux Reconstruction Problem in Nodal Reactor Analysis," Joint International Conference on Mathematical Methods and Supercomputing in Nuclear Applications, M&C+SNA 19-23 April 1993, Karlsruhe, Germany.
31. K. Koebke and L. Hetzelt, "On the Reconstruction of Local Homogeneous Neutron Flux and Current Distributions of Light Water Reactors from Nodal Schemes," Nucl. Sci. Eng., **91**, 123, 1985.
32. B. O. Cho, "Specification of FLUXD of COPS," Siemens/KWU Work-Report BT25/1993/E048, March 4, 1993.
33. C. H. Lee *et al.*, "Determination of Local Power Distribution Considering Spectral History Effect in Nodal Methods," Proceedings of International Conference on Mathematics and Computations, Reactor Physics, and Environmental Analyses, Portland, Oregon, April 30 - May 4, 1995.
34. C. H. Lee and Y. J. Kim, "An Adaptation of the SAV Standard Nuclide Chain for the CASMO-3/MEDIUM-3 Procedure," Journal of the Korean Nuclear Society, **26**, No.2, June, 1994.
35. M. R. Wagner, K. Koebke and H. J. Winter, "A Nonlinear Extension of the Nodal Expansion Method," International Topical Meeting on Advances in Mathematical Methods for the Solution of Nuclear Engineering Problems, **2**, 43, Munich, 1981.
36. D. S. Rowe, "COBRA III-C: A Digital Computer Program for Steady-State and Transient Thermal Hydraulic Analysis of Rod Bundle Nuclear Fuel Elements," BNWL-1695, Battelle-Pacific Northwest Laboratories, 1973.
37. R. E. Masterson and L. Wolf, "COBRA III-P: An Improved Version of COBRA for Full

Core Light Water Reactor Analysis," Nuclear Engineering and Design, **48**, 293, 1978.

38. J. W. Jackson and N. E. Todreas, "COBRA III-C/MIT-2: A Digital Computer Program for Steady-State and Transient Thermal Hydraulic Analysis of Rod Bundle Nuclear Fuel Elements," MIT-EL81-018, MIT, 1981.

39. Yoo, Y. J. *et al.*, "Development of a subchannel analysis code MATRA applicable to PWRs and ALWRs," J. Korean Nuclear Society 31, 314-327 (1999).

40. C. L. Wheeler *et al.*, COBRA-IV-I: An Interim Version of COBRA for Thermal-Hydraulic Analysis of Rod Bundle Nuclear Fuel Elements and Cores, BNWL-1962 (1976).

41. H. Finnemann, "Representation of Control Rods using the Nodal Expansion Method (NEM)," Siemens/KWU Technical-Report R121-E285/77, December 15, 1977.

42. J. L. Biffer, W. B. Terney and F. S. Zimnock, "CECOR 2.0 - General Description, Methods and Algorithms," Nuclear Power Division, Combustion Engineering, Inc., NPSD-103-P, 1980.

43. K. B. Lee *et al*, "Correction of the Control Rod Cusping Effect Using One-Dimensional Fine Mesh Flux Profiles," Proceedings of the KNS Spring Meeting vol II, Seoul, Korea, Oct. 1988.

44. J. Harris and K. A. Jones, "Code Manual INCORE 3.7," WCAP-8492, March, 1975.

45. K. B. Lee *et al*, "Current Conservation Factors for Consistent One-Dimensional Neutronics Modeling," J. Korea Nuclear Society, vol. 32, number 3, pp.235-243, June 2000.

서 지 정 보 양 식

수행기관보고서번호	위탁기관보고서 번호	표준보고서 번호	INIS 주제코드
KAERI/TR-2061/2002			

제목 / 부제	MASTER-3.0: 코드 방법론
연구책임자 및 부서명	조 병 오 (동력로기술개발팀)
연 구 자 및 부 서 명	주 한 규 (동력로기술개발팀) 조 진 영 (동력로기술개발팀) 송 재 승 (동력로기술개발팀) 지 성 균 (동력로기술개발팀)

출 판 지	대전	발행기관	한국원자력연구소	발행년	2002.2.
페 이 지	125 p.	도 표	있음(√),없음( )	크 기	26 cm
참고사항	원자력 연구개발 중장기 과제				
비밀여부	공개(√),대외비( ),__급비밀		보고서종류	기술보고서	
연구위탁기관			계약 번호		

초록 (15-20 줄)

MASTER-3.0 (Multi-purpose Analyzer for Static and Transient Effects of Reactors) 코드는 정상상태 및 천이상태의 사각형 또는 육각형 핵연료집합체로 구성된 원자로를 3차원으로 모사할 수 있는 노심설계 코드이다. 다군 또는 2군 중성자 확산방정식을 풀기 위해 사각형 핵연료집합체를 사용하는 노심에는 NIM (Nodal Integration Method), NEM (Nodal Expansion Method), AFEN (Analytic Function Expansion Nodal Method)/NEM 혼용 방법, NNEM (Non-linear Nodal Expansion Method), NANM (Non-linear Analytic Nodal Method) 방법들이 사용자의 선택에 따라 이용 가능하며, 육각형 핵연료집합체를 사용하는 노심에는 NTPEN (Non-linear Triangle-based Polynomial Expansion Nodal Method) 방법, AFEN (Analytic Function Expansion Nodal)/NEM 혼용 방법 또는 NLFM (Non-linear Local Fine-Mesh Method) 이 이용되고 있다. 계산의 효율 증대 및 시간 단축을 위하여 coarse-mesh rebalancing, Krylov Subspace 방법, 에너지군 축약/확대 방법, asymptotic extrapolation 방법들이 사용되고 있다. MASTER-3.0 코드는 CASMO-3 또는 HELIOS 로부터 마련된 각 핵종의 미시단면적으로 연소계산을 수행한다. 또한, MSS-IAS (Method of Successive Smoothing with Improved Analytic Solution)를 이용하여 각 핵연료집합체 내의 핵연료봉에 관한 정보를 구할 수 있다. 열수력 계산을 위해서 핵연료 온도표를 이용하는 기능과 COBRA3-C/P 또는 MATRA 코드로 계산하는 기능도 갖추고 있다. MASTER-3.0 코드는 실제 설계에 효율적으로 사용되기 위하여 WH형과 CE형 노심 및 SMART 원자로를 비롯한 일반 가압경수로 노심에서 설계 단계별로 필요로 하는 자료를 출력하는 기능도 갖추고 있다.

주제명키워드 (10 단어내외)	MASTER-3.0 코드방법론, 노심설계, 노달방법, 정상상태, 천이상태, 정방형, 육각형핵연료, CASMO-3, HELIOS, COBRA, MATRA

BIBLIOGRAPHIC INFORMATION SHEET

Performing Org. Report No.	Sponsoring Org. Report No.	Standard Report No.	INIS Subject Code
KAERI/TR-2061/2002			

Title / Subtitle	MASTER-3.0: METHODOLOGY MANUAL
Project Manager and Dept.	Cho, Byung-Oh (Advanced Reactor Technology Development Team)
Researcher and Dept.	Joo, Han Gyu (Advanced Reactor Technology Development Team) Cho, Jin Young (Advanced Reactor Technology Development Team) Song, Jae Seung (Advanced Reactor Technology Development Team) Zee, Sung-Quun (Advanced Reactor Technology Development Team)

Publication Place	**Taejon**	Publisher	**KAERI**	Publication Date	2002.2.
Page	125 p.	Ill. & Tab.	Yes(√), No( )	Size	26 cm
Note					

Classified	Open(√), Restricted( ), __Class Document	Report Type	**User Manual**
Sponsoring Org.		Contract No.	

Abstract (15-20 Lines)

MASTER-3.0 (Multi-purpose Analyzer for Static and Transient Effects of Reactors) is a nuclear design code based on the multi-group diffusion theory to calculate the steady-state and transient pressurized water reactor core in a 3-dimensional Cartesian or hexagonal geometry. Its neutronics model solves the space-time dependent neutron diffusion equations with NIM (Nodal Integration Method), NEM (Nodal Expansion Method), AFEN (Analytic Function Expansion Nodal Method)/NEM Hybrid Method, NNEM (Non-linear Nodal Expansion Method) or NANM (Non-linear Analytic Nodal Method) for a Cartesian geometry and with NTPEN (Non-linear Triangle-based Polynomial Expansion Nodal Method), AFEN (Analytic Function Expansion Nodal)/NEM Hybrid Method or NLFM (Non-linear Local Fine-Mesh Method) for a hexagonal one. Coarse mesh rebalancing, Krylov Subspace method, energy group restriction/prolongation method and asymptotic extrapolation method are implemented to accelerate the convergence of iteration process. MASTER-3.0 performs microscopic depletion calculations using microscopic cross sections provided by CASMO-3 or HELIOS and also has the reconstruction capability of pin information by use of MSS-IAS (Method of Successive Smoothing with Improved Analytic Solution). For the thermal-hydraulic calculation, fuel temperature table or COBRA3-C/P or MATRA model can be used selectively. In addition, MASTER-3.0 is designed to cover various PWRs including SMART as well as WH- and CE-type reactors, providing all data required in their design procedures.

Subject Keywords (about 10 words)	MASTER-3.0 code, Core Design, Nodal Method, Steady-State, Transient, Cartesian or hexagonal geometry, CASMO-3, HELIOS, COBRA, MATRA